Functional characterization of the novel lncRNA LINC00941 in tissue homeostasis and disease

D I S S E R T A T I O N

zur Erlangung des Doktorgrades der Naturwissenschaften (Dr. rer. nat.)
der Fakultät für Biologie und Vorklinische Medizin
der Universität Regensburg

vorgelegt von Johannes Graf

aus Burglengenfeld

im Jahr 2020

Das Promotionsgesuch wurde eingereicht am:

13.11.2020

Die Arbeit wurde angeleitet von:

PD Dr. Markus Kretz

Unterschrift:

1 Abstract

The skin with the epidermis provides the outermost effective barrier against environmental challenges such as pathogen invasion, UV-radiation, or prevention of extensive water loss. To fulfill its duties, the epidermis has to be constantly regenerated in order to maintain the protective function. During this highly elaborate process of epidermal rejuvenation, progenitor keratinocytes conduct a terminal differentiation program which is accompanied by a versatile expression of specific differentiation proteins and ultimately results in flattened anucleated cells that are embedded in an extracellular lipid layer.

In light of these profound alterations in gene expression, it is not surprising that epidermal homeostasis is controlled by an extensive network of signaling pathways and transcription factors. Recently, also the involvement of several long non-coding RNAs (lncRNAs) for this vital process has been uncovered. Several lncRNAs act as regulators of cellular homeostasis; however, few of these molecules were functionally characterized in a mature human epidermal tissue environment.

This work aims to characterize the lncRNA LINC00941 which was initially identified from full transcriptome sequencing of progenitor versus differentiated keratinocytes. LINC00941 is enriched in progenitor keratinocytes and acts as a repressor of keratinocyte differentiation upon onset of differentiation in both *in vitro* cultures as well as organotypic epidermal tissue and at the same time is increased in squamous cell carcinoma samples. Global RNA-sequencing ultimately proved the necessity of LINC00941 for a proper terminal differentiation program and hinted towards an epigenetic mechanism. This was further supported by the finding that LINC00941 appears to interact with the Nucleosome Remodeling Deacetylase (NuRD) complex indicating that LINC00941 might regulate expression of differentiation genes through modulation of activity or recruitment of this chromatin-remodeling complex. Additionally, Chromatin Isolation by RNA Purification (ChIRP) revealed various RNA occupancy sites of LINC00941 throughout the genome, highly similar to binding sites of the transcription factor family E2F.

Converse expression of LINC00941 during normal epidermal homeostasis and cutaneous squamous cell carcinoma (cSCC) progression hinted towards a role of LINC00941 during skin cancer development. Altered cell invasion as well as migratory potential mediated by LINC00941 further support the impact of LINC00941 in SCC progression.

In conclusion, an in-depth characterization of the human LINC00941 has been conducted in epidermal homeostasis development. Additionally, first results have been gained for epidermal disorders including squamous cell carcinoma. Thus, further analysis of LINC00941 might provide insights into a common mode of action for normal epidermal development as well as for disorders of epidermal growth, differentiation, and regeneration including squamous cell carcinoma.

List of abbreviations

AA	amino acid
A/A	antibiotic/antimycotic
AEBSF	4-(2-aminoethyl) benzenesulfonyl fluoride
Amp	Ampicillin
ANCR	anti-differentiation ncRNA
APS	ammonium persulfate
ATAC	Assay for Transposase Accessible Chromatin
BANCR	BRAF-regulated lncRNA
BCA	bicinchoninic acid
BCC	basal cell carcinoma
BCS	bovine calf serum
bp	base pair
Cas9	CRISPR associated protein 9
cDNA	complementary DNA
Cdk4	cyclin-dependent kinase 4
CDS	coding sequence
ChEA	ChIP Enrichment Analysis
ChIP	Chromatin Immunoprecipitation
chr	Chromosome
CMV	Cytomegalovirus
CRISPR	Clustered Regularly Interspaced Short Palindromic Repeats
CSF	codon substitution frequency
Ctrl	control
Cy5	Cyanine5
d, D	day
Da	Dalton (unified atomic mass unit)
DAG	Diacylglycerol
DAPI	4',6-diamidino-2-phenylindole
DB	dialysis buffer
diff	differentiated
DMSO	dimethyl sulfoxide
DMEM	Dulbecco's modified Eagle's medium
DNA	deoxyribonucleic acid
DNMT1	DNA (cytosine-5) methyltransferase 1
dNTP	deoxynucleotide triphosphate
DPBS	Dulbecco's phosphate-buffered saline
DTT	Dithiothreitol
dTTP	deoxythymidine triphosphate
et al.	et alia
EDC	epidermal differentiation complex
EDTA	ethylenediaminetetraacetic acid
EGF	epidermal growth factor
ERCC	External RNA Controls Consortium
EZH	Enhancer of zeste homolog
f	femto
FBS	fetal bovine serum
FC	fold change
Fendrr	FOXF1 adjacent non-coding developmental regulatory RNA
FISH	fluorescence *in situ* hybridization
FRIP	fraction of reads in called peak regions
g	gram
GADD	growth arrest and DNA damage-inducible protein
GEO	Gene Expression Omnibus
GFP	green fluorescent protein
GO	gene ontology
goi	gene of interest
gRNA	guideRNA
h	hour
HaCaT	human adult skin keratinocytes propagated under low Ca^{2+} conditions and elevated temperature
HDAC	histone deacetylase
HDR	homology-directed repair
HEK	human embryonic kidney
HEPES	4-(2-hydroxyethyl)-1-piperazineethanesulfonic acid
HF	high fidelity
hg19 / hg38	human genome build 19/38
HKGS	human keratinocyte growth supplement
HOTAIR	HOX transcript antisense RNA
hPGK	human phosphoglycerate kinase
IF	Immunofluorescence
IGV	Integrative Genomics Viewer
IP_3	inositol trisphosphate
JMJD3	Jumonji domain containing protein 3
k	kilo
KC	keratinocyte
KD	knockdown
DA	Dalton

KGM	keratinocyte growth medium
KO	knockout
l	liter
LB	lysogeny broth
LCE	late cornified envelope
lnc-mg	myogenesis-associated lncRNA
lncRNA	long non-coding RNA
LTR	long terminal repeat
m	milli
M	molar
µ	micro
MAPK	mitogen-activated protein kinase
miRNA	microRNA
min	minute
mio	million
MOPS	3-morpholinopropane-1-sulfonic acid
mRNA	messenger RNA
MUNC	MyoD upstream no-coding
mut	mutated
n	nano
n	number (of samples)
NA	not available
n.d.	not determined
NHEJ	non-homologous end joining
NLS	nuclear localization signal
nt	nucleotides
OD	optical density
ORF	open reading frame
p	pico
PAGE	polyacrylamide gel electrophoresis
PBS	phosphate buffered saline
PCA	principal component analysis
PCR	polymerase chain reaction
pH	power of hydrogen
PICSAR	p38 inhibited cutaneous squamous cell carcinoma associated lincRNA
PIP2	phosphatidylinositol bisphosphate
PNK	polynucleotide kinase
PRC	polycomb repressive complex
PRINS	psoriasis susceptibility-related RNA gene induced by stress
RACE	rapid amplification of cDNA ends
rcf	relative centrifugal force
RIPA	radio immunoprecipitation assay
rpm	rounds per minute
RNA	ribonucleic acid
RT	room temperature
RT-qPCR	reverse transcription-quantitative polymerase chain reaction
s	second
SCC	squamous cell carcinoma
SDS	sodium dodecyl sulfate
SENCR	smooth muscle and endothelial cell-enriched migration/differentiation-associated lncRNA
Seq	sequencing
SFM	serum-free medium
si	short interfering
SLIC	sequence- and ligation-independent cloning
SMRT-2	SCC misregulated transcript 2
SPRR	small proline-rich protein
SRA1	steroid receptor RNA activator 1
SRAP	steroid receptor RNA activator protein
TAE	Tris acetate EDTA buffer
TBS	Tris-buffered saline
TE	Tris EDTA buffer
TEMED	tetramethylethylenediamine
TGS	Tris glycine SDS buffer
TINCR	terminal differentiation induced ncRNA
tracrRNA	trans-activating CRISPR RNA
Tris	Tris(hydroxymethyl)aminomethane
U	unit
UCSC	University of California at Santa Cruz
USA	United States of America
UTX	ubiquitously transcribed tetratricopeptide repeat, X chromosome
UV	ultraviolet
V	Volt
v.	version
v/v	volume by volume
VSV-G	G glycoprotein of the vesicular stomatitis virus
WB	wash buffer
WB	western blot
w/v	weight by volume
XIST	X-inactive-specific transcript
YFP	yellow fluorescent protein

2 Introduction

2.1 The human skin

The human skin is the outermost barrier covering the whole surface of the body. This barrier is necessary to protect from a variety of external influences such as heat, radiation, mechanical stress, or invasion of harmful or contagious substances but also comprises regulation of the body temperature or prevention of extensive water loss [1–6]. These duties can be fulfilled through the sophisticated composition of the human skin into three layers: hypodermis, dermis and epidermis (Figure 1A). The innermost hypodermis mainly consists of fat tissue and is essential for thermal insulation, whereas the dermis as middle layer is forming a connective tissue which retains water, provides stability and includes sensory receptors, sweat glands, hair follicles, and blood vessels being crucial for oxygen and nutrient supply of epidermal cells[7]. Together with its associated appendages the epidermis is the outermost layer[8]. Due to its exposed location, the epidermis is most important in preventing the loss of fluid components of the body to the environment and in protecting the body from a variety of environmental influences. It provides physical, chemical, biochemical (antimicrobial, innate immunity), and adaptive immunologic barriers although the whole skin structure actively participates in the host defense[3]. Between the dermis and the outermost epidermis lies a highly specialized matrix structure, the basement membrane. This undulating basement membrane adheres the epidermis to the dermis[7]. On the other hand, it separates the two compartments physically providing a stabilizing as well as dynamic interface[9].

2.1.1 General architecture of the human skin

The vast majority (90 - 95 %) of the various cell types in the epidermis are keratinocytes undergoing a specific differentiation process resulting in the production of flattened anucleated cells (corneocytes). The cells are passing through different stages of differentiation while all of them having specific functional and structural features[10]. This complex and highly regulated process is a prerequisite for the continuous renewal of the epidermis and thus finally forming a protective barrier. Due to its exposed position within the human body, this barrier is constantly weakened by environmental influences or ruptured by mechanical stress. Thus, it has to be continuously renewed by succeeding keratinocytes. In humans, this highly elaborate process, balancing the reservoir of progenitor cells and

terminally differentiating keratinocytes, takes 28 days and is known as epidermal homeostasis[11].

Being the outermost layer of the human skin, the epidermis is the first and most effective barrier against external influences and is composed of four different strata which can be distinguished by the presence of keratinocytes in distinct differentiation states (Figure 1B)[12,13].

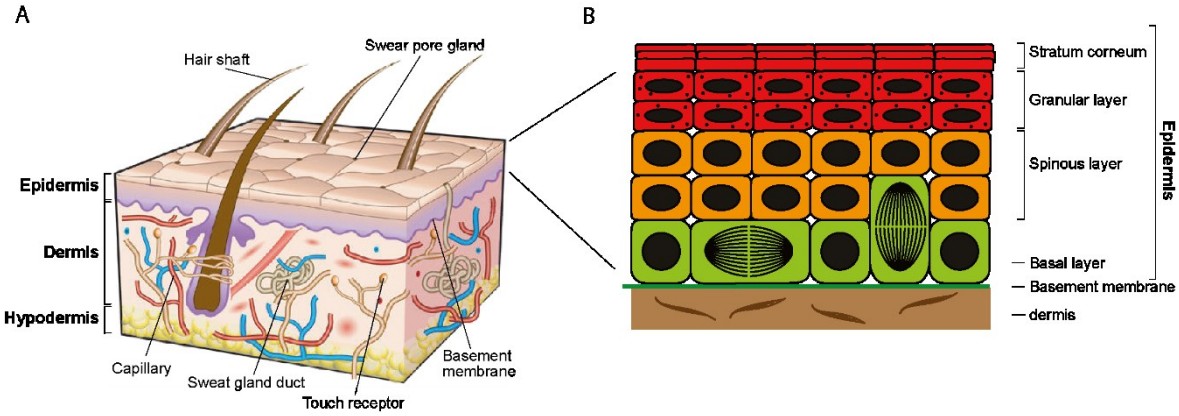

Figure 1: Cross section of human skin and schematic overview of epidermal layers
(A) Schematic overview of the human skin, showing the three layers, hypodermis, dermis, and epidermis as well as the therein included appendages (modified after MacNeil et al.[8]). (B) magnification of the epidermis, comprising the basal layer, spinous layer, granular layer, and the stratum corneum (modified after Solanas et al.[14]).

The process of epidermal homeostasis already begins in the stratum basale (basal layer) with undifferentiated keratinocytes which are mitotic active and therefore responsible for the continuous renewal of the epidermis. The basal layer is characterized by the expression of keratin 5 and keratin 14. In the classic model for epidermal regeneration, those keratinocytes are claimed to be stem cells which give rise to short-lived progenitors known as transit-amplifying cells (TA-cells) undergoing terminal differentiation after a few rounds of division[14–17]. Upon several rounds of cell division, these TA-cells would eventually lose their potential for division and would conduct a terminal differentiation program as the cells migrate to the apical site of the epidermis[18,19]. Studies, however, contradict this model and claim that one uniform population of committed progenitor keratinocytes undergoes symmetric and asymmetric cell divisions with a fixed probability[16,20]. Whereas the cells from the symmetric cell division maintain the pool of committed progenitor cells, the progeny from asymmetric cell division is committed to terminal differentiation[14,19]. More recently Lineage-tracing studies figured out that epidermal homeostasis is maintained by a population of cells termed progenitors generating progenitor and differentiating daughters with equal

probability, thus ensuring that homeostasis is achieved across the progenitor cell population[21]. During their maturation, cells synthesize and express different structural proteins and lipids[22].

The initial activation of this differentiation program is triggered by increasing calcium concentrations in combination with signals from cell-cell contacts and becomes first apparent in the suprabasal layers where the existing keratins 5 and 14 are replaced by newly synthesized keratin 1 and keratin 10 filaments. Keratin monomers bundle to intermediate filaments which comprise the predominant cytoskeletal component of the epidermis and gain resilience to mechanical stress [23]. They are attached to the cell membrane via desmosomes and form a rigid structure within the cytoplasm. During the transition from the granular layer to the stratum corneum, keratinocytes undergo drastic changes and even apoptosis to eventually form a protective skin barrier.

While migrating towards the skin surface, keratinocytes synthesize two types of granules: lamellar bodies and keratohyalin granules. Lamellar bodies containing mainly glycosphingolipids, free sterols, and phospholipids can be detected in granular cells, whereas electron-dense keratohyalin granules contain proteins involved in the aggregation of keratin filaments and in the formation of the cell envelope, such as profilaggrin and loricrin[17,22,24].

Many differentiation-associated proteins, such as involucrin, loricrin, and filaggrin, can be uniquely found in the epidermis and are expressed in the terminally differentiated layers of the epidermis[17,25–27]. Loricrin is expressed in the granular layer during differentiation and comprises 70-85 % of the total protein mass of the cornified layer at the end of differentiation[17]. Loricrin functions as a key structural cornified-envelope protein and undergoes different types of crosslinking[28]. Human profilaggrin is synthesized as a large highly phosphorylated precursor protein of around 500 kDa, containing 10 - 12 complete filaggrin repeats [23,29–31]. Elevating intracellular calcium levels trigger the release of profilaggrin from the keratohyalin granules which ultimately becomes dephosphorylated and cleaved into filaggrin monomers that are subsequently bundled with the present keratin into macrofibrils resulting in gradual flattening of the cells[26,32–35]. Concomitantly, transglutaminases introduce isopeptide bonds between these macrofibrils and other structural proteins like members of the S100 protein family, loricrin, late cornified envelope proteins (LCEs), small proline rich proteins (SPRRs), and involucrin forming a rigid protein shell termed “cornified envelope”[32,36–38]. Finally, the lamellar bodies fuse with the plasma membrane and secrete the enclosed lipids into the extracellular space generating a lipid

lamella which is crucial for maintaining the epidermal water barrier[37]. As a result of this process, the cornified envelopes of terminally differentiated keratinocytes are tightly connected via modified desmosomes and embedded in extracellular lipid lamellae, thus providing the indispensable barrier against external challenges and loss of essential body fluids[36,39].

2.1.2 Human epidermal differentiation complex

Mammalian genomes contain several large lineage-specific gene loci harboring functionally related and mostly co-regulated genes which frequently form conserved clusters or loci (> 0.5 Mb) in the mammalian genomes[40,41]. Spanning 1.9 Mb on the human chromosome 1 and encoding roughly sixty proteins essential for proper keratinocyte differentiation and epidermal barrier formation, the epidermal differentiation complex (EDC) is indispensable for epidermal homeostasis[42,43]. Interestingly, gene distribution within the EDC is not random but genes encoding for proteins with similar functional and structural properties are clustered accordingly into distinct genomic locations (Figure 2).

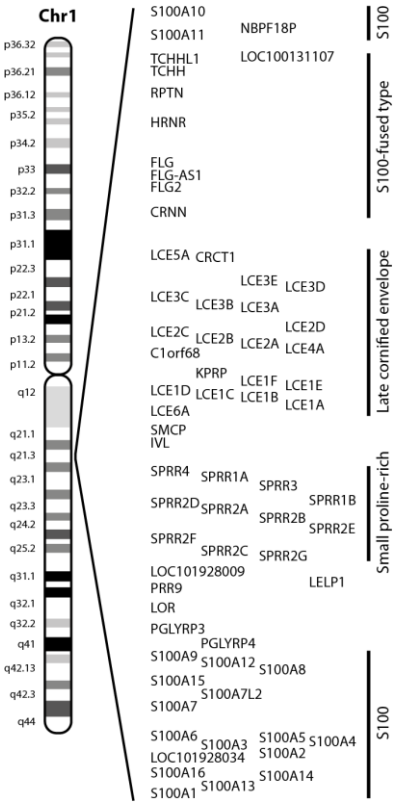

Figure 2: Overview of the human epidermal differentiation complex and its encoded genes
The human chromosome 1 is shown on the left and the respective cytogenetic bands are indicated. Furthermore, the area of the epidermal differentiation complex with its encoded genes (according to the RefSeq release 2016) is magnified and the main gene clusters are indicated on the right. Modified after Kypriotou et al. [43]

The EDC contains three clustered families of genes encoding: (a) the flanking calcium-binding proteins (S100 family), (b) the group of precursor proteins of the cornified envelope involucrin, loricrin, the SPRRs, and the LCE proteins[44,45] (c) the 'fused gene' proteins filaggrin, filaggrin-2, trichohyalin, trichohyalin-like protein, hornerin, repetin, and cornulin which evolved from families (a) and (b).

(a) The S100 familiy

The S100A family of 17 genes and 6 pseudogenes is located on human chromosome 1q21. These genes limit the EDC on both sides flanking the cornified envelope precursor and fused gene families [43,46]. Generally, S100 genes are composed of three exons, of which the second and third contain the open reading frame. S100 proteins are characterized by two EF-hands separated by a hinge region[47]. S100 proteins have diverse functions, but distinct members are associated with abnormal epidermal differentiation[45,48,49].

(b) The cornified envelope precursor family.

The EDC proteins IVL, SPRRs and LOR have similar structures with strong homologies in their glutamine and lysine-rich amino and carboxy-terminal domains. They are cross-linked by transglutaminases and have unique internal domains consisting of diverse glutamine-, proline- and serine-rich repeats, respectively[39,50,51]. The cornified envelope composition differs according to epithelium type and species[39,52,53]. This requires a tight differential regulation of the EDC genes to assure the unique identity of the particular cornified envelope. In combination with the interspersed genes for loricrin and involucrin, the LCE and SPRR cluster account for the majority of proteins present in the cornified envelope of terminally differentiated keratinocytes[43].

(c) The fused gene family

The S100 fused type protein family of the EDC evolved by fusion of ancestors of the two previously described families ((a) and (b)). They possess two amino-terminal Ca^{2+}-binding EF-hand motifs, most closely related to S100A8, a unique central repeat domain and a C-terminal domain specific for each protein. Similar to the S100A gene family, fused genes contain three exons, and the second and third exon encode the entire protein sequence. They are primarily expressed in stratified epithelia. Filaggrin, repetin, hornerin, and cornulin are major cytoplasmic matrix proteins associated with intermediate filament proteins and minor components of the cornified envelope[42,43].

2.1.3 Regulation of human epidermal homeostasis

Since generation of a functional epidermis is accompanied by radical changes in gene expression, multiple regulatory mechanisms are required to orchestrate these changes. Most important for keratinocyte differentiation are increasing levels of extra- and intracellular calcium concentrations. Several differentiation proteins are dependent on Ca^{2+}, but also numerous signalling pathways are regulated by calcium. These include the formation of desmosomes, adherens and tight junctions, or activation of various kinases and phospholipases, producing second messengers and regulate intracellular free calcium[54–57]. In addition to that, E-cadherin-catenin complex mediated cell-cell contacts as well as the activated form of vitamin D_3 are involved in the regulation of cell differentiation[58–61]. All these stimulate the hydrolysis of phosphatidylinositol bisphosphate (PIP_2) by increased activity of phospholipase C into the secondary messengers inositol trisphosphate (IP_3) and diacylglycerol (DAG)[56,62]. IP_3 then activates IP_3 receptor to release Ca^{2+} from intracellular stores[63]. DAG, on the other hand, together with the released Ca^{2+} activates protein-kinase C which triggers intracellular signaling pathways including the mitogen-activated protein kinase (MAPK) pathway[63,64]. The MAP kinases pathway comprises major signaling cascades with sequential phosphorylation and activation of kinases that ultimately results in the activation of transcription factors, and thus ultimately induces the expression of differentiation genes[65–68]. Apart from the described exemplary mechanism, several other signaling pathways, including Notch, TGF- β or IKK/NF-κB, are crucial for keratinocytes differentiation and eventually induce the expression of differentiation genes[66,69]. In the human epidermis, localized expression of the Notch-ligand Delta in keratinocyte stem cells has been proposed to induce development of neighboring Notch1-expressing keratinocytes to transit-amplifying cells through a negative feedback mechanism of lateral inhibition[70]. Notch/delta signalling therefore determines the boundaries of stem-cell clusters to differentiated keratinocytes[70,71]. Few other molecular markers have been identified as fundamental mediators of keratinocyte differentiation. They include members of the c-jun/c-fos family, GRHL3, Klf4, MAF:MAFB, OVOL1/2 or ZNF750, BMI1, CEBPs, MYC, and GATA-3 transcription factors (TFs), integrins, Wnt/β-catenin, HH, SGK3, p63, and some bone morphogenetic proteins [65,72–77]. In particular, p63 is considered a master regulator of morphogenesis, identity, and regenerative capacity of stratified epithelia by either direct induction of differentiation genes or regulation of several chromatin modifiers[78–81]. Loss of p63 in keratinocytes impacts basement membrane formation, cell adhesion as well as stratification[80–82]. One example for the regulation of chromatin modifiers is the recruitment

of the histone deacetylases 1 and 2 (HDAC1/2) in order to omit the expression of cell cycle arrest genes or alteration of the accessibility of epidermal enhancers in combination with the BAF chromatin remodeling complex[83,84].

Several other epigenetic mechanisms including chromatin remodeling or DNA methylation by DNMT1 or GADD45A/B have also been identified in keratinocytes[85,86]. Additionally, various histone modifications are discovered to play a role during epidermal differentiation. Thus, several differentiation-associated genes are known to be suppressed in progenitor cells by the repressive histone mark H3K27me3, established in a conjoined action of the methyltransferase subunits EZH1 and EZH2 of the polycomb repressive complex (PRC) and its counterpart the demethylases JMJD3 and UTX[85,87–89].Similar reports revealed differences for deposition of various histone modification such as H3K4me1, H3K27ac, H4K20me1, or H3K9ac between progenitor and differentiated keratinocytes [84,90–92].

An additional layer of epigenetic regulation originates from large scale nuclear remodeling during which distinctive differences in nuclear architecture and micro-environment occur. These include a decrease in nuclear volume, relocation of the epidermal differentiation complex to the nuclear periphery, and its association with active nucleoli for induction of gene expression[93]. In addition to direct regulation of tissue-specific genes, p63 and several other transcription factors promote formation of distinct higher order chromatin structures in tissue-specific gene loci[94].

In conclusion, a conjoined effort of a plethora of intracellular signaling pathways, transcription factors as well as epigenetic mechanisms is mandatory to orchestrate the profound changes in the gene expression pattern during epidermal homeostasis.

2.1.4 Defective epidermal homeostasis results in skin cancer progression

Given the complex composition and the highly elaborate regulatory networks involved in epidermal homeostasis, accumulation of disrupted expression of genes controlling proliferation and differentiation lead to cancer development. Further understanding of the processes that drives progression from normal epithelium to invasive cancer might provide new targets for the prevention and treatment of skin cancer and other disorders of epidermal growth, differentiation, and regeneration. The three major forms of skin cancer occur in the epidermis and arise either from keratinocytes as the basal cell carcinoma (BCC) and the cutaneous squamous cell carcinoma (cSCC) or from pigment producing melanocytes in the case of melanoma[96–98]. The primary cause for keratinocyte carcinomas is chronic exposure

to ultraviolet radiation. But common risk factors also include alcohol consumption, fair skin pigmentation, chronic cutaneous infection, human papillomavirus infection, and immune suppression[96–101].

Whereas keratinocyte carcinomas BCC and cSCC are the most common forms of skin cancer with increasing incidence globally, melanomas account for a higher number of deaths and in general correlates with poor prognosis [98,100]. However, if recognized and treated prior to metastasis, melanoma is almost always curable by surgical excision[96,102,103]. While BCC is the most common human malignancy, cSCC accounts for the majority of deaths among keratinocyte carcinomas[104,105]. In contrast to BCC, which rarely metastasizes, the existing risk of metastasis for cSCC is a deadly threat owing to its ability to metastasize to any organ in the human body if not recognized and excised immediately[105]. Both BCC and cSCC harbor a substantial mutational burden mainly due to cumulative UV exposure typically observed as C → T transitions in the DNA [106–109]. Several studies using BCC and cSCC murine models suggest that these cancers arise from multiple cellular origins, *e.g.* from different stem cell populations in the basal layer of the epidermis, hair follicle bulge, or sebaceous gland[110]. Additionally, like many other cancers, cSCCs and BCCs are often associated with epigenetic deregulation and aberrant DNA methylation which also contribute to cancer progression[111,112].

Basal cell carcinoma

As the name already indicates, BCC arises from nonkeratinizing progenitor keratinocytes located in the basal layer of the epidermis and is characterized by slow growing and rarely metastasizing cells. Nevertheless, BCC patients frequently suffer from major tissue damage resulting in serious mutilating deformations and loss of vital structures[96,97,113]. From a mechanistic point of view, BCCs are often strongly associated with aberrant activation of the Hedgehog signaling pathway due to loss of the patched 1 tumor suppressor gene (PTCH1) and activation of the G protein-coupled receptor smoothened (SMO)[114]. But also other activating mutations in the sonic hedgehog signaling pathway have been reported[115,116]. Interestingly, activation of the platelet-derived growth factor receptor α (PDGFRα), which has been shown to be upregulated in BCC, activates the Ras/MAPK pathway and is at least one important mechanism by which hedgehog signaling mediates tumor formation[117].

Cutaneous squamous cell carcinoma (cSCC)

Despite a high frequency of UV-induced mutations, BCCs and cSCCs do not harbor many common genetic alterations. As cSCC is not a uniform disease but rather a heterogenous group of tumors, inactivation of tumor suppressor p53 or NOTCH1 and constitutive activation of the Ras/Raf pathway can be commonly detected[106–109]. Though being only the second most common form of skin cancer in the USA, at the same time it shows the highest metastatic potential and the highest mortality after formation of aggressive metastasis[96,118,119]. UV-radiation-mediated mutagenesis is thought to be the major environmental factor promoting this type of cancer[96]. Thus, it is not surprising that UV-induced p53 loss of function mutations is the key event in cutaneous SCC carcinogenesis[119]. Other important mutations occur in the CDKN2A locus generating insufficient or non-functional p16 as an inhibitor of cyclin-dependent kinase 4 (Cdk4). This finally leads to an unleashed cell cycle control which is mediated through loss of inhibition of Cdk4 activity[120–122]. Additionally, elevated Cdk4 expression is often associated with SCC development[123]. In combination with oncogenic forms of Ras proteins, increased expression of Cdk4 is sufficient to induce invasive human neoplasia resembling squamous cell carcinoma [96,124]. Surprisingly, however, expression of oncogenic Ras proteins alone drives keratinocytes into senescence. Only the combination of oncogenic Ras and an unleashed cell cycle, for example by overexpression of Cdk4 or blocking the NF-κB signaling pathway, results in SCC generation[125–127]. Consistent with this, release of the cell cycle control by a blockade in the NF-κB signaling pathway and simultaneous expression of oncogenic Ras can also transform human epidermis into a highly aggressive invasive neoplasia which presents itself indistinguishable from SCC[125,128]. In contrast to its fundamental role in SCC development, it is astonishing that amplification of Ras genes or activating mutations have only been reported for the minority of SCC samples[129–131]. But presumably, activation occurs through a number of upstream factors[129–131]. Apart from the above described proteins, several other markers have been reported to distinguish SCC from normal skin[100,108,132] Histologically and biochemically, the keratinocyte derived SCC cells can be distinguished from healthy keratinocytes by their altered proliferative capacity as well as their reduced expression of keratinocyte differentiation proteins. In fact, suppression of gene expression for several key differentiation genes is a hallmark of SCC development and was frequently reported over the past years[133–135].

In keratinocyte carcinomas, particularly in cSCCs, several members of the novel class of long non-coding RNAs (lncRNAs) are differentially expressed as compared to normal skin or keratinocytes, suggesting a role for them in cSCC progression but also normal tissue development (covered in chapter 2.2.4)[136–141].

2.2 Long non-coding RNAs

2.2.1 Identification and classification of long non-coding RNAs

For years, one central dogma has been irreversible for molecular biologists[142,143]:

- *DNA is transcribed into RNA which is eventually translated into a functional protein.* -

The first step of this central dogma is the synthesis of RNA from DNA known as transcription. The second step involves a change of code from nucleotide sequences to amino acid sequences and is called translation. Proteins are very important molecules being essential for all living organisms. By dry weight, proteins are the largest unit of cells. Proteins are involved in almost all cell functions, and a different type of protein is devoted to each role with tasks ranging from general cellular support to cell signaling and locomotion. On the other hand, RNA was long time only contemplated as the inevitable intermediary required for protein production. However, this picture changed as genome sequencing projects revealed that complex organisms have lower numbers of protein coding genes than anticipated. Although two thirds of our genome are actively transcribed, only less than 2 % of the transcribed genes are actually encoding for proteins[144–146]. Several classes of non-coding RNAs (ncRNAs) control basic cellular functions, such as translation (transfer RNAs, ribosomal RNAs), RNA editing (small nucleolar RNAs), or splicing (small nuclear RNAs). These classes of ncRNA have been known for a long time and are essential for the normal function of the cell. More recently, short regulatory ncRNAs (20-30 nt in length) including microRNAs, endogenous short-interfering RNAs (siRNAs), or piwi-associated RNAs (piRNAs), acting as crucial regulators of gene expression were identified[147–150]. A further group of regulatory RNAs, the long non-coding RNAs (lncRNAs), has gained widespread attention since the last decades. Research in this field is still at the beginning to understand the significant roles of lncRNAs for a multitude of cellular processes as well as for tissue homeostasis. However, most lncRNAs lack strong sequence conservation prompting suggestions that they might not be functional [151–155].

Per definition, lncRNAs are over 200 nucleotides in length and can be localized in the nucleus or the cytoplasm of the cell. Additionally, lncRNAs can be spliced, capped, and/or polyadenylated which makes them structurally resembling mRNAs [136,156–160]. In general, lncRNAs lack a protein-coding potential but often form a complex secondary structure of hairpins and loops resulting from the partial complementary basepairing of the nucleotides[161,162]. However, the strict classification of a lacking protein-coding potential was questioned by recent reports about lncRNAs associating with ribosomes and translation of small functional peptides from lncRNA templates [163–166]. Though some lncRNAs are extremely stable, some are rapidly degraded after transcription[167,168]. A rapid turnover of lncRNAs enables a dynamic cellular response via specifically induced lncRNAs, for instance in DNA damage, immune response, and cellular differentiation [169–171].

There are various classes of lnRNAs, often differing in the region or their orientation within genes. Scattered all over the genome, long intergenic non-coding RNAs are transcribed from distinct loci, often from their own promoters, whereas intronic lncRNAs are transcribed from intronic regions within protein-coding gene[155,172,173]. Depending on the overlap and the orientation to the host gene, this rather general classification can be further refined into several more defined subclasses[174,175]. Bidirectional lncRNAs are produced divergently from the same promoter of a protein-coding gene. Circular RNAs (circRNA) are a recently discovered group of lncRNAs structurally different from most lncRNAs. They are produced by back splicing of precursor mRNAs or lncRNAs resulting in covalently closed circular RNAs without polyadenylation[176]. Apart from being included into other transcriptional units, lncRNAs themselves can host protein-coding genes or other ncRNAs like circRNAs, tRNAs, miRNAs, and especially snoRNAs[160,177–181].

This high degree of complexity in lncRNA loci is even further increased by the presence of different isoforms per gene locus, resulting from a combination of alternative splicing, alternative polyadenylation, and employing alternative transcription start sites which highlights the requirement for a careful lncRNA locus characterization[153,179,182].

Interestingly, many lncRNAs are cell-type specific expressed during cell differentiation and tissue development, whereas inappropriate and aberrant expression of lncRNAs in various pathological conditions is becoming evident suggesting a central role of lncRNAs during different cellular processes [183]. And indeed, lncRNAs have been proven essential regulators for fundamental processes such as cellular differentiation, epigenetic imprinting, cell cycle control, apoptosis, X-chromosome inactivation, promoter-specific gene regulation, and

nuclear import[137,157,184–190]. Furthermore, aberrant lncRNA signatures are a hallmark of several severe diseases including numerous types of cancer which impressively highlights their tremendous significance on almost every aspect of the life cycle[136,191].

2.2.2 Molecular mechanisms of lncRNA function

Although we are aware of several thousand different lncRNAs in humans today with new lncRNAs being identified on a regular basis, only a small number of lncRNAs has been mechanistically characterized in detail[179]. In general, the regulatory role of lncRNAs is based on binding to specific effector molecules by sequence complementarity or structural recognition to mediate gene expression. But additionally, the single-stranded structure of lncRNAs and the folding into unique secondary and tertiary structures gives them the ability to bind to RNA, DNA, or proteins and this way controls diverse cellular functions [192–194] (Figure 3). LncRNAs typically exhibit a strict cell and tissue-specific expression and subcellular localization, thus indicating a strongly controlled regulatory role for distinct lncRNAs [179,195]. Specific localization of distinct lncRNAs to cytoplasm, nucleus, or other cellular compartments is likely to reflect their function (Figure 3). In addition, some lncRNAs are secreted in extracellular vesicles and exosomes and can exert their effect in adjacent cells and in cells in other tissues [196,197]. In general, lncRNA mechanism of action can be divided into four main types: signals, guides, decoys, and scaffolds[192]. By employing solely one of the above mentioned archetypes or a combination of those, lncRNAs are able to fulfill their multifaceted functions which are mostly reasoned by a regulatory function on gene expression at the transcriptional and the posttranscriptional level. Furthermore, another classification scheme subdivided them into nuclear lncRNAs mediating gene transcription, or cytoplasmic lncRNAs controlling post-transcriptional events and mRNA stability[198,199]. Depending on the localization of the lncRNA gene in respect to the position of transcriptional control, *cis*- (lncRNA regulates gene expression in the vicinity of its own locus) or *trans-acting* (spatial separation of lncRNA expression and transcriptional control) lncRNAs can be distinguished[192,200].

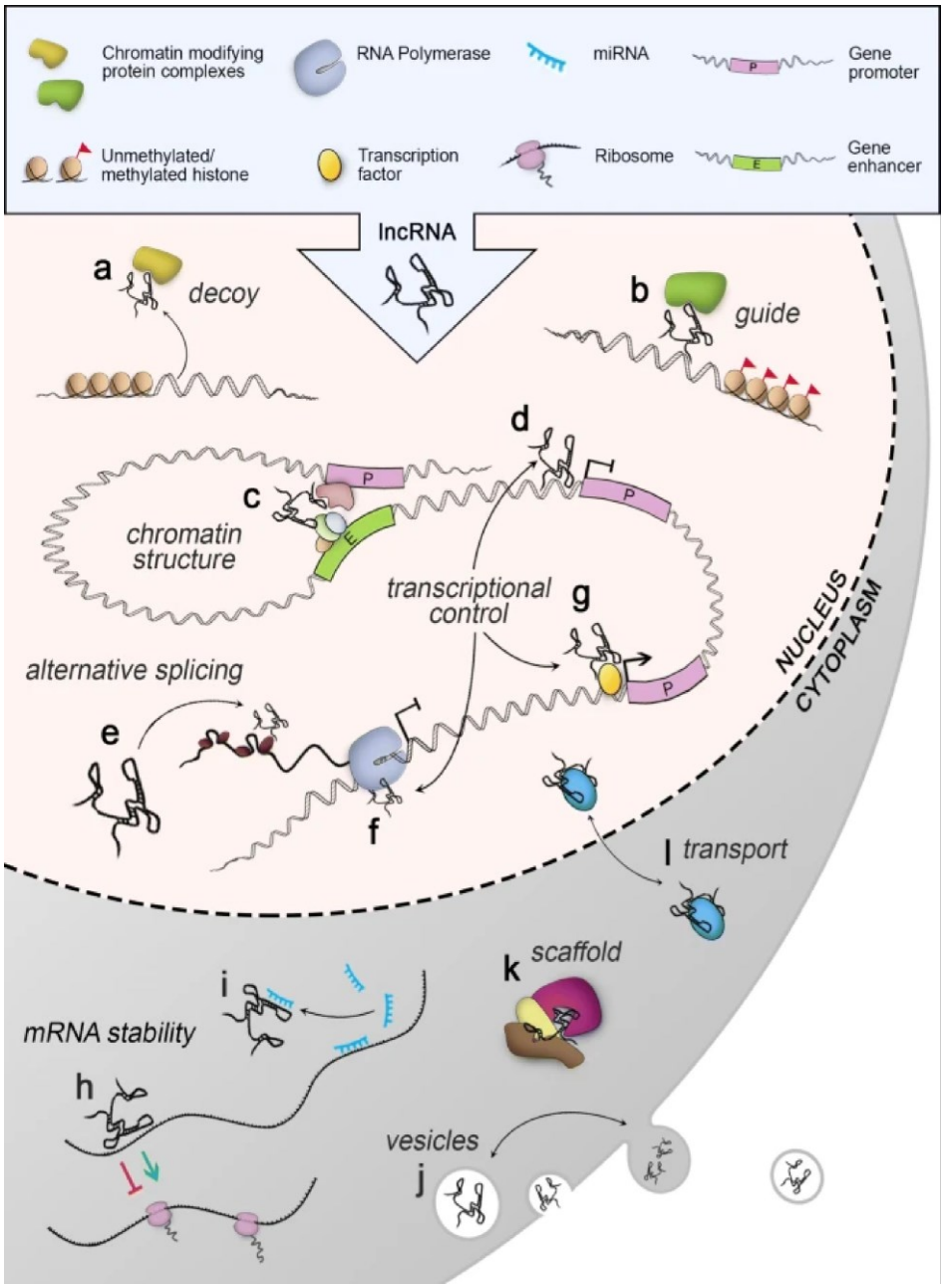

Figure 3: High diversity of regulatory functions of lncRNA in the nucleus and the cytoplasm [201]
Nuclear lncRNAs can act as a (a) decoy or (b) guide for chromatin-modifying complexes. (c) lncRNAs can alter or (d and f) block the chromatin accessibility (e) lncRNAs can regulate alternative splicing (g) lncRNAs can activate factors necessary for transcription.
Cytoplamic lncRNAs can (h) regulate mRNA stability by binding to mRNAs (i) sequester miRNAs (j) be secreted to extracellular vesicles (k) serve as scaffolds for ribonucleoprotein complex assembly (l) impact the intracellular transport of proteins.

One of the best studied examples for transcriptional gene regulation in *cis* is the lncRNA X-inactive-specific transcript (XIST) which is crucial for mammalian dosage compensation. XIST is exclusively expressed from one of the two X-chromosomes in females and coats the future inactive X chromosome during early development and thus represses its

transcription[202]. This occurs with the aid of several protein binding events that take place along the length of the transcript. These have been well investigated and trigger a series of events that lead to conformational reorganization, chromatin modifications, and ultimately transcriptional silencing of this X-chromosome[203–206]. Studies also identified many other proteins binding directly to Xist including SHARP and others[205,207]. In contrast to this, dosage compensation in flies is achieved by transcriptional activation of the single X-chromosome in males. During this process, the functionally redundant lncRNAs roX1 and roX2 target the male-specific lethal complex to the X-chromosome where hypertranscription is achieved by increasing H4K16 acetylation[208,209].

Another well-characterized lncRNA is the 2.2 kb HOX transcript antisense RNA (HOTAIR) which was first identified to be associated with Sporadic Thoracic Aortic Aneurysm through regulation of extracellular matrix deposition and apoptosis of human aortic smooth muscle cells [210]. HOTAIR is expressed from the HOXC locus but represses transcription of the distant HOXD locus. This repression is mediated through its 5´end interacting with chromatin remodeling complexes such as polycomb repressive complex 2 (PRC2) or the LSD1/ REST/ CoREST complex and leads to silencing of genes on the HoxD cluster via H3K27 trimethylation and H3K4 demethylation [157,185].

Besides, the above-mentioned histone and chromatin modifications, lncRNAs were also found to directly control Pol II activity, to influence the cellular localization of transcription factors or to act as transcriptional co-regulators[173,211–213]. Moreover, lncRNAs are also able to control gene expression on a post-transcriptional level by regulating RNA splicing, RNA editing, mRNA stability, mRNA translation efficiency as well as miRNA-mediated mRNA destabilization[173,214]. *MALAT1,* for example, has been shown to be associated with relocation of splicing factors to nuclear speckles and thus may have a role in controlling alternative splicing of certain mRNAS[215]. Other lncRNAs function as competitive endogenous RNAs by occupying similar binding sequences of miRNAs, and thus sequestering the miRNAs and changing the expression of their downstream target genes[216,217].

2.2.3 LncRNAs control tissue homeostasis and organ development

Given the largely cell-type and also differentiation state specific expression pattern of lncRNAs, it is not surprising that lncRNAs are crucial regulators of organ and tissue development and homeostasis[136,218]. Linc-MD1, for example, activates muscle-specific gene expression in human and murine myoblasts via sponging miR-133 and miR-135[217]. Skeletal

muscle differentiation and regeneration are also promoted by the lncRNAs H19, SENCR, MUNC, or lnc-mg[219–222]. One of the first discovered examples for the homeostasis of the heart was *Braveheart* which activates a core cardiovascular gene network through interaction with the Zinc-finger motif-containing transcription factor CNB and possibly mediates epigenetic regulation of cardiac commitment by interacting with components of the PRC2 complex[223]. Additionally, proper murine heart development is ensured by the recruitment of the histone modifying complexes PRC2 and TrxG/MLL through the lncRNAs Fendrr and Carmen[224,225].

Moreover, several lncRNAs are exclusively expressed in the brain and the nervous system to ensure proper brain development, synapse formation and function, stress responses, and age-associated changes. Evf2, for example, recruits transcription factors in *cis* and *trans* during murine ventral forebrain development while Pinky regulates neurogenesis in the embryonic and postnatal brain in combination with the splicing factor PTBP1[187,226].

Apart from indispensable roles during muscle, heart and brain development, lncRNAs are also well-established regulators in various organs, including bones, lung, liver, fat as well as intestinal tissue, and even the homeostasis of the largest human organ - the skin - is tightly controlled by several lncRNAs[73,218].

2.2.4 Roles of lncRNAs in epidermal tissue homeostasis and skin diseases

In epidermal homeostasis, there is a strict regulation of maintaining the undifferentiated state and proliferation on one hand as well as the initiation of the differentiation program leading to cell death on the other hand. Two lncRNAs were found to be involved in this process: the 858 bp long ANCR (anti-differentiation non-coding RNA) as a maintainer of proliferation and the 3.7 kb long TINCR (Terminal differentiation induced non-coding RNA) which is required for epidermal differentiation [137,227]. Highly induced during terminal differentiation, TINCR was one of the first discovered lncRNAs featuring a crucial function for maintenance of epidermal homeostasis. Depletion of TINCR leads to reduced expression of differentiation markers at both mRNA and protein levels, whereas the epidermis stratified normally. Gene expression of these regulated genes is controlled via a post-transcriptional mechanism, where TINCR forms short double stranded RNA duplexes with several differentiation protein mRNAs. This interaction is mediated by short 25 nt TINCR - box motifs that are repeated in TINCR itself and as well strongly enriched in interacting mRNAs. Specific interactions become subsequently bound by the protein Staufen1, ultimately

resulting in mRNA stabilization and therefore sustained expression of differentiation genes[137].

Whereas TINCR is essential for keratinocyte differentiation, the anti-differentiation ncRNA (ANCR) has an opposing effect on keratinocyte differentiation. ANCR was shown to be significantly down-regulated upon differentiation and appeared to contribute to the maintenance of a non-differentiated state in progenitor keratinocytes (Figure 4). Although the exact mechanism has not been established so far, loss of ANCR in undifferentiated keratinocytes induced ectopic expression of differentiation markers, ultimately proving that ANCR is essential for maintaining the undifferentiated cell state within the epidermis[227]. Recent studies suggest that ANCR suppresses the transcription factors MAF/MAFB expression in association with the PRC2 component EZH2[73]. Interestingly, TINCR is also involved in controlling MAF/MAFB mRNA stability, and thus both TINCR and ANCR exert their regulatory function in epidermal homeostasis at least partially via the same pathway[73].

Progenitor renewal associated non-coding RNA (PRANCR) is one of the most recently characterized lncRNAs involved in epidermal homeostasis [228]. Depletion of PRANCR leads to reduced proliferative capacity and differentiation of keratinocytes. PRANCR regulates the expression of several genes coding for cell cycle regulators including E2F transcription factor target genes [228]. In addition, SCC misregulated transcript-2 (SMRT-2) is a recently identified lncRNA induced during differentiation of epidermal keratinocytes[138]. Depletion of SMRT-2 results in repression of several genes associated with epidermal differentiation and development[138]. SMRT-2 was hypothesized to function upstream of zinc finger protein 750 (ZNF750) and Kruppel like factor 4 (KLF4)[138]. ZNF750 functions downstream of p63 in driving epidermal differentiation by upregulating KLF4 [229]. Moreover, ZNF750 upregulates expression of lncRNA TINCR [230]. Taken together, these observations provide a regulatory link between SMRT-2, ZNF750 and TINCR for epidermal keratinocyte differentiation (Figure 4).

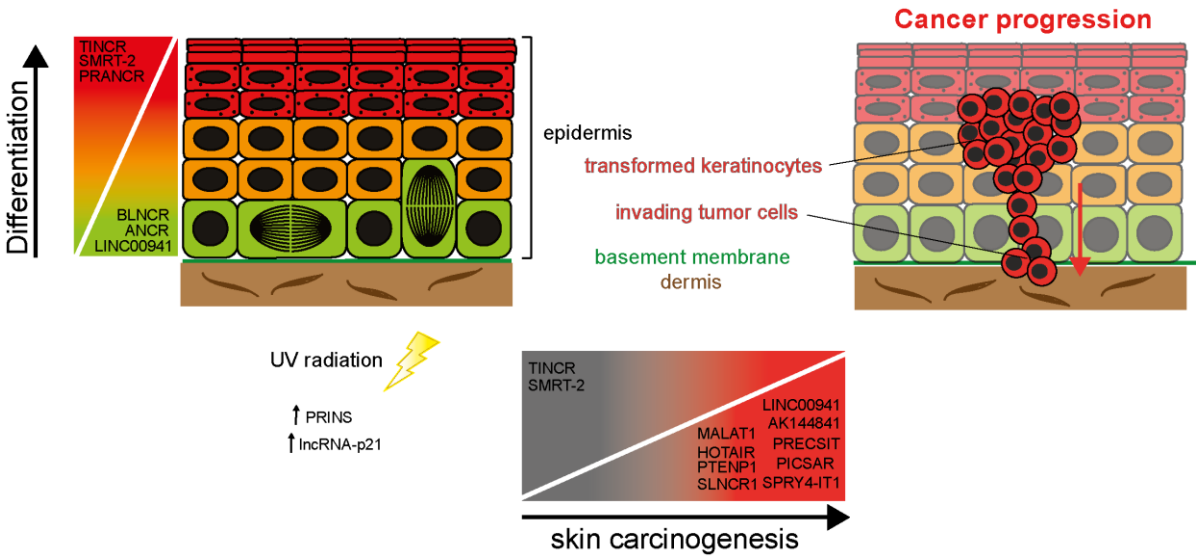

Figure 4: Overview of lncRNAs implicated in epidermal homeostasis in normal skin and in cutaneous SCC progression.
Solar ultraviolet radiation (UVR) induces a stress response and altered expression of specific lncRNAs such as PRINS and lincRNA-p21 in normal keratinocytes. Cumulative exposure to UVR predisposes epidermal keratinocytes to DNA damage and malignant transformation which eventually leads to development of invasive cSCC. Several lncRNAs have been shown to be involved in cutaneous homeostasis.

However, not only proper keratinocyte differentiation is maintained by lncRNAs but also generation and progression of several skin diseases and cancer types are accompanied by aberrant lncRNA expression. As aberrant keratinocyte differentiation and stem-cell characteristics are involved in KC tumor development[231,232], it is not surprising that the expression of keratinocyte differentiation inducing lncRNAs, SMRT-2, and TINCR is strongly downregulated in cSCC[137,138,233].

Poor differentiation of cSCC is associated with risk for metastasis and poor prognosis [231,232]. TINCR and SMRT-2 both promote differentiation of keratinocytes and may this way serve in a protective role in keratinocyte carcinogenesis [137,138]. Accordingly, decreased expression of TINCR and SMRT-2 has been detected in human cSCCs[137,138] and a notable decrease in TINCR expression has been reported in murine cSCC tumors compared to normal skin[233]. In addition, marked suppression of SMRT-2 expression has been noted in Ras-driven human organotypic epidermal neoplasia[138]. Taken together, these two TINCR and SMRT-2 may function as potential tumor suppressors in cSCC. In this context, it is interesting that ZNF750, which upregulates the expression of TINCR in keratinocytes, was recently shown to exert a tumor-suppressive role in SCCs of head and neck, lung, cervix, and skin[230].

The expression of beta1-adjacent long non-coding RNA (BLNCR) is also downregulated during keratinocyte differentiation, preceding downregulation of ITGB1, which codes for integrin β1, an epidermal stem cell marker adjacent to BLNCR gene [234,235]. BLNCR and ITGB1 are both transcriptionally regulated by transcription factors p63 and AP-1. Loss of BLNCR and ITGB1 expression may be an early event resulting in loss of proliferative capacity of keratinocytes and in subsequent terminal differentiation[234].

P38-inhibited cutaneous squamous cell carcinoma-associated lincRNA (PICSAR) represents the earliest evidence of a functionally characterized lncRNA in cSCC [139]. The expression of PICSAR is upregulated in cSCC tumor cells in culture and in vivo compared to normal human epidermal keratinocytes[139]. Elevated expression of PICSAR was noted *in vivo* cSCC suggesting a role for PICSAR at the early stage of epidermal carcinogenesis[139]. Silencing of PICSAR expression potently suppresses growth of human cSCC xenografts[139]. Interestingly, PICSAR serves as a regulatory link between p38 and MAPK pathways[139]. In addition, this lncRNA potently regulates cell adhesion and migration by regulating integrin expression and may this way contribute to cSCC progression and invasion[236].

P53-regulated carcinoma-associated STAT3-activating long intergenic non-protein coding transcript (PRECSIT) is a recently identified lncRNA with elevated expression in cSCC [237]. This nuclear-enriched lncRNA is downregulated by p53 signaling in cSCC tumor cells *in vivo*[237]. Furthermore, loss of PRECSIT inhibits cSCC cell invasion by repressing STAT3 expression and activation. Additionally, production of matrix metalloproteinases (MMPs) is downregulated suggesting a tumor-promoting function for PRECSIT[237].

Distinctive expression of the lncRNA AK144841 has been observed in a murine model very similar to human cSCCs[238,239]. Sustained activation of HRAS, which is caused by highly carcinogenic DMBA, results in induction of EGFR and its ligands in this cSCC mouse model [240,241]. A potential human ortholog with homology to AK144841 has been shown to be expressed at high level in cSCC cell lines compared to normal keratinocytes suggesting a potential role in human cSCC progression [238].

Besides, a subset of UV-induced lncRNAs has been functionally characterized[242–245]. In keratinocytes, the expression of lincRNA-p21 is markedly induced by UVB through a p53-dependent mechanism and it exerts a tumor suppressive role by triggering UVB-induced apoptosis and cell cycle arrest [245]. Accordingly, a tumor suppressive function for lincRNA-

p21 has been reported in head and neck SCC[246]. The primate-specific lncRNA PRINS (psoriasis susceptibility-related RNA gene induced by stress) for example affects psoriasis susceptibility as well as the innate immune response of the skin and generally functions in the keratinocyte stress response[244,247].

Also in melanoma, the most dangerous form of skin cancer originating from melanocytes, several lncRNAs like SPRY4-IT1, MALAT1, HOTAIR, PTENP1, or SLNCR1 feature an aberrant expression pattern indicating a lncRNA involvement in melanoma progression[102,248,249]. Another well-known example for a melanoma lncRNA is the 693 bp BRAF-regulated lncRNA (BANCR) which controls cell motility and survival of melanoma cells and hence directly correlates with their metastatic potential[250,251]. Further studies addressing the mechanistic details of BANCR-mediated melanoma progression were able to unravel that BANCR controls and suppresses the MAPK pathway activity and leads to upregulation of Notch2 via sponging of miR-204[252–254].

In summary, lncRNAs have been proven to be crucial regulators of epidermal homeostasis and their aberrant expression is tightly linked to several skin diseases including multiple forms of skin cancer. Thus, lncRNAs are not only valuable markers for skin diseases or keratinocyte differentiation but expand knowledge about the underlying modes of action. This might offer new approaches for the development of therapeutics for skin diseases.

2.3 Detection of LINC00941 and preliminary results

Initially identified from full transcriptome sequencing of differentiated versus undifferentiated keratinocytes, LINC00941 was discovered as a novel long non-coding RNA. This lncRNA was drastically repressed during keratinocyte differentiation and induced in SCC samples as compared to site-matched tissue control samples from the same donors (Figure 5)[137,138,227].

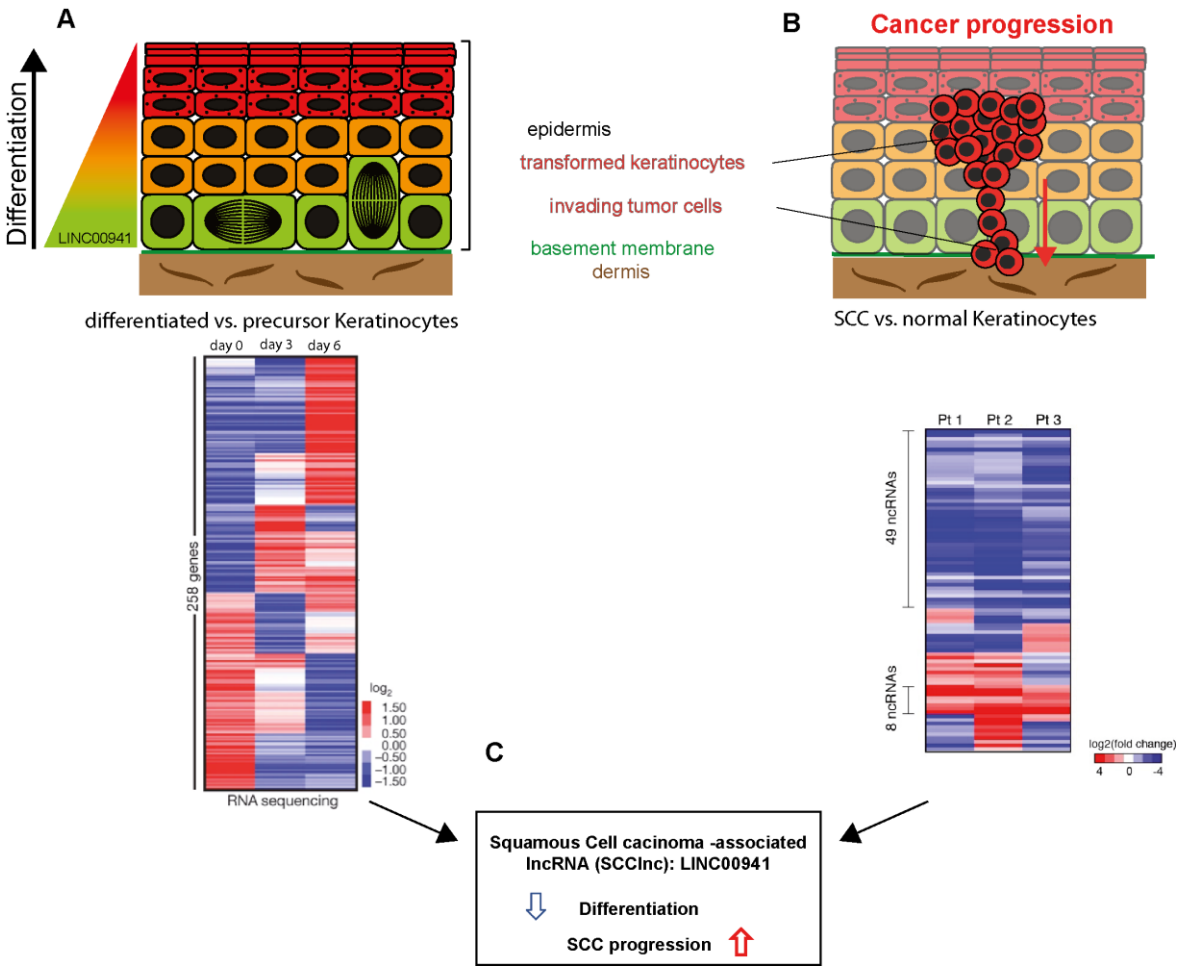

Figure 5: Screening of keratinocytes for lncRNAs (adapted after Kretz et al. and Lee et al. [227,255])
(A) Screening for differentially expressed lncRNAs during epidermal differentiation (B) Screening for lncRNAs altered in cutaneous squamous cell carcinoma compared to site-matched controls. (C) LINC00941 as one candidate, which is downregulated during epidermal differentiation and induced during cancer progression.

Preliminary knockdown studies revealed a potential role of LINC00941 as a suppressor of the terminal differentiation in progenitor and weakly differentiated keratinocytes. Upon knockdown of LINC00941, several differentiation genes within the epidermal differentiation complex, where many essential differentiation genes are clustered, showed enhanced expression. Interestingly, LINC00941 is also increased in SCC samples compared to healthy tissue control. At the same time, lack of differentiation is a hallmark of SCC cells.

Taken together, this might be a hint that LINC00941 commonly and conversely controls both epidermal homeostasis as well as SCC progression.

3 Objective

Several long non-coding RNAs (lncRNAs) act as regulators of cellular homeostasis; however, few of these molecules were functionally characterized in a mature human tissue environment. This work aimed to characterize the novel lncRNA LINC00941 in epidermal homeostasis. Given the proposed function of LINC00941 during regular keratinocyte differentiation and its dysregulation in human squamous cell carcinoma, the aim of this PhD project was to shed more light on the exact role of LINC00941 throughout those processes. To this end, first the previously uncharacterized lncRNA gene locus was characterized in more detail. For this purpose, potential LINC00941 isoforms as well as their expression pattern during keratinocyte differentiation were analyzed.

Furthermore, the role of LINC00941 on epidermal homeostasis was investigated in *in vitro* differentiation as well as in mature tissue environment. Full transcriptome analysis in LINC00941 depleted organotypic tissue was performed and revealed a potential epigenetic mechanism which was investigated further on chromatin as well as on protein level.

Finally, insights from these studies were used to postulate and test a hypothesized molecular mechanism of LINC00941 during the course of keratinocyte differentiation and SCC progression.

4 Results

4.1 Characterization of LINC00941

4.1.1 LINC00941 expression

To identify previously unrecognized lncRNAs involved in human epidermal homeostasis, transcriptome sequencing analyses of non-differentiated and differentiated human keratinocytes were conducted recently. This revealed a number of lncRNAs that are dynamically regulated throughout this process. One of these lncRNAs, LINC00941, which is encoded on chromosome 12, was found to be most highly expressed in undifferentiated progenitor keratinocytes (on average approximately 59 ± 14 copies per cell) and significantly reduced in abundance upon onset of terminal differentiation. Correspondingly, qRT-PCR analysis confirmed reduction of LINC00941 expression throughout all time points of calcium-induced differentiation of human keratinocyte cultures as well as of differentiation in organotypic epidermis (Figure 6A-B). Since LINC00941 abundance decreases upon keratinocyte differentiation, a role for this lncRNA in non- or poorly differentiated strata of the epidermis was postulated.

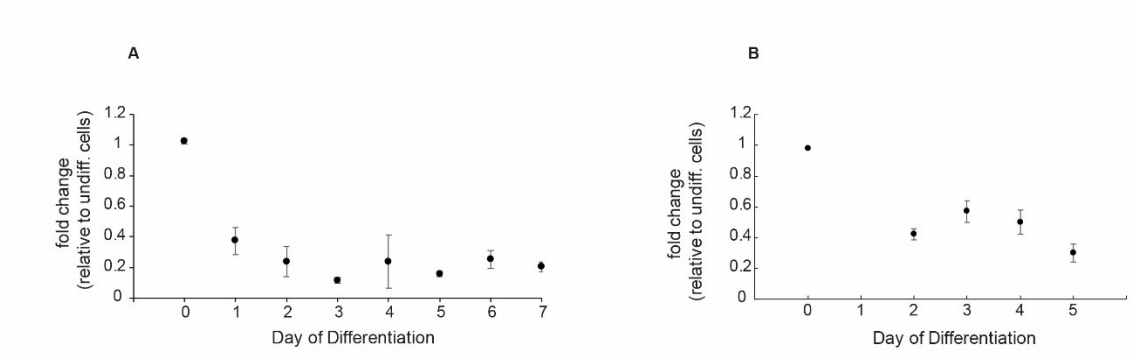

Figure 6: Expression of LINC00941 in keratinocytes
(A) expression of LINC00941 in Ca^{2+} induced keratinocytes during differentiation. (B) LINC00941 expression in organotypic epidermis

While LINC00941 was recently reported to play a role in development of hepatocellular carcinoma, nothing was known about its role in regulation of epidermal tissue homeostasis[256]. Additionally, LINC00941 is expressed in multiple human tissues, suggesting a ubiquitously role in many cell types (Figure 7).

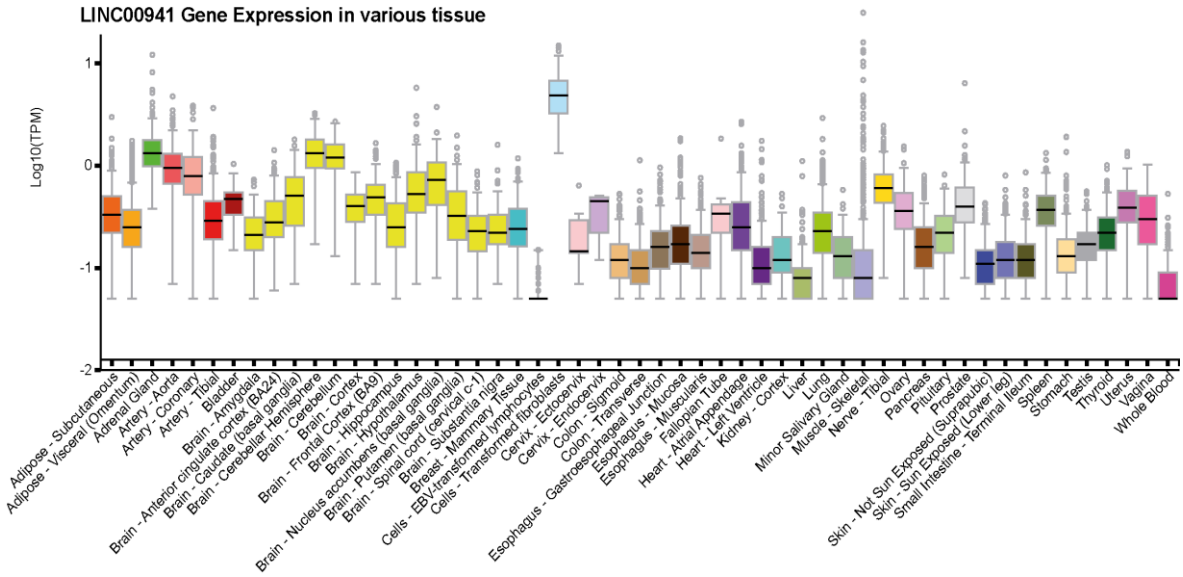

Figure 7: LINC00941 expression in different tissue types (data obtained from the GTex portal)

4.1.2 Subcellular localization

To give first insights into its possible function, unravelling the subcellular localization of a given lncRNA is a first approach. Hence, a subcellular fractionation approach followed by RT-qPCR analysis was chosen to reveal the localization of LICN00941 in undifferentiated keratinocytes (Figure 8).

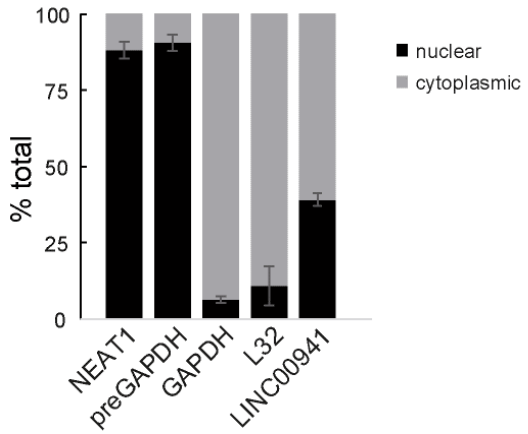

Figure 8: Subcellular localization of LINC00941
Analysis of nuclear and cytoplasmic RNA fractions of undifferentiated keratinocytes by RT-qPCR. The localization of cytoplasmic markers (GAPDH and RPL32), nuclear markers (NEAT1 and preGAPDH) as well as LINC00941 was assessed and the enrichment in each fraction was calculated.

Given the facts that almost all subcellular fractionation approaches are not able to completely separate the cytosolic and nuclear fraction, no perfect separation into a nuclear and cytosolic fraction was anticipated in this experiment. Contrary, here enrichment of the assessed marker

transcripts clearly indicates a decent separation of cytoplasmic and nuclear fraction since the cytosolic markers GAPDH as well as RPL32 are clearly enriched in the cytosolic over the nuclear fraction, whereas the nuclear markers NEAT1 and preGAPDH are clearly enriched in the nuclear fraction. In summary, the expected pattern for the cytosolic and nuclear marker transcripts could be observed in general, and thus the localization of LINC00941 could be analyzed in this experiment.

Cellular fractionation of undifferentiated human keratinocytes indicated presence of LINC00941 in both cytoplasmic (62%) and nuclear (38%) compartments with an increased cytoplasmic enrichment. Nevertheless, significant amounts of LINC00941 were also detected in the nuclear fraction when compared to mRNAs (Figure 8).

Complementary to this subcellular fractionation approach, single molecule RNA fluorescence *in situ* hybridization (smRNA-FISH) as well as a new RNA fluorescence *in situ* hybridization technique (RNAScope) were performed to study the localization of LINC00941[257,258]. Single-molecule visualization in individual cells was achieved through use of a novel probe design strategy and a hybridization-based signal amplification system to simultaneously amplify signals and suppress background[258,259]. Despite various attempts with different labelling reagents, amplification strategies, and numerous variations of the applied protocol, however, no conclusive results for LINC00941 could be obtained by smRNA-FISH (data not shown). Thus, it appears that smRNA-FISH for this particular transcript was especially challenging. Therefore, no final statement for the LINC00941 localization could be made due to the technical difficulties for smRNA-FISH.

In contrast to this, RNAScope was performed as threedimensional z-stacks in primary keratinocytes and was applicable since the utilized positive controls repeatedly exhibited the expected subcellular localization and the negative control was characterized by a complete lack of signal. Analysis of the z-stacks showed a clear cytosolic distribution for the POL2RA mRNA serving as a positive cytoplasmic control, whereas the negative control prokaryotic dapB mRNA showed no signal in keratinocytes (data not shown). LINC00941 could be observed mainly cytosolic, but still nuclear signals were detectable (Figure 9). Knockdown of LINC00941 in undifferentiated keratinocytes, however, clearly abolishes cytoplasmic signals for LINC00941, but the nuclear transcripts remain (marked with white arrow, Figure 9). This is consistent with the known cytoplasmic location of the RNA-induced silencing complex (RISC)[260,261]. However, for complete subcellular localization studies a nuclear marker has to be involved.

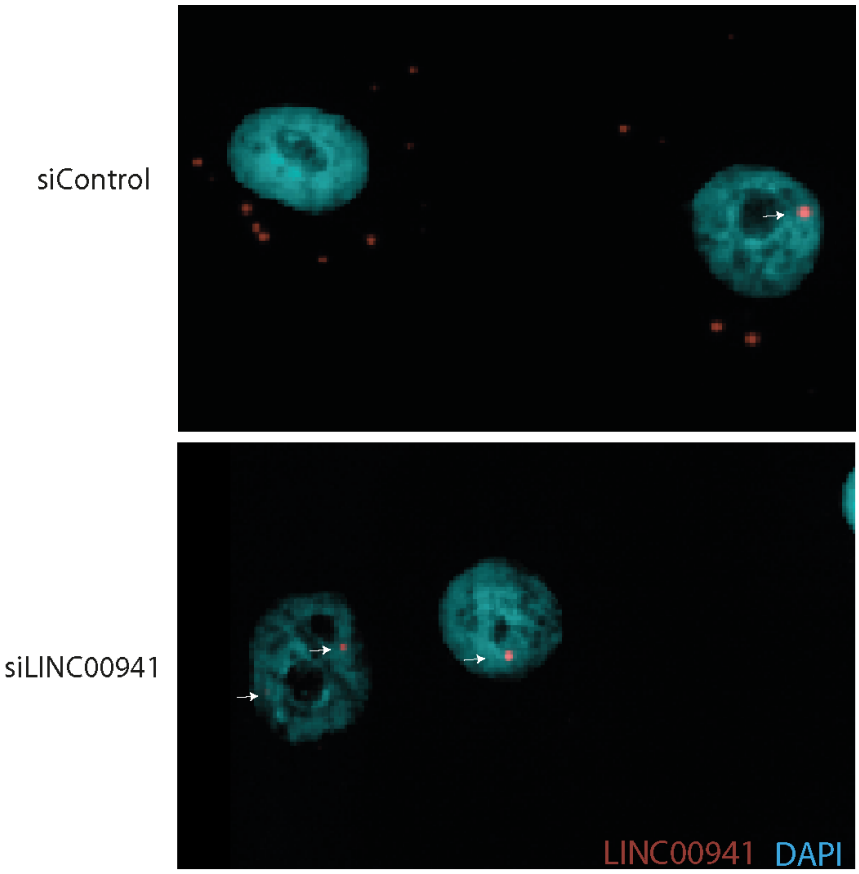

Figure 9: Reconstructed 3D image of single RNA molecule detection in undifferentiated keratinocytes using RNAscope probes and signal amplification system.
Knockdown of LIN00941 in undifferentiated keratinocytes. Arrows mark retained nuclear signals

In summary, cytoplasmic and nuclear LINC00941 molecules could be clearly identified in both fractionation and *in situ* methods. Nevertheless, results from this analysis should be interpreted as a first indication rather than a final proof of the LINC00941 localization. LINC00941 might exhibit a dual nuclear and cytoplasmic distribution and so may therefore play multiple roles in different cellular compartments, which was already shown for several other lncRNAs[262–264].

4.1.3 Annotations for LINC00941

At the beginning of this project, LINC00941 was annotated on the forward strand on chromosome 12 containing 5 exons with a length of 1645 bp (ENST00000547804.1) (ENST00000547804.1)[265,266]. Later, a new transcript appeared in the Ensembl genome browser with a different 5'end being annotated (ENST00000650286.1). To validate the annotation of LINC00941, rapid amplification of cDNA ends (RACE) was performed. 3´RACE revealed several different alternative-splicing and alternative polyadenylation

isoforms regarding the 3´end in undifferentiated keratinocytes. 5´RACE showed no conclusive results. Nanopore-sequencing was performed (work from Daniela Strauss) identifying different LINC00941 isoforms which could be clearly mapped to the previous annotation (an overview is given in Figure 10)[266–269]. To further analyze the 5´start site of LINC00941, RACE and Nanopore-Sequencing results were compared to FANTOM5 CAGE (Cap Analysis Gene Expression) data in order to finally map 2 different start sites for LINC00941.

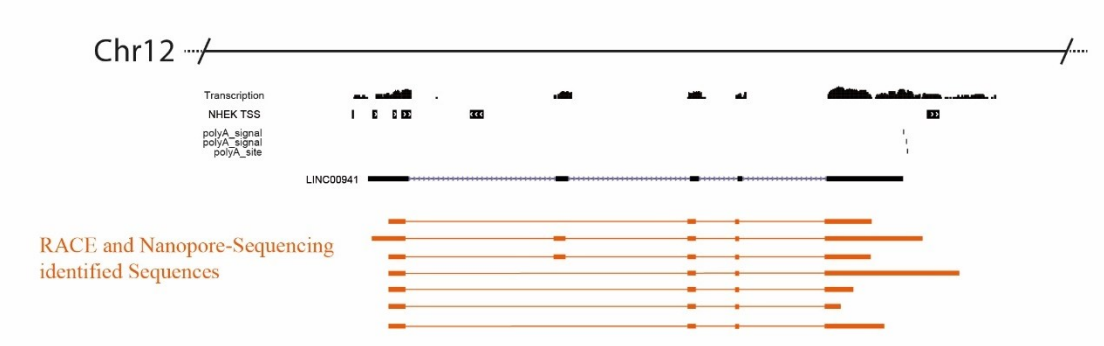

Figure 10: Comparison of different LINC00941 isoforms detected by RACE and Nanopore-Sequencing

Most identified isoforms were lacking Exon 2 in both RACE and Nanopore sequencing. But due to the nonquantitative nature of RACE and Nanopore-Sequencing, it was hard to identify one final isoform. Nevertheless, in all approaches one isoform with 1327 bp was enriched. Additionally, Northern Blot analysis with 16 different LINC00941 antisense oligos covering the whole transcript to detect all isoforms was performed (sequences can be found in Table 14). This Northern Blot was conducted in undifferentiated keratinocytes with total RNA and Poly-A selected RNA (Figure 11). That assay consistently showed only one band at roughly 1300 bp enriched in Poly-A selected RNA.

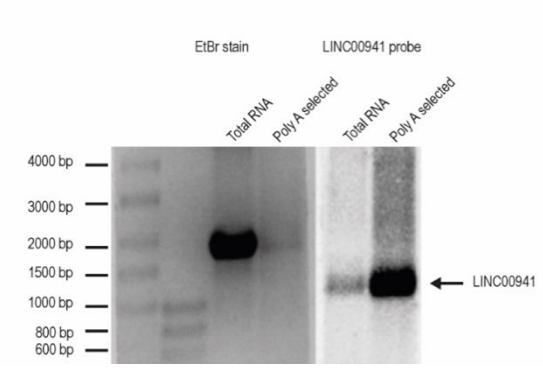

Figure 11: Northern Blot analysis with only one identified band

In summary, several LINC00941 transcripts with different 3´ends could be identified in keratinocytes with probably one dominant LINC00941 isoform of 1327 bp missing exon 2 (the complete sequence and genomic coordinates are given in the appendix 9.2, Table 28 and Table 29). With the LINC00941 transcript structure in hand, the challenge to unravel the function of LINC00941 in keratinocytes was addressed and is shown in the next chapter.

4.1.4 Protein coding potential of LINC00941

A few reports could already confirm the existence of bifunctional lncRNAs acting as RNA as well as encode for small peptides[163,165,166,270–272]. Thus, it remains a challenge in the lncRNA field to discriminate whether transcripts contain a predicted open reading frame, act as a coding or non-coding transcript, or as a combination of both. In order to verify the annotation of LINC00941 as a long non-coding RNA, Coding-Potential Assessment Tool (CPAT) , iSeeRNA, Lncident, and Coding Potential Calculator (CPC2) were utilized to assess the coding potential of the nucleotide sequences[273–276]. With these bioinformatic algorithms a lack of protein-coding potential could be identified (Figure 12) strongly indicating that LINC00941 solely acts as a long non-coding RNA.

Tool	Result	Interpretation
coding-potential assessment Tool (CPAT, Wang et al. 2013)	0.0911	non-coding
lSeeRNA (Sun et al. 2013)	0.978	non-coding
Lncident (Han et al. 2016)	0.003	non-coding
coding-potential calculator (CPC2, Kang et al. 2017)	0.0246	non-coding

Figure 12: Investigation of the protein coding potential of LINC00941 using different bioinformatical algorithms.

4.2 Epidermal homeostasis controlled by LINC00941

4.2.1 Generation of LINC00941 knockout cell lines

Due to high remaining levels of RNA in preliminary knockdown-based LINC00941-deficient keratinocytes (see chapter 2.3), another approach to diminish the residual activity of siPool-mediated LINC00941 knockdowns was necessary. Thus, LINC00941 knockout cells were chosen to be generated as a substitute. However, primary keratinocytes were unsuitable for this approach since they possess only a very limited number of cell doublings *in vitro*[277–279]. After the long process of clonal growth and selection for knockout clones, cell

doublings will be restricted. Another drawback of primary keratinocytes are variations of different donors.

Thus, the immortalized keratinocyte cell lines N/TERT1 and N/TERT2G, which were described to differentiate in an epidermal environment, were utilized for the generation of LINC00941 knockout cell lines[280]. Additionally, both cell lines have been karyotyped already to assess their ploidy. N/TERT2G is diploid (46, XY) and N/TERT1 is diploid with an additional chromosome 20 (47, XY, +20)[280,281]. In a first step towards generating a LINC00941 knockout cell line, the ability of these cell lines to differentiate in a calcium-induced keratinocyte differentiation cultures (Figure 13) as well as in regenerated organotypic epidermal tissue cultures was assessed[281].

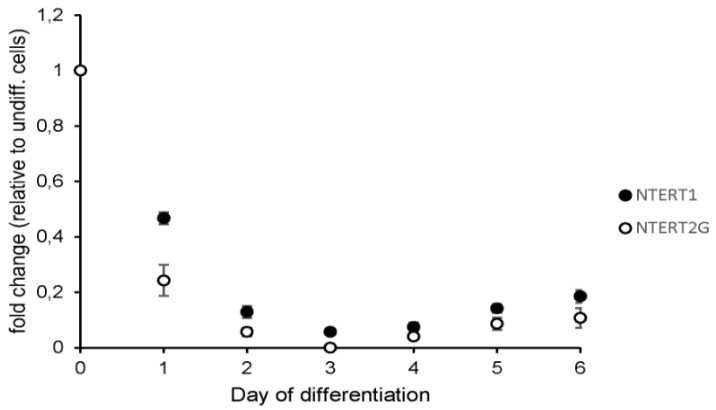

Figure 13: Expression of LINC00941 in two N/TERT cell lines

This pilot experiment clearly indicated that both N/TERT cell lines were suitable in this experiment as they express normal levels of LINC00941 and conduct a similar differentiation program like primary keratinocytes. Due to the addition of chromosome 20 in the N/TERT1 cell line, the N/TERT2G was used to generate knockout cell lines.

In theory, knockout cell line generation works as described in the following: After transfection of a plasmid encoding chimeras of the desired guideRNAs (gRNAs) and the required trans-activating CRISPR RNA (tracrRNA), the gRNAs should target the Cas9 endonuclease (also encoded on the plasmid) to the intended genomic cutting sites via base complementarity between the gRNA and the DNA[282,283]. Next, Cas9 cleaves the DNA specifically at the targeted sites and the resulting DNA double-strand breaks are repaired either via non-homologous end joining (NHEJ) or homology-directed repair (HDR) mechanism[282]. In this case, only the NHEJ of two cutting sites flanking the LINC00941 locus

would generate the desired genomic LINC00941 deletion, as HDR with potentially remaining wild type alleles would reconstitute the initial state with no genomic alteration.

To screen for potential knockout events, a single PCR approach was used first to detect wild-type as well as knockout events. Due to the large locus (around 8kb) to be cut out, the PCR could not detect wildtype alleles in this PCR setting. Therefore, a new strategy was utilized to only amplify both the 5´ and the 3´end of the lncRNA in order to check for a knockout event (Figure 14).

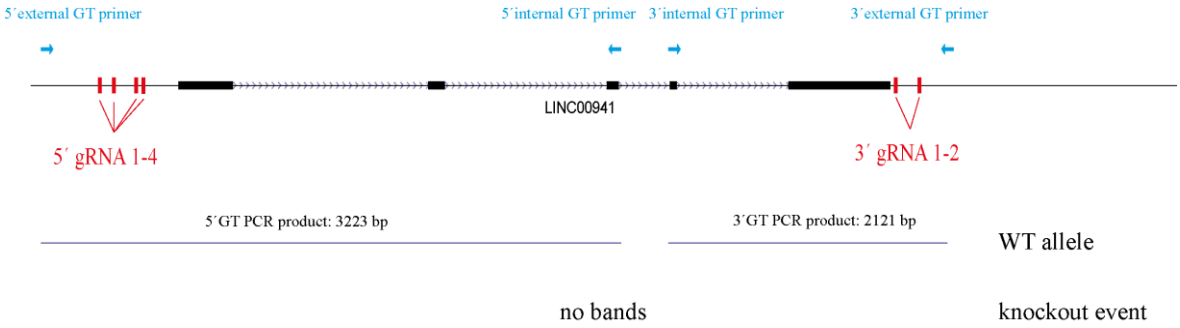

Figure 14: CRISPR-Cas9 based knockout and PCR screening strategy for the LINC00941
(WT: wildtype, gRNA: guideRNA)

Here, the wildtype allele could be detected, whereas no homozygous or heterozygous knockout event happened in various trials. Despite various reports about efficient genomic editing using the CRISPR/Cas9 system in different cell lines, especially in keratinocytes, successful knockout studies of lncRNAs are still sparse due to the fact that keratinocytes are prone to terminal differentiation and proliferate only for few passages in monoculture. Clonal growth of single clones for a longer time is therefore very challenging.

4.2.2 LINC00941 acts as negative regulator of keratinocyte differentiation

Since LINC00941 abundance decreases upon keratinocyte differentiation, a role for this lncRNA in non- or poorly differentiated strata of the epidermis was postulated. To test a role of LINC00941 in poorly stratified layers, siRNA-mediated knockdown of LINC00941 was performed in keratinocyte differentiation cultures, the expression of several key differentiation markers was assessed by RT-qPCR. An efficient loss of LINC00941 (< 10% remaining) resulted in an increased abundance of mRNA levels for early (Keratin 1) and late differentiation genes (SPRR3 and Filaggrin) suggesting a functional relevance of LINC00941 in preventing premature progression of the terminal differentiation program (Figure 15A-B).

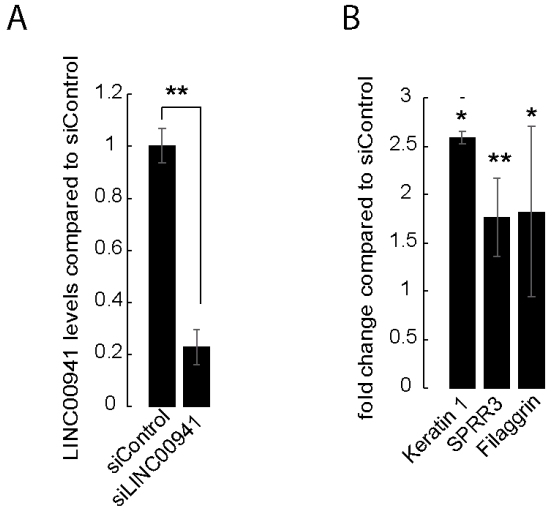

Figure 15: LINC00941 depletion leads to differentiation defects
(A) Depletion of LINC00941 by siRNAs leads to (B) increased expression of differentiation marker mRNAs as obtained by RT-qPCR (n=3-4). Data are presented as mean ± SD. Statistical significance was tested by an unpaired t-test and corrected for multiple testing after Bonferroni (*adj. P-value < 0.05, **adj. P-value < 0.01, ***adj. P-value < 0.001).

To examine the impact of LINC00941 on the proliferative potential of keratinocytes, a knockdown of LINC00941, followed by staining of Ki-67, a marker strictly associated with cell proliferation, was performed (Figure 16A-B). The fact that the Ki-67 protein was present during all active phases of the cell cycle but was absent from resting cells, made it an excellent marker for determining the growing fraction of a given cell population. No significant difference in Ki-67 positive cells could be detected in LINC00941 deficient cells.

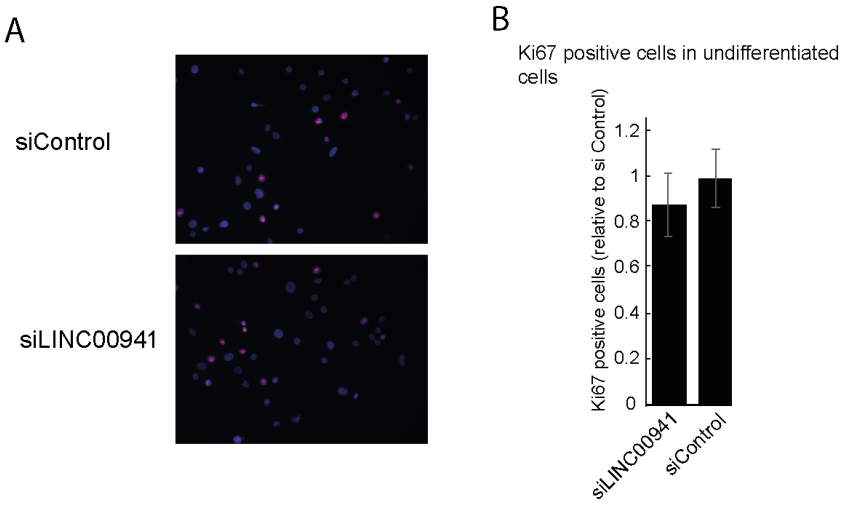

Figure 16: Ki-67 staining to examine the proliferative potential of LINC00941 deficient keratinocytes
(A) staining of Ki-67 positive cells (B) counting of Ki-67 positive cells in comparison to control

Whether LINC00941 alone is sufficient to ectopically keep keratinocytes in the progenitor state was examined by lentiviral based overexpression of LINC00941 followed by RT-qPCR analysis of differentiation marker mRNA levels. Compared to the GFP control,

overexpression of 12-fold increased LINC00941 levels was achieved (Figure 17A). Upon LINC00941 overexpression reduced transcript levels for keratin1 (KRT1), filaggrin (FLG) and loricrin (LOR) could be detected (Figure 17B). This further supported the role of LINC00941 as a negative regulator of keratinocyte differentiation.

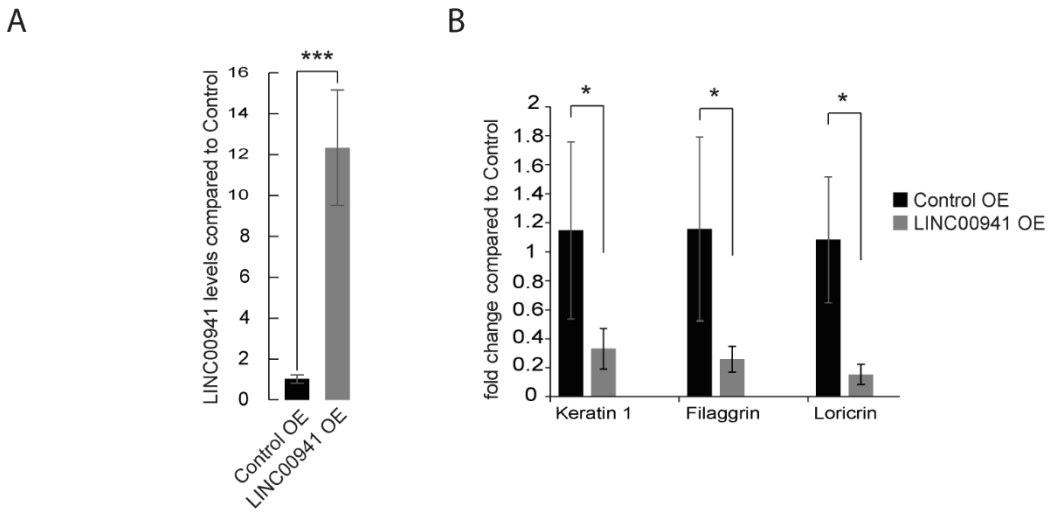

Figure 17: LINC00941 overexpression in day 3 differentiated keratinocytes leads to reduced expression of differentiation markers
(A) LINC00941 overexpression on d3 of differentiation leads to (B) reduced expression of differentiation markers as obtained by RT-qPCR (n=3-4). Data are presented as mean ± SD. Statistical significance was tested by an unpaired t-test and corrected for multiple testing after Bonferroni (*adj. P-value < 0.05, **adj. P-value < 0.01, ***adj. P-value < 0.001).

4.2.3 Epidermal tissue generation requires LINC00941

Since LINC00941 regulates keratinocyte differentiation *in vitro* (4.2.2), it was interesting to test whether LINC00941 also represses keratinocyte differentiation in a mature tissue environment. For this purpose, LINC00941 knockdown was conducted in epidermal tissue cultures. LINC00941-deficient human organotypic epidermis was generated and compared to matching control tissue.

Similar results as observed with primary keratinocytes were found. LINC00941-deficient organotypic epidermis differentiated prematurely as indicated by increased mRNA and protein abundances of keratin 10 (crucial for early differentiation) as well as SPRR4 and Loricrin (late differentiation genes) (Figure 18A-C). These results indicate an important role for LINC00941 in repressing not only premature keratinocyte differentiation *in vitro* but also in human epidermal tissue homeostasis.

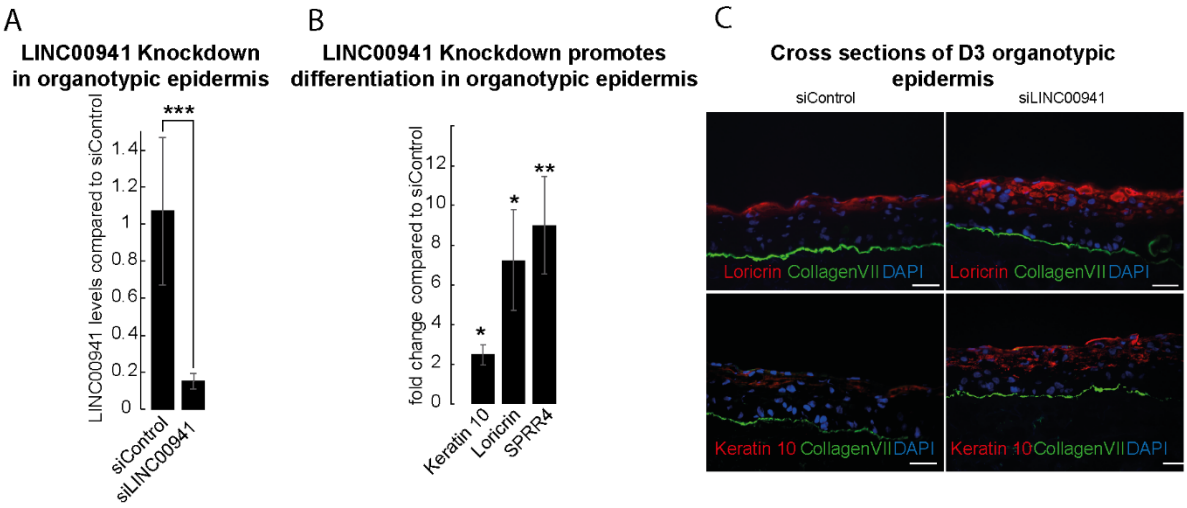

Figure 18: LINC00941 acting as a negative regulator of keratinocyte differentiation
(A) LINC00941 knockdown in d3 organotypic epidermis leads to (B) increased expression of differentiation markers as obtained by RT-qPCR (n=4) (C) Immunofluorescence analysis shows increased levels of early and late differentiation proteins. Collagen VII (col VII, green) stain indicates the basement membrane; nuclei are shown in blue, and the differentiation proteins keratin 10 and loricrin are shown in red (n = 4 tissue cultures/knockdown group; one exemplary picture for each group is depicted). Scale bar: 50 µm. Data are presented as mean ± SD. Statistical significance was tested by an unpaired t-test and corrected for multiple testing after Bonferroni (*adj. P-value < 0.05, **adj. P-value < 0.01, ***adj. P-value < 0.001).

Similar to the cell culture model, a lentiviral based overexpression of LINC00941 was performed in organotypic epidermis. Here, also an overexpression of LINC00941 of 11-fold could be detected (Figure 19A). Overexpression of LINC00941 led to a diminished differentiated epidermis as indicated by decreased mRNA abundances of the late differentiation genes Loricrin (LOR) as well as late cornified envelope proteins 1D and 2D (LCE1D and LCE2D) (Figure 19B). In comparison to LINC00941-deficient organotypic epidermal tissue, LINC00941-overexpressing tissue was much thinner, and therefore no conclusive result for protein abundances of respective differentiation markers could be drawn. In contrary to the reported induction of keratinocyte differentiation upon an increase of cellular stress levels triggered by lentiviral infection, a decrease in differentiation markers upon lentiviral-mediated overexpression of LINC00941 might be indicative for a repressing role of LINC00941 in human epidermal homeostasis [284,285].

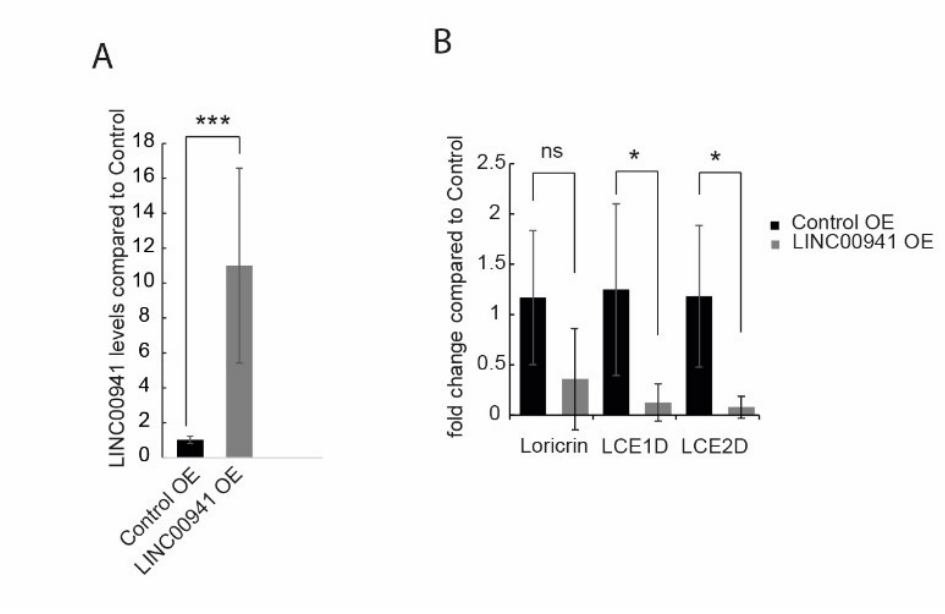

Figure 19: Overexpression of LINC00941 in organotypic epidermis
(A) Overexpression of LINC00941 in d3 organotypic epidermis leads to (B) decreased expression of differentiation markers as obtained by RT-qPCR (n=4). Data are presented as mean ± SD. Statistical significance was tested by an unpaired t-test and corrected for multiple testing after Bonferroni (*adj. P-value < 0.05, **adj. P-value < 0.01, ***adj. P-value < 0.001).

To further test the impact of LINC00941 on proliferation, a Ki-67 stain was performed in LINC00941-deficient as well as in LINC00941-overexpressing organotypic epidermis, and similar to the cell culture model no significant differences could be obtained (data not shown). Both loss of LINC00941 and ectopically overexpressed LINC00941 do not diminish the proliferative potential in undifferentiated keratinocytes in the basal layer indicating that the LINC00941 transcript is essential but not sufficient for preventing premature progression of terminal differentiation. More likely is a role of LINC00941 in poorly differentiated keratinocytes.

4.2.4 LINC00941 regulates keratinocyte differentiation on a global level

In order to obtain a comprehensive picture of the global impact of LINC00941 knockdown on epidermis development, a full transcriptome sequencing approach of LINC00941-depleted and control tissue at days 2 and 3 after onset of epidermal homeostasis was performed. To this end, four and five biological replicates, respectively, of regenerated organotypic epidermis with and without LINC00941 depletion were harvested; the isolated RNA was subjected to poly-A enrichment followed by library preparation and next generation sequencing, respectively (Figure 20A). A sequencing depth of 22 to 39 million

mapped reads per sample was received (Table 30), and the subsequent principal component analysis proved comparability between the transcriptomes of the biological replicates for each timepoint and distinct clustering in a control and LINC00941 depletion group (Figure 20B). Thus, differential gene expression analysis was done for each timepoint using a customized DeSeq2 script and the obtained results were successfully verified by RT-qPCR for selected transcripts confirming the validity of the obtained RNA-Seq analysis (Figure 30C, appendix chapter 9.1).

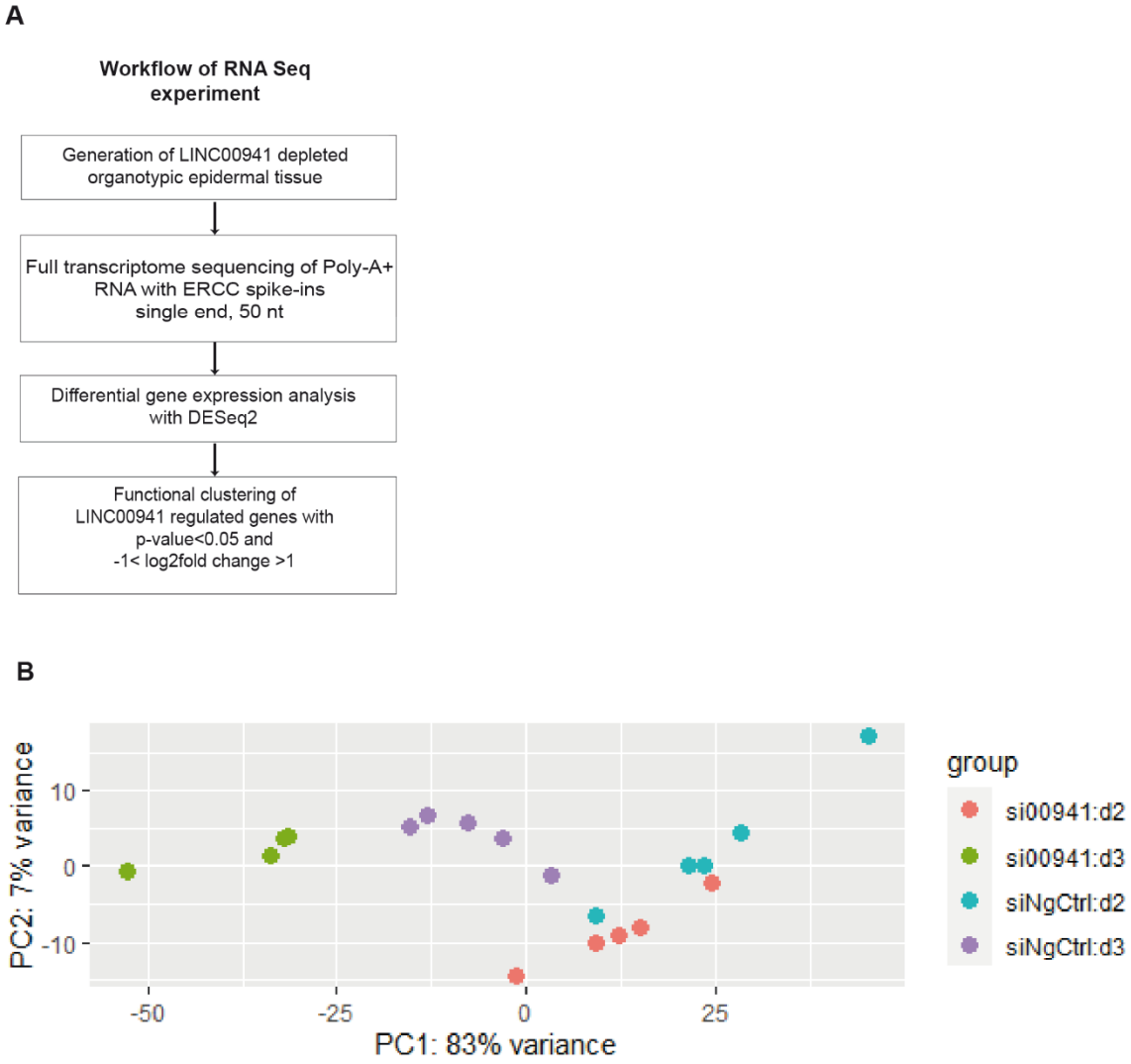

Figure 20: Global analysis of the effect of LINC00941 knockdown in organotypic epidermis
(A) Workflow of the performed RNA-Seq experiment (B) Principal component analysis of the transcriptome upon LINC00941 depletion on d2 and d3 in regenerated organotypic epidermal tissue shows good clustering of control samples (siNgCtrl) and LINC00941 depleted tissue (si00941) for both analyzed timepoints of differentiation, PC = principal component.

First, the efficient knockdown of LINC00941 with 12% and 22% remaining transcript amounts on day 2 or day 3, respectively, (Figure 21A-B) was verified. This ultimately

resulted in numerous differentially expressed genes (-1 > $\log_2$ (fold change) > 1 and an adjusted p-value < 0.05; lists of differential expressed genes are included in the appendix, chapter 9.6).

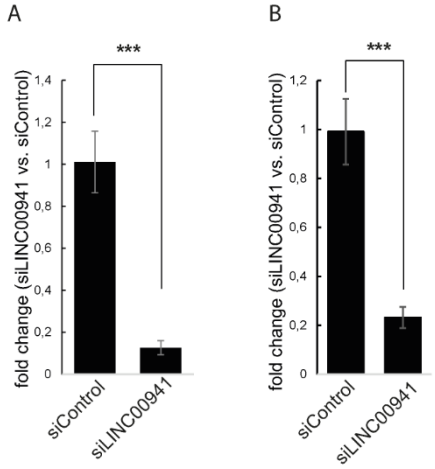

Figure 21: Validation of knockdown for RNA-Seq
LINC00941 knockdown efficiency (siLINC00941) in epidermal tissue on (A) day 2 or (B) day 3 of differentiation as obtained by qRT–PCR measurements (n = 4–5 epidermal tissue cultures/knockdown group). Data are presented as mean ± SD. Statistical significance was tested by an unpaired t-test and corrected for multiple testing after Bonferroni (***adj. P-value < 0.001).

On day 2 of differentiation a total of 240 genes were differentially expressed, 111 genes were downregulated and 129 genes were upregulated upon LINC00941 depletion (Figure 30A, chapter 9.1). On day 3, the majority of the 314 total genes showed increased expression (223 upregulated versus 91 downregulated genes; Figure 22A). Gene ontology (GO) term analysis of all deregulated genes in LINC00941-deficient tissue showed strong enrichment of genes involved in processes crucial for epidermal differentiation such as keratinization, keratinocyte differentiation, generation of a cornified envelope, and peptide cross-linking (Figure 22B). These findings provide further evidence for a role of LINC00941 in repressing the epidermal differentiation program. To investigate potential hot spots of LINC00941-regulated genes across the human genome, enrichment of LINC00941-altered genes compared to the relative distribution of Ensembl genes across all human chromosomes were analyzed (Figure 30D, chapter 9.1). The strongest enrichment could be detected on chromosome one, with a significant accumulation of altered genes in the epidermal differentiation complex (1q21.3; EDC; Figure 22C).

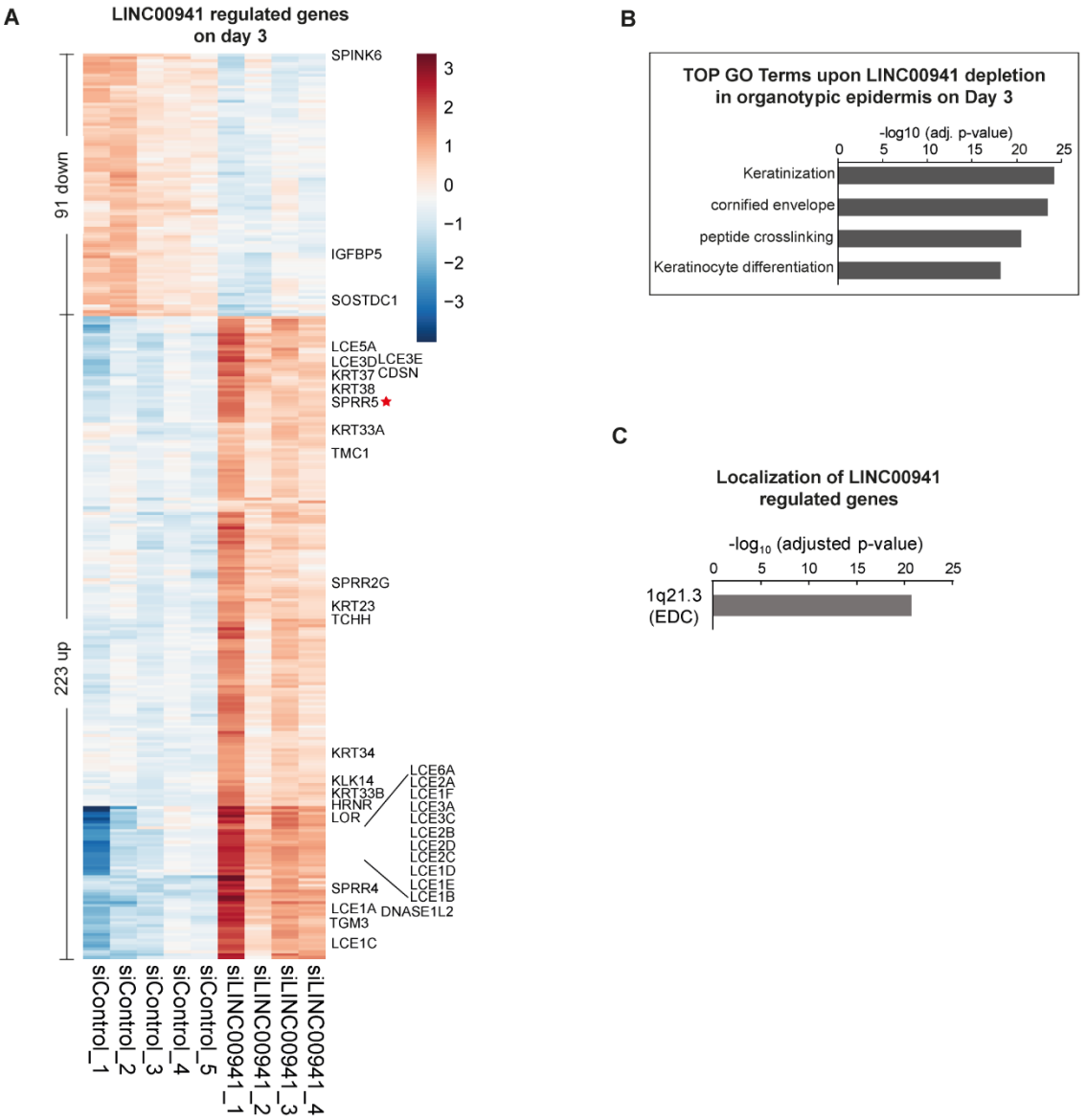

Figure 22: LINC00941 is a suppressor of keratinocyte differentiation
(A) Heatmap of differentially expressed genes (Padj < 0.05 and-1 > log2FC > 1) upon LINC00941 depletion on day 3 in organotypic epidermal tissue with marked keratinocyte differentiation genes (n = 4–5 epidermal tissue cultures/knockdown group). (B) GO term analysis of regulated (Padj < 0.05 and -1 > log2FC < 1) genes in LINC00941-deficient organotypic epidermal tissue on day 3 (n = 4–5 epidermal tissue cultures/knockdown group (C) Differentially expressed genes in day 3 LINC00941-depleted epidermal tissue cluster within the epidermal differentiation complex (EDC)

The EDC spans 1.9 Mb and harbors roughly sixty genes, many of which are coding for proteins involved in keratinocyte differentiation and epidermal barrier formation (see chapter 2.1.2). Thus, a more detailed analysis of the LINC00941 regulated genes within the EDC was performed. Correspondingly, 28 well-characterized genes crucial for epidermal differentiation located within the EDC show premature expression in LINC00941-depleted epidermal tissue (Figure 23). These include Loricrin, SPRR4, and 16 out of 18 LCE genes.

Thus, LINC00941 is not only capable of repressing key differentiation genes and preventing premature onset of differentiation in human epidermal tissue but controls different gene clusters indicating a possible epigenetic mechanism of LINC00941.

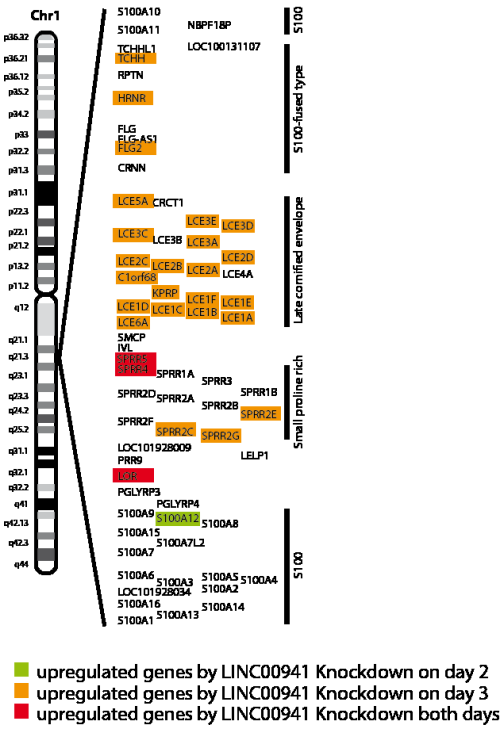

Figure 23: Regulated genes in the EDC upon knockdown of LINC00941
Graphical depiction of clusters regulated upon LINC00941 knockdown in d2 and d3 organotypic epidermis

4.3 Role of LINC00941 in keratinocyte development

LncRNAs are known to be key regulators of chromatin states, yet the nature and sites of RNA-chromatin interaction are mostly unknown[286]. Since LINC00941 controls different gene clusters in the epidermal differentiation complex (see chapter 4.2.4) and has also shown partially nuclear localization during subcellular fractionation experiments (see chapter 4.1.2), first protein interaction studies were employed to identify potential interacting protein complexes. Afterwards, chromatin association of LINC00941 was analyzed.

4.3.1 Protein Interaction of LINC00941

RNA-protein complexes play a central role in the regulation of fundamental cellular processes such as mRNA splicing, localization, translation, and degradation. Recently, many strategies have been developed to comprehensively analyze these complex and highly dynamic RNA–protein networks. Hence, an unbiased RNA-centric approach that subsequently involves mass spectrometry, which is a powerful tool for identifying proteins

bound to a given RNA, was conducted to identify protein interaction partners of LINC00941. I*n vitro* transcribed and biotinylated LINC00941 was used to co-immunoprecipitate associated proteins of interest, followed by SDS page and detection by mass spectrometry. Here, pulldown of LINC00941 was performed in undifferentiated keratinocytes as well as in a cutaneous squamous carcinoma cell line UT-SCC7 (see chapter 4.4.1). In this SCC cell line LINC00941 is 7-fold enriched. Pull-down of LINC00941 revealed interaction with caspase-14. Differentiation of keratinocyte involves an activation of intracellular proteolytic cascade mainly mediated by members of the caspase family which cleave each other and various intracellular targets[287,288]. Caspase-14 is the only member of the caspase family that shows a restricted tissue expression in epidermal differentiation. Knockout studies of caspase-14 in mice have suggested a critical role in the proteolytic processing of filaggrin indicating a role of Caspase-14 in terminal differentiation leading to skin barrier formation[27,289–291].

Additionally, in undifferentiated keratinocytes LINC00941 seemed to interact with several components of the Nucleosome Remodeling Deacetylase (NuRD) complex (Figure 24A). To further validate these results, interaction of LINC00941 with MTA2 as one of the core components of the NuRD complex was tested. Surprisingly MTA2 showed the same expression pattern as LINC00941 in keratinocytes. Pull-down with in vitro transcribed, biotinylated LINC00941 RNA and cell lysates from primary keratinocytes, followed by SDS page and detection with α-MTA2 antibody was performed and interaction of LINC00941 with MTA2 could be verified (Figure 24B).

Correspondingly, GO-term analysis of proteins interacting with LINC00941 compared to a size matched control RNAs showed enrichment for terms associated with nucleosomal RNA binding, chromatin remodelling, histone deacetylation, and NuRD complex (Figure 24C).

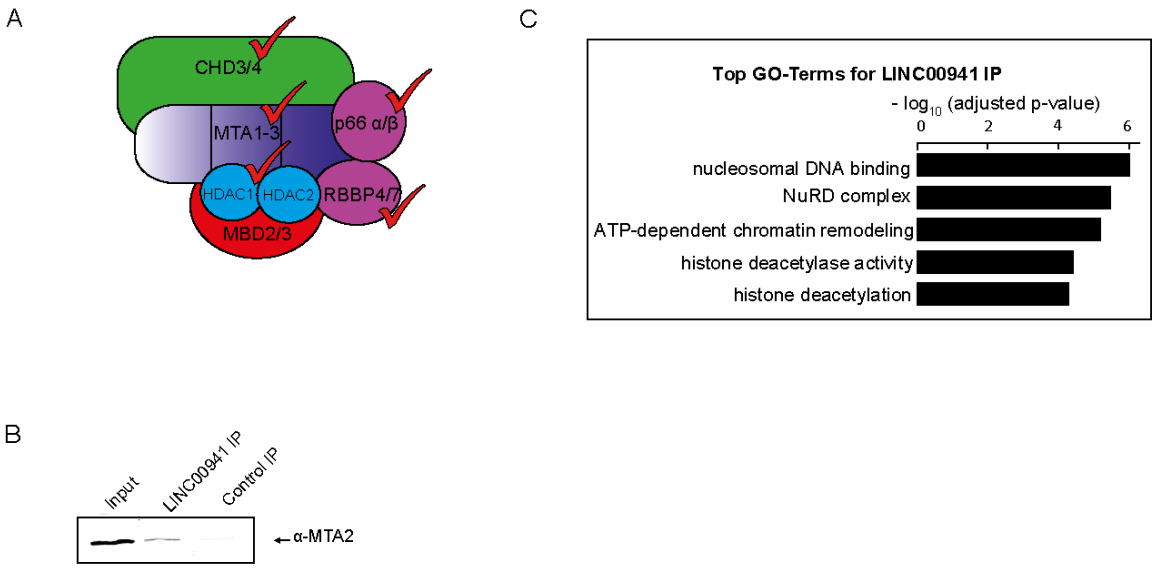

Figure 24: LINC00941 interacts with the Nucleosome Remodeling Deacetylase complex
(A) Schematic representation of major NuRD complex components. Red check marks depict proteins interacting with LINC00941 as shown by mass spectrometry analyses of proteins pulled down with in vitro transcribed, biotinylated LINC00941. (B) Pull-down with in vitro transcribed, biotinylated LINC00941 RNA and cell lysates from primary keratinocytes, followed by SDS page and detection with αMTA2 antibody. (C) GO term analysis of proteins specifically interacting with LINC00941.

NuRD complexes consist of multiple subunits including the dermatomyositis-specific autoantigen Mi-2α or β (CHD3 or CHD4), the histone deacetylases HDAC1/2, the histone binding proteins RbAp46/48, the methyl-CpG binding domain protein MBD3, and the metastasis-associated proteins MTA1/2/3[292–294]. The complexes have chromatin remodeling and histone deacetylation properties and function primarily in transcriptional repression[295]. Components of NuRD complexes have been found to play important roles in embryonic development and homeostasis in various organisms and human tumorigenesis[293,296,297]. The exact composition of NuRD complexes varies depending on targets and cell types and plays distinct roles in cell proliferation, survival, and differentiation. Surprisingly, mice deficient of several components of the NuRD complex, such as Chd4 or Mta2 as well as Hdac1+2 double-deficient mice, showed defective epidermal homeostatic activity with significant similarities to the phenotypes seen with LINC00941 knockdown[84,298,299].

These findings indicate that LINC00941 might regulate expression of differentiation gene cluster as observed on a global level (see chapter 4.2.4) through modulation or recruitment of this chromatin-remodeling complex.

4.3.2 Investigating the potential epigenetic mechanism of LINC00941

To investigate a potential role of LINC00941 in recruiting the NuRD complex to target chromatin sites, Chromatin Isolation by RNA Purification (ChIRP) was implied. ChIRP is based on affinity capture of a target lncRNA-chromatin complex by tiling antisense-oligos which then generates a map of genomic binding sites at a resolution of several hundred bases with high sensitivity and low background[300]. One potential source of noise in ChIRP-seq is the precipitation of nonspecific DNA fragments from off-target hybridization of the pool of oligonucleotide probes. In order to eliminate such artifacts, all probes were split into two pools (all even probes were in one set and all odd probes in another). As the two different sets of probes shared no overlapping sequences, the only target they have in common is the RNA of interest and its associated chromatin. Four independent ChIRP-seq runs with "even" and "odd" probes were performed separately. Only the shared signal from all four independent ChIRP-seq experiments was considered to be a meaningful signal; a signal present in only even or odd experiments alone was not interpreted. ChIRP-Seq was performed on endogenous LINC00941 RNA in undifferentiated primary keratinocytes. Binding sites of LINC00941 in each sample were called using model-based analysis of ChIP-seq (MACS) against its corresponding input. 3028 LINC00941 binding-sites could be identified with high enrichment in promoter regions (Figure 25A)[301]. To further analyze peaks, these binding sites were associated to the nearest genes that were less than 10 Kb away from the transcription start site. Gene ontology terms analysis of these genes showed enrichment for RNA-binding proteins as well as kinase and phosphotransferase activity (Figure 25B). No binding site in of LINC00941 in the EDC could be identified, thus suggesting a regulation of EDC gene clusters in *trans* and not in proximity of LINC00941 transcription site.

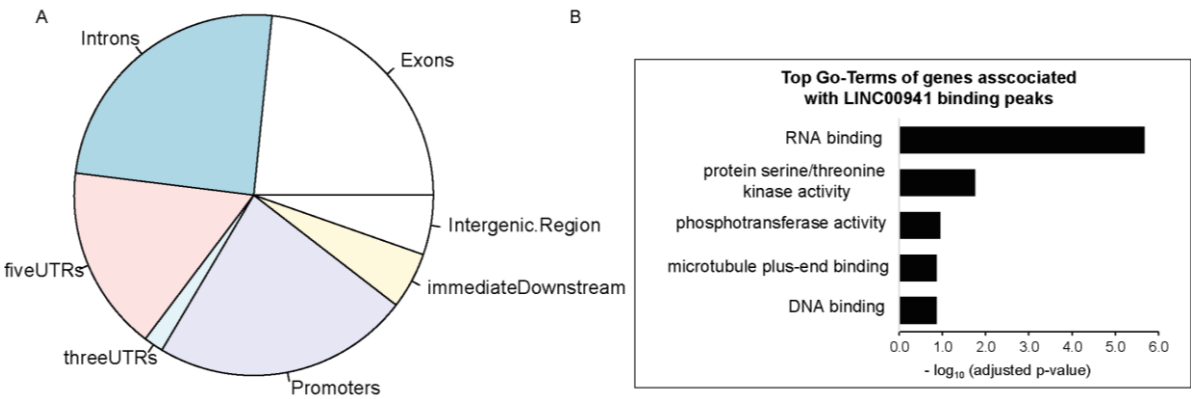

Figure 25: ChIRP-Seq reveals binding sites of LINC00941 all over the genome
(A) LINC00941 occupancy in different genomic features (B) Gene ontology analysis of LINC00941 associated peaks.

Moreover, to investigate a potential role of LINC00941 in recruiting the protein complexes to target chromatin sites, only the promoter associated genes were extracted and further analyzed. Motif analysis of promoter associated LINC00941 ChIRP-Seq Peaks revealed a significantly enriched DNA motif that was highly similar to the E2F4 and E2F6 binding motif as well as to their heterodimic binding partner TFDP1 (Figure 26A-B)

A

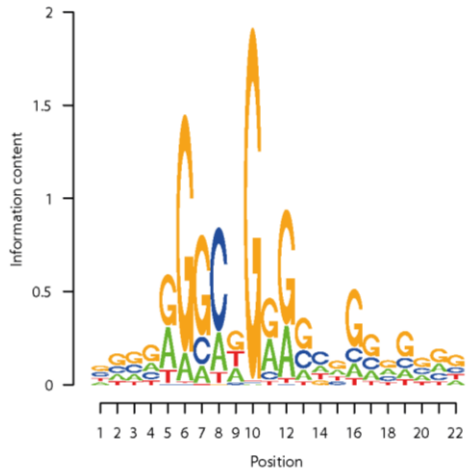

B

ID	name	similarity
MA0470.1	E2F4	0.55360556825289
MA0471.1	E2F6	0.548560857317162
MA1122.1	TFDP1	0.520620883602226
MA0750.2	ZBTB7A	0.464983141544377
MA0645.1	ETV6	0.451712641553582
MA0057.1	MZF1(var.2)	0.422019462616277
MA0056.1	MZF1	0.418124537237931
MA1100.1	ASCL1	0.375751827164036
MA0814.1	TFAP2C(var.2)	0.371407886263032
MA0163.1	PLAG1	0.368644219084189

Figure 26: Motif search for promoter regions bound of LINC00941
(A) cytosin-guanin-rich motif enriched among LINC00941 binding sites at promoters (B) motif search of most similar motifs.

The E2F family has been implicated in controlling diverse critical cellular and organismal functions including regulation of differentiation, development and tumorigenesis[302,303]. There are eight genes for E2F family members encoded in the human genome[303,304]. The highest degree of homology among the E2F family members is in their DNA-binding domains, which is consistent with the finding that they can all bind to the same consensus motif *in vitro*[305]. Most E2F family members are complexed with a member of the dimerization partner (DP) family of transcription factors to fulfill their function[303,306].

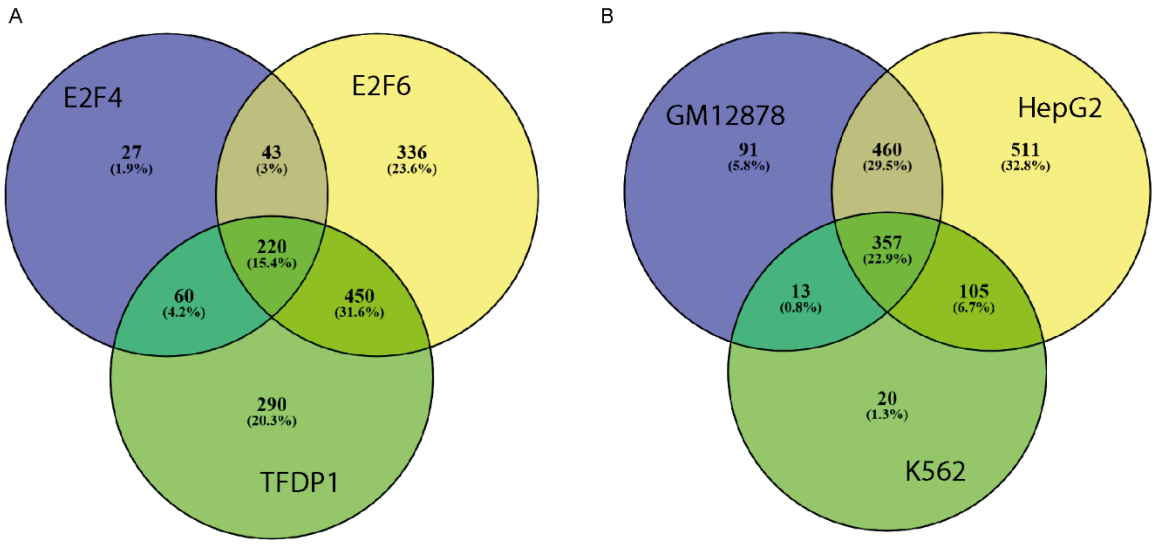

Figure 27: Overlap of E2F4 binding sites with LINC00941 binding sites in three different cell lines
(A) Overlap of publicly available ChIP-Seq datasets with LINC00941 binding sites (B) Overlap of E2F4 ChIP-Seq datasets with LINC00941 binding sites in the three different cell lines GM12878, HepG2 and K562

Due to lack of ChIP data in keratinocytes, publicly available ChIP-Seq datasets of the three transcription factors with the highest similarity (E2F4, TFDP1 and E2F6) were overlapped with LINC00941 associated peaks. Here, ChIP-Seq analyses from E2F4, E2F6, and TFDP1, which were all performed in K562 cells, were used. Peaks from the ChIP analyses were overlapped with LINC00941 and each overlap was further analyzed. Almost 16% of genes exhibiting LINC00941 association were also shown to be bound by E2F4, E2F6, and TFDP1 suggesting to be common targets of all four molecules and therefore hinting towards a common mechanism (Figure 27A). Gene ontology (GO) term analysis of common targets showed only enrichment of genes involved in RNA-binding (data not shown).

Additionally, utilizing publicly available ChIP datasets for E2F4 in three different cell types (HepG2, K562 and GM12878) and overlapping these datasets with the peaks of the ChIRP analysis, common features could be identified to be regulated by both LINC00941 and E2F4 respectively (Figure 27B). For this purpose, all peaks from the ChIP analyses were overlapped with LINC00941 binding sites. Afterwards, only the overlaps of each set were further analyzed. An overlap of 357 cell line independent common LINC00941 and E2F4 peaks could be observed.

4.4 Role of LINC00941 in cutaneous squamous carcinoma

4.4.1 Invasion assay

The upregulation of LINC00941 in human squamous cell carcinoma samples compared to their site matched healthy tissue controls has already implied an important function for LINC00941 in either cancer onset or development. This led to the hypothesis that high expression of LINC00941 might inhibit differentiation of keratinocytes and therefore might increase tumor progression.

In order to test this hypothesis, an experiment was performed in collaboration with Kunal Das Mahapatra (laboratory of Andor Pivarcsi at the Karolinska institute, Sweden). First, cSCC cell lines were profiled for the expression of LINC00941 in comparison to normal keratinocytes. In most SCC derived cell lines, a clear overexpression of LINC00941 could be observed (Figure 28A).

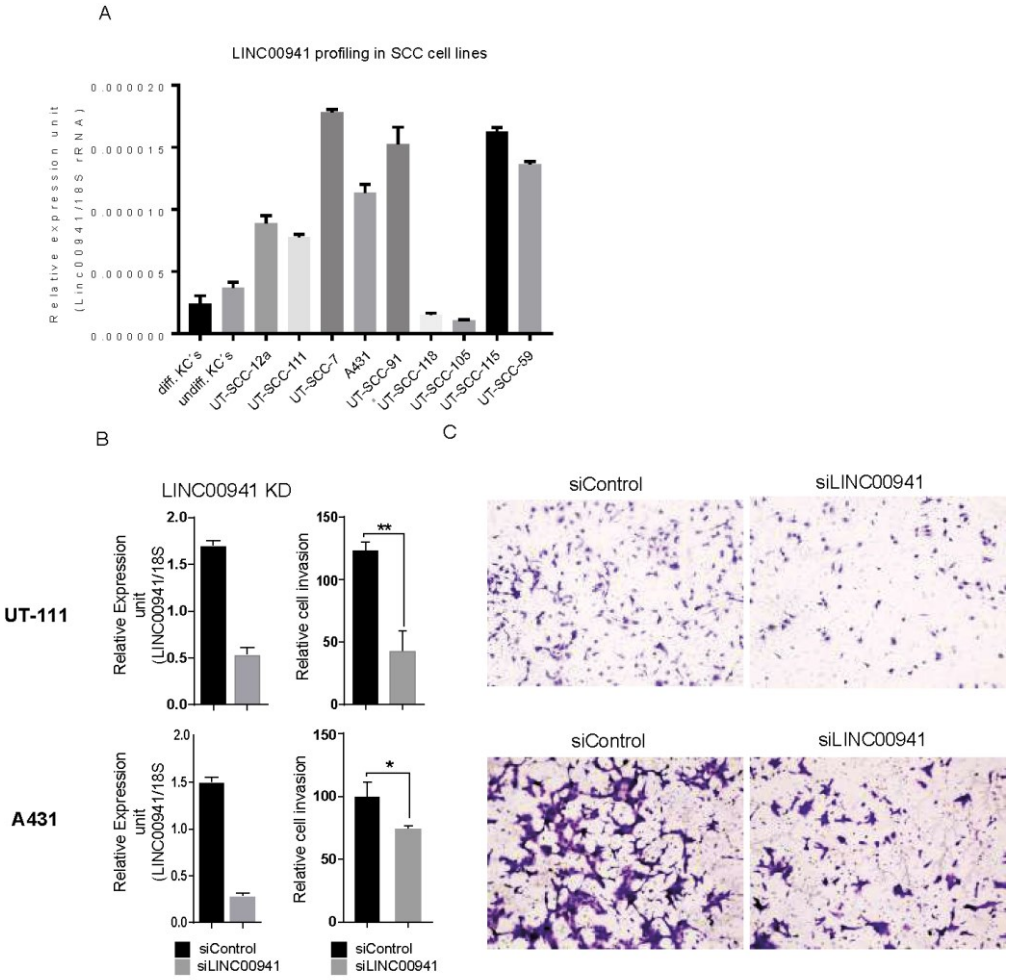

Figure 28: Loss of LINC00941 inhibit invasion of SCC keratinocytes
(A) Profiling of LINC00941 expression in comparison to normal keratinocytes (B) SiRNA-mediated depletion of LINC00941 in keratinocyte cell lines derived from squamous cell carcinoma (SCC)-patients (shown here: UT-111 and A431) led to (C) inhibition of cell invasion in Matrigel invasion assays

Afterwards, an Matrigel invasion assay was performed in two cell lines (UT-111 and A431) with a moderate overexpression of LINC00941. The Matrigel invasion Assay provides an in vitro system to study cell invasion of malignant and normal cells[307]. The transwell migration and invasion assays may be used to analyze the ability of single cells to directionally respond to various chemo-attractants, whether they are chemokines, growth factors, lipids, or nucleotides[308–310]. Knockdown of LINC00941 led to a decreased invasion of keratinocytes in both SCC cell lines (Figure 28B-C).

As deregulated lncRNAs might function in signaling pathways which are already mutationally activated or suppressed in cSCC, LINC00941 might play a role at the early stage of epidermal carcinogenesis.

4.4.2 Analysis of cell migration

Collective cell migration is a hallmark of wound repair, cancer invasion and metastasis, immune responses, angiogenesis, and embryonic morphogenesis. The migration of epidermal keratinocytes is the basis for skin reepithelialization during wound healing. Wound healing is a complex cellular and biochemical process necessary to restore structurally damaged tissue. It involves dynamic interactions and crosstalk between various cell types, interaction with extracellular matrix molecules, and regulated production of soluble mediators and cytokines. In cutaneous wound healing, skin cells migrate from the wound edges into the wound to restore skin integrity[311].

The *in vitro* scratch assay using monolayers of primary human epidermal keratinocytes is a straightforward and effective method to assess their migratory capacity (Figure 29A)[312]. The mechanical scratch of a confluent monolayer directly disrupts the adhesion of the keratinocytes both to one another and to the underlying matrix resembling the physical trauma of a wound in an *in vitro* assay.

Here, confluent LINC00941-deficient monolayers as well as control cultures were generated. All the experimental groups showed significant migration and narrowing of the scratch area by 10 hours. In comparison with control cultures, a delayed closure could be examined in LINC00941-deficient cultures (Figure 29: Scratch assay in LINC00941 deficient keratinocytes). The scratch area of control cultures was occupied by migrating keratinocyte cells after around 10 hours, whereas the LINC00941-deficient cultures showed

significant migration and only narrowing (35-47%) of the scratch area by 12-15 hours (Figure 29B). As described before, knockdown of LINC00941 led to decreased invasion in a matrigel invasion assay (see chapter 4.4.1), and also lower migrating potential was observed as expected.

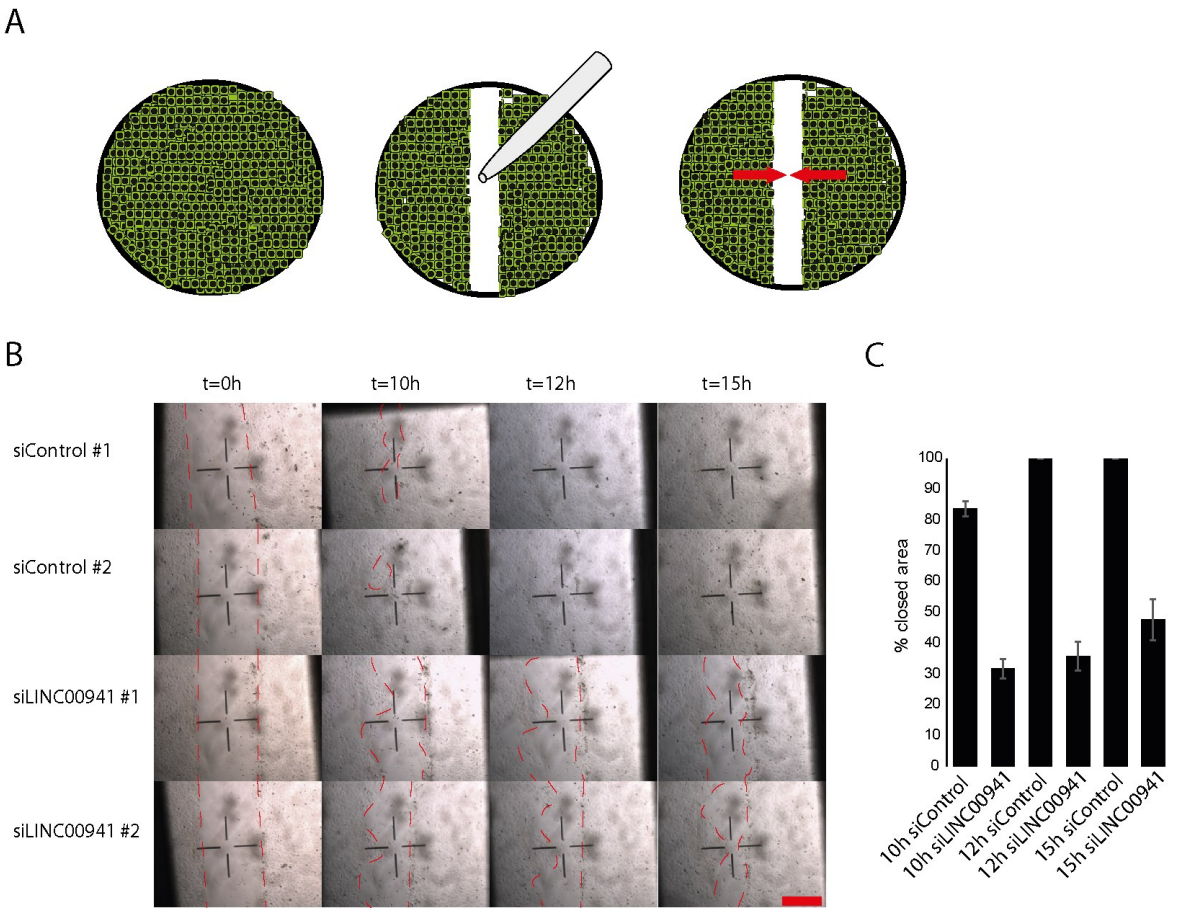

Figure 29: Scratch assay in LINC00941 deficient keratinocytes
(A) Principle of a scratch assay. (B) Time course of migrating keratinocytes upon LINC00941 knockdown. (C) Quantification of closed area relative to t=0 hours. Scale bar: 100 µm. Data are presented as mean ± SD.

Taken together, the lower migration potential and the lower invasive potential of LINC00941-deficient SCC cell lines strongly suggest a functional impact of LINC00941 in invasion, perhaps through a similar interdependent mechanism as seen in regulation of epidermal homeostasis. Indications for a tumor activating effect of LINC00941 can be deduced from the performed experiments, but subsequent studies are required to elucidate the functional role of LINC00941 in physiological conditions and SCC progression.

5 Discussion and outlook

5.1 Characterization of the LINC00941 transcript

To shed first light on the molecular mechanism of a given lncRNA, deciphering the cellular localization and expression of lncRNA isoforms of a specific locus, together with a comprehensive transcript characterization seemed necessary.

To this end, first subcellular fractionation in combination with RT-qPCR was employed during this project, hinting towards a dual localization of LINC00941 with increased cytoplasmic enrichment (chapter 4.1.2; Figure 8). Nevertheless, significant amounts of LINC00941 were also detected in the nuclear fraction when compared to mRNAs. As a complete separation of the cytosolic and nuclear fraction is difficult to achieve, single molecule *in situ* hybridization methods were used for further characterization. Other reports about lncRNA localization in skin utilized single molecule FISH analysis for example rather than a biochemical fractionation approach[137]. Advances in single-molecule methods have been invented to visualize lncRNAs in single cells at single-molecule resolution in order to characterize the subcellular localization of a given lncRNA.

Especially, the here used RNAScope method seemed to be applicable to keratinocytes since the utilized cytoplasmic positive controls repeatedly exhibited the expected cytoplasmic subcellular localization. Additionally, the negative control was characterized by a complete lack of signal. RNAScope showed a mainly cytosolic localization for LINC00941, however, nuclear signals were also detectable. Knockdown of LINC00941 in undifferentiated keratinocytes, however, clearly abolishes cytoplasmic signals for LINC00941, but the nuclear transcripts remain which is consistent with the known cytoplasmic location of the RNA-induced silencing complex (RISC)[260,261]. For complete subcellular localization studies an additional nuclear marker has to be involved. Nonetheless, LINC00941 might exhibit a dual nuclear and cytoplasmic distribution and thus might play multiple roles in different cellular compartments. One example of a lncRNA with these properties is the recently described PYCARD-AS1[262]. This lncRNA can localize to the PYCARD promoter where it facilitates DNA methylation and H3K9me2 modification by recruiting the chromatin-suppressor proteins DNMT1 and G9a. Moreover, both PYCARD-AS1 and PYCARD mRNA can interact with each other via their 5′ overlapping region, leading to inhibition of ribosome assembly in the cytoplasm for PYCARD translation[262].

Taken together, these inconclusive results should be interpreted as a first indication rather than a final proof of the LINC00941 localization. The conducted subcellular fractionation as well as the RNAScope approach should be further adapted in order to eventually unravel the subcellular localization of LINC00941 in keratinocytes and finally in epidermal tissue. Establishment of RNAScope in organotypic tissue and, subsequently, in human epidermis would be a big step towards characterization not only due to detecting the subcellular localization but also the distribution of LINC00941 during the time course of differentiation. So far, there are only indications for an increased localization of LINC00941 in undifferentiated keratinocytes.

With the advance in sequencing technologies over the recent years, numerous novel lncRNA transcripts have been identified and it became evident that several lncRNA isoforms can arise from one gene locus through a combination of alternative splicing, polyadenylation or promotor usage[153,313–315]. With LINC00941 being a novel lncRNA locus whose transcript has been annotated as a 1645 nt long lncRNA and regarding the recent miscellaneous annotations for this gene locus in the Ensembl and FANTOM5 release, an exact isoform characterization for LINC00941 became indispensable[265,316]. Thus, in order to elucidate the start and end point of the transcript with single nucleotide resolution, RACE analyses with a 5'cap dependent and a 3'-poly-A based strategy as well as long read Nanopore-Sequencing were conducted (chapter 4.1.2; Figure 11). Interestingly, both strategies revealed different 3´ends. Nanopore-sequencing reproducibly detected a 5'start site corresponding to FANTOM5 CAGE 5´start site. Combining these approaches with northern blot, one polyadenylated dominant LINC00941 isoform with 1327 bp could be identified in undifferentiated keratinocytes.

Recapitulating the obtained insights, there might be a dual localization and one dominant isoform in undifferentiated keratinocytes. However, the presented results might impact different roles of LINC00941 in various cellular compartments during epidermal differentiation (chapter 2.2.2). During the course of epidermal homeostasis, different stage-specific isoforms might be expressed and subsequently localized to different compartments. In the process of terminal differentiation, however, no final statement could be made about possible changes neither regarding localization nor expression of specific isoforms. These possible changes have to be biochemically verified with several isoform specific northern blots. These northern blots should be performed in time courses with fractionated keratinocytes to obtain insights into possible switches of isoforms and localization.

Combining these results with knowledge obtained with RNAScope in epidermal tissue, this will shed more light into the exact role of LINC00941 during epidermal homeostasis.

Moreover, unravelling how LINC00941 is embedded into other processes controlling epidermal homeostasis might lead to a better and more comprehensive understanding of other lncRNAs during epidermal homeostasis. Considering the transcriptional control of TINCR and ANCR regarding epidermal transcription factors MAF/MAFB, there seems to be a highly complex and elaborate network of lncRNAs and transcription factors regulating each other and collectively controlling epidermal tissue homeostasis[73].

5.2 LINC00941 as a novel player in epidermal homeostasis

Transcriptome sequencing analyses of non-differentiated and differentiated human keratinocytes revealed a number of lncRNAs that are dynamically regulated throughout terminal differentiation. LINC00941, which is encoded on chromosome 12, is most highly expressed in undifferentiated progenitor keratinocytes and significantly reduced in abundance upon onset of terminal differentiation, leading to a hypothetic role non- or poorly differentiated strata of the epidermis.

In order to reduce the cellular stress levels and the possible rescue effect of residual LINC00941 molecules, a CRISPR/Cas9 mediated LINC00941 depletion strategy was employed as a substitute for the electroporation based LINC00941 knockdown. As primary keratinocytes were unsuitable for a LINC00941 knockout cell line generation due to their limited amount of cell passages, the N/TERT keratinocyte cell lines were employed and successfully validated as a suitable model system for this experiment.

Since the transient transfection approach did not yield any LINC00941 knockout cell lines, a lentiviral delivery system promised to be more efficient for a stable genomic integration of gRNAs as well as the Cas9 endonuclease into wild type NTERT2G cells. This would ensure prolonged and constant expression of Cas9 and gRNAs at the same time, and thus might decrease the cellular stress level as well as increase the probability for genomic deletions.

The biggest drawback of knockout studies is that keratinocytes are prone to terminal differentiation and proliferate only for few passages in monoculture. The long process of clonal growth of single clones as well as the combination with harsh selection ultimately leads to growth arrest or death of transfected keratinocytes.

As successful knockout of lncRNAs in keratinocytes are still rarely reported, in this project siRNA-Pool mediated knockdowns were utilized as an alternative to investigate loss of function of LINC00941 in epidermal homeostasis.

Loss of LINC00941 transcript, in *in vitro* differentiated keratinocytes and in organotypic epidermal tissue cultures resulted in induced expression of several key differentiation markers on both mRNA and protein levels (Figure 15, Figure 18), whereas overexpression of LINC00941 resulted in decreased expression of differentiation genes (Figure 17). Moreover, the global RNA-sequencing approach of LINC00941 deficient epidermal tissue versus control tissue revealed that LINC00941 controls gene expression for a plethora of genes. Since the top GO-terms for genes, altered upon LINC00941 depletion, were associated with epidermal development and homeostasis, this experiment proved the importance of LINC00941 for keratinocyte differentiation (Figure 22). Strikingly, LINC00941 apparently controls the gene expression of almost the whole neighboring SPRR and LCE gene clusters over the course of the differentiation program suggesting a regulatory role of LINC00941 not in proximity of its site of transcription but in *trans* on chromosome 1 (Figure 22; Figure 23). These *trans*-regulatory roles of lncRNAs can be categorized into at least three major subgroups. First, lncRNAs can regulate chromatin states and gene expression at regions distant from their transcription site. Second, lncRNAs influence the nuclear structure or organization to orchestrate transcription or third, modulate the interaction and activity of interacting molecules[200]. Thus, assuming that LINC00941 exerts its cellular function as a *trans-acting* lncRNA and including the unclear subcellular localization, various modes of action are imaginable. Guidance of transcription factors, assembly of an active transcription machinery as well as altering the genomic accessibility or the histone marks at the regulated gene loci in the nucleus are potential mechanisms. Alternative regulation of enhancer elements especially in the EDC are possible (discussed in the next chapter)[69,317]. Similarly, LINC00941 might be responsible for the regulation of post-transcriptional events such as mRNA stability and translational control in the cytoplasm. Also, a combination of nuclear and cytoplasmic mechanisms might be possible.

In addition to that, LINC00941 deficiency led to induced expression of an uncharacterized gene locus comprising the recently annotated SPRR5 transcript[318]. Interestingly, significant induction of SPRR5 could be detected upon LINC00941 depletion. SPRR5 RNA was barely detectable in progenitor keratinocytes but strongly induced upon differentiation. The SPRR5 gene locus is located within the epidermal differentiation complex between the late cornified

envelope (LCE) gene cluster and the small proline-rich protein gene cluster. siRNA-Pool - mediated depletion of SPRR5 in keratinocytes and organotypic epidermis resulted in defective differentiation as seen by reduced levels of many early and late differentiation mRNAs and proteins. Interestingly, 54,8 % of genes induced in LINC00941-deficient epidermis were repressed in SPRR5-depleted organotypic tissue suggesting a common mode of action for both molecules. Additionally, co-depletion of LINC00941 and SPRR5 led to reduced levels of several conversely regulated differentiation proteins, suggesting that LINC00941-mediated repression of differentiation might indeed be, at least in part, mediated by repression of SPRR5[318].

As the analysis of regulated genes from the RNA-Seq experiment in LINC00941 depleted organotypic epidermis hints towards a regulation of complete clusters in the epidermal differentiation complex, a nuclear *trans-acting* mechanism in non or poorly differentiated cells was investigated further with a ChIRP-Seq experiment (chapter 4.3.2)[319]. Numerous publications reported a crucial role of activating and repressing histone marks in epidermal differentiation, which are controlled by many different molecular machineries (see also 2.1.3), and therefore an epigenetic mechanism for LINC00941 seemed also possible. Epigenetic mechanisms of the control of gene expression include several levels of regulation that can be based on: (a) changes in DNA methylation, (b) changes in the distribution of core histone variants, (c) changes in the nucleosome positioning relative to specific DNA sequences, and (d) changes in higher-order chromatin folding and genome organization[320–323].

5.3 Evidence for an epigenetic mechanism of LINC00941

As discussed above, LINC00941 might epigenetically control gene expression from the LCE and SPRR gene clusters in a *trans-acting* mechanism. Interaction studies of LINC00941 revealed binding to several distinct proteins including caspase-14 and several components of the NuRD complex. Caspase-14, which shows a restricted tissue expression in epidermal differentiation, is also strongly increased during terminal differentiation of keratinocytes, already suggesting a part in skin barrier formation[289]. Caspase-14 expression already starts in the spinous layer and it is active in the dehydrating environment of the cornified layer, where it has an important function in formation of the epidermal barrier leading to protection against UVB and water loss[291]. Furthermore, knockout studies of caspase-14 in mice have suggested a critical role in the maintenance of cornification through proteolytic processing of filaggrin[27,289–291]. Interaction of caspase-14 with LINC00941 might alter the activity or

the substrate specifity of caspase-14. Recent studies report several lncRNAs regulating caspases in various tissue types. This includes T-ALL-R-lncRNA that suppresses caspase-3 and is associated with T-cell acute lymphoblastic leukemia, HOXA-AS2 which suppresses cleavage of caspase-3, -8, and -9 in promyelocytic leukemia cell lines, or AFAP1-AS1 which inhibits caspase-3 cleavage in esophageal squamous cell carcinoma[324–327]. Proteomic approaches in LINC00941 deficient keratinocytes could lead to the identification of additional LINC00941-specific caspase-14 substrates. This ultimately could contribute to understand the role of caspase-14 together with LINC00941 in the skin.

Additionally, interaction of LINC00941 with components of the NuRD complex indicates first evidence for an RNA-mediated epigenetic mechanism (chapter 4.3.1). Supplementary, reports about mice deficient of several components of the NuRD complex such as Chd4 or Mta2 as well as Hdac1+2 double-deficient mice showed defective epidermal homeostatic activity with significant similarities to the phenotypes observed with LINC00941 knockdown[84,298,299]. Furthermore, LINC00941 pulldown could verify interaction with MTA2 as one of the core components of the NuRD complex. MTA2 has been shown to interact directly with the tumor suppressor p53 and it modulates its steady-state acetylation level[328]. Over-expression of MTA2 has been associated with deacetylation of p53[329]. This correlates with impaired ability of p53 to arrest cell growth and to mediate apoptosis[328].

In general, upon purification and characterization of the NuRD complex, ATP-dependent nucleosome remodeling activity coupled to histone tail deacetylase function could be identified[330]. NuRD complexes were found to consist of several subunits with varying composition dependent on targets and cell types. Initially identified as a transcriptional silencer or repressor, more complex roles on gene transcription including gene activation have been found[331,332]. In addition, many other significant biological functions (e.g. DNA repair) have been attributed to NuRD through its modifications of chromatin and post-translational modification of other transcription factors independent of regulating gene expression[331,332].

Interaction of LINC00941 with the NuRD-complex might either affect the activity or affinity of the NuRD-complex or might influence the guidance of the complex to specific loci, and might therefore alter the chromatin landscape of distinct loci as already observed for another lncRNA PAPAS (promoter and pre-rRNA antisense)[333]. PAPAS interacts directly with DNA forming a DNA-RNA triplex structure that guides associated CHD4/NuRD to the rDNA promoter and thereby regulates transcription[333]. A similar mechanism might be imaginable

for the interaction of LINC00941 and the NuRD complex. Including the fact that LINC00941 regulates gene expression from the LCE and SPRR gene clusters, guidance of the complex to specific loci and alteration of the chromatin landscape might be a possible. One of these loci might be the recently discovered specific regulatory enhancer 923. Sitting between the LCE and SPRR locus, the enhancer 923 responded to the developmental and spatio-temporal cues at the onset of epidermal differentiation in the mouse embryo[317]. Chromatin states of proliferating keratinocytes are marked by fewer interactions of 923 and do not express EDC genes. In contrast, differentiated keratinocytes are characterized by greater observed 923-mediated interactions with EDC gene promoters. LINC00941 together with the NuRD complex could either directly alter the chromatin state of the EDC by repressing the enhancer 923 in undifferentiated keratinocytes or could remodel the chromatin state of other loci, which are important for regulating epidermal homeostasis. This includes transcription factors or other chromatin modifying machineries. To test a direct impact of LINC00941/NuRD complex interaction on keratinocyte differentiation, several experiments could be performed to further strengthen this epigenetic hypothesis.

First, Assay for Transposase-Accessible Chromatin using sequencing (ATAC-Seq), a technique used in molecular biology to assess genome-wide chromatin accessibility, could be utilized here [334]. Changes in accessibility of distinct loci upon loss of either LINC00941 or NuRD components might give hints on a cooperative regulation. Second, Chromatin immunoprecipitation (ChIP) of several NuRD subunits should be performed upon LINC00941 knockdown to detect changes in binding sites of NuRD components[335]. For further analysis, comparative chromosomal conformation capture (3C) assays in proliferating and differentiated LINC00941-deficient keratinocytes might reveal multiple chromatin interactions in keratinocytes[336].

Finally, NuRD complex binding-deficient LINC00941 mutants should be generated. Once, the minimal fragment of LINC00941 capable of binding NuRD will be identified, RNA pull-down followed by mass spectrometry could be performed to verify interaction with the complex analog to full-length LINC00941. A minimal LINC00941 binding fragment might act as a dominant negative regulator of LINC00941 / NuRD-dependent regulation of epidermal homeostasis. This could be the basis for establishing a molecular tool to correct homeostatic defects of the epidermis as present in several skin diseases.

Furthermore, it should also be considered that LINC00941 might alter the distribution of histone modifications during the course of differentiation. Several differentiation-associated

genes are known to be suppressed in progenitor cells by the repressive histone mark H3K27me3 and are activated by demethylation upon induction of the terminal differentiation program[90]. Similar reports revealed differences for deposition of various histone modification such as H3K4me1, H3K27ac, H4K20me1, or H3K9ac between progenitor and differentiated keratinocytes [84,90–92]. In addition to that, LINC00941 might also affect the DNA methylation state, which has been found to be a crucial regulator of maintaining the keratinocyte progenitor state as loss of the DNA methyltransferase 1 (DNMT1), and thus a decreased DNA methylation rate at certain gene loci leads to premature keratinocyte differentiation[337]. These potential changes in distribution of histone modifications have to be tested in depth. Therefore, ChIP with following high throughput sequencing should be performed in the future. Here, several either repressing or activating histone modifications should be examined upon LINC00941 knockdown during the time course of differentiation.

In contrast to the regulation of complete clusters in the epidermal differentiation complex upon LINC00941 loss, no direct binding of LINC00941 in the epidermal differentiation complex could be identified in the ChIRP experiment. ChIRP-seq for LINC00941 has identified focal, specific, and numerous binding sites. In contrast to histone modifications, which often broadly occupy certain genomic elements (e.g., promoters, enhancers, transcribed exons, or silent genes), the interspersed and gene-selective nature of lncRNA occupancy more resembles transcription factors[319]. Motif enrichment analysis revealed that LINC00941 accesses the genome through specific GC rich DNA sequences in a highly discriminating fashion. The overlap of the binding sites with common transcription factor profiles and motif search analysis detected a high correlation with E2F transcription factor binding motifs. Especially, E2F4, and E2F6 showed high similarity to the detected binding motif. Additionally, the binding motif for TFDP1 as a known dimerization factor for the E2F family could be identified.

The E2F family has been implicated in controlling diverse critical cellular (entrance into S phase, regulation of mitosis, apoptosis, DNA repair, and DNA damage checkpoint control) and organismal (regulation of differentiation, development, and tumorigenesis) functions[302,303]. In humans, eight genes for E2F family members encoded in the genome[303,304]. The highest degree of homology among the E2F family members is in their DNA-binding domains which is consistent with the finding that they can all bind to the same consensus motif *in vitro*[305].

Most E2F family members are complexed with a member of the dimerization partner (DP) family of transcription factors to fulfill their function[303,306]. E2F4 binds DNA cooperatively

with DP proteins and is found in the promoter region of a number of genes whose products are involved in cell cycle regulation or in DNA replication[338–340]. E2F6 lacks the transcriptional activation pocket and protein binding domains. E2F6 appears to regulate a subset of E2F-dependent genes whose products are required for entry into the cell cycle but not for normal cell cycle progression[305,341]. This may silence expression via the recruitment of a chromatin remodeling complex containing histone H3K9 methyltransferase activity[342]. Common binding sites for LINC00941 and the E2F family hint towards a collectively regulated set of genes. Therefore, there might be a common mode of action. But, as many different potential mechanisms for LINC00941 and the E2F family are imaginable, future directions would aim to characterize the interplay of LINC00941 and the E2F transcription factor family.

In keratinocytes, ChIP experiments of E2F family members followed by high throughput sequencing, should be performed and compared with LINC00941 binding sites in the genome. Identification of molecules controlled by E2F as well as by LINC00941 might add further puzzle pieces in the highly complex network of lncRNAs and transcription factors regulating each other and controlling epidermal tissue homeostasis in a conjoined effort.

In summary, in depth functional, mechanistic and biochemical characterization of the Ribonucleoprotein particle, consisting of either LINC00941 and the NuRD complex or LINC00941 and Caspase-14, respectively, is necessary. Besides, the interplay with the E2F transcription factor family has to be analyzed in the future. The proposed analyses thus provide important novel insights into the mechanisms of lncRNAs in processes as epidermal growth, differentiation and regeneration.

5.4 Functional impact of LINC00941 in SCC-progression

LINC00941, proven to be functionally important for human epidermal homeostasis, is upregulated in human squamous cell carcinoma samples compared to healthy tissue controls (see chapter 2.3)[227,255]. This already implies an important function for LINC00941 in either cancer onset or development. Several analyses were performed to test whether LINC00941 plays a functional role in regulating cutaneous squamous cell carcinoma progression. Loss of LINC00941 led to reduced invasion of SCC-keratinocytes in a Matrigel invasion assay, whereas an increased differentiation could be observed in normal epidermal tissue (Figure 18, Figure 28). Since suppression of differentiation is an integral process during epidermal

squamous cell carcinoma, a reverse relationship between tissue differentiation and neoplastic progression was expected and observed. Additionally, knockdown of LINC00941 led to a slower migration of keratinocytes in scratch assays. Altogether, this led to the hypothesis that high levels of LINC00941 promote neoplasia or tumor progression in cutaneous squamous cell carcinoma. Despite a vast amount of lncRNAs have been reported to have an aberrant expression pattern in cancer and in particular in skin cancer progression, their significant role for carcinogenesis is still not completely clear (see chapter 2.2.4). Current knowledge about lncRNAs as regulators of SCC progression and about their molecular modes of action is still limited and impressively highlights the importance of elucidating the functional role of lncRNAs in physiological conditions and keratinocyte cancer development[201]. Recently identified examples for lncRNAs playing a functional role in SCC progression are PICSAR and PRECSIT[139,237]. The lncRNA PICSAR was found to be upregulated in SCC cells compared to normal keratinocytes and promotes growth of SCC by regulating ERK1/2 activity[139]. In addition, PICSAR upregulates expression of integrins resulting in increased cell adhesion and decreased cell migration on collagen I and fibronectin in SCC cells[139,236].

Another identified lncRNA with elevated expression in SCC compared to normal skin is PRECSIT[237]. Loss of PRECSIT inhibits SCC cell invasion by repressing STAT3 expression and activation[237].

Similar to PICSAR and PRECSIT, LINC00941 exhibits elevated expression in SCC samples. Loss of LINC00941 leads to reduced invasion and migration of SCC keratinocytes (see chapters 4.4.1 and 4.4.2). Regarding the combination of these results with the diminished differentiation phenotype obtained by forced LINC00941 expression (see chapters 4.2.2 and 4.2.3) together with the lack of differentiation being a hallmark of skin cancer, LINC00941 seems to play a dual role during differentiation as well as during skin cancer progression. Further indications for a role of LINC00941 in tumorigenesis are a potential interaction with components of the NuRD complex (see chapter 4.3.1) and sharing a similar binding motif as the E2F transcription family (see chapter 4.3.2). Components of the NuRD complex as well as the E2F family are already known to play distinct roles in human tumorigenesis, thus indicating a potential synergetic role of LINC00941 with these molecules[297,342,343].

Taken together, results obtained from normal epidermal homeostasis should be conveyed to SCC progression to analyze the interplay of LINC00941 together with the NuRD complex as well as the E2F family. To shed further light on the possible link between LINC00941

and carcinogenesis, the commonly used colony formation assay, scratch assay or a transwell invasion assay might be applied in the future[307,344].
To obtain a better understanding of these pro-tumorigenic functions of LINC00941, the impact of LINC00941 loss could be studied in an invasive three-dimensional organotypic neoplasia tissue model, which recapitulates natural features of tumor progression. Additionally, the impact of LINC00941 on tumor development can be assessed by an *in vivo* tumor formation assay[345].

Since both experiments need adequate and long-lasting LINC00941 loss, knockdown of LINC00941 might not be sufficient. But this problem can only be overcome by a LINC00941 knockout. Unfortunately, successful knockout studies of lncRNAs in keratinocytes are still sparse. A big breakthrough on the way to detect the mechanism of LINC00941 would be the establishing of a successful LINC00941 knockout cell line (see chapter 4.2.1 and 5.1).

Subsequently, these cells can be used to generate invasive organotypic neoplastic tissue. For that purpose, an organotypic model of Ras/Erk MAPK-driven epithelial neoplasia can be used. In order to transform organotypic human epidermal tissue into invasive neoplasia, human HRasG12V and simultaneous Cdk4 have to be overexpressed. Oncogenic Ras overexpression alone leads to cell cycle arrest in G1 phase, whereas Cdk4 co-expression bypasses Ras growth suppression and induces invasive human neoplasia resembling squamous cell carcinoma[125,346]. Next, these tumorigenic keratinocytes can be seeded onto a dermal matrix with embedded fibroblasts, and the resulting tissue can be harvested six or eight days after seeding. Invasion of keratinocytes into the dermal matrix can be analyzed by immunofluorescence analyses[124,345](see chapter 2.1.4).

In a further approach, the influence of LINC00941 loss on tumor formation and growth should be addressed *in vivo* in a Xenograft model. Therefore, the tumorigenic keratinocytes as described above with additional overexpression of a luciferase-YFP fusion protein can be injected into the flank of immunodeficient mice. Then tumor growth can be monitored over time by *in vivo* luciferase measurements and volumetric tumor measurements.

Afterwards, experiments should be expanded to analyze the interplay between LINC00941 and NuRD components as well as E2F family members (in a similar manner as described in chapter 5.3). Correspondingly, experimental groups showing an effect on cell invasion can subsequently be tested for changes in chromatin regulation, NuRD complex assembly, or

occupancy of differentiation genes/gene clusters using ChIP-seq, ATAC-seq, and mass spectrometry analyses.

The obtained data about the role of the novel lncRNA LINC00941 in normal epidermal development as well as in skin diseases contribute to a more profound characterization and further understanding of the complexity of lncRNAs in general. Further analysis of LINC00941 should aim to a profound description of its specific mode of action in the intriguing regulatory network of epidermal homeostasis. These new insights should be conveyed towards the involvement in skin cancer progression or the generation of other skin diseases.

6 Materials and methods

6.1 Antibodies and beads

6.1.1 Antibodies

Table 1: Primary antibodies used during this thesis

Name	Source	Dilution (Fixative)	Application	Supplier
α-β-actin	mouse, monoclonal AC-15	1:5,000	WB	Sigma-Aldrich, A1978
α-β-actin	mouse, monoclonal AC-15	1:10,000	WB	Abcam, ab6276
α-collagen VII	rabbit, polyclonal	1:400 (dependent on diff. marker)	IF staining	Merck Millipore, 234192
α-collagen VII	mouse, monoclonal LH7.2	1:800 (dependent on diff. marker)	IF staining	Merck Millipore, MAB1345
α-collagen VII	mouse, monoclonal clone32	1:1,000 (methanol/acetone 1:1)	IF staining (tissue: 7.3.1)	Merck Millipore, MAB2500
α-Filaggrin	mouse, monoclonal	1:50 (ethanol)	IF staining	Santa Cruz Biotechnology, sc-66192
α-Loricrin	rabbit, polyclonal	1:800 (acetone)	IF staining	Covance, PRB-145P
α-Loricrin	rabbit, polyclonal	1: 1,000	WB	Covance, PRB-145P
α-Keratin1	rabbit, polyclonal	1:1,000	WB	Covance, PRB-149P
α-Keratin1	rabbit, polyclonal	1:2,000 (methanol)	IF staining	Covance, PRB-149P

Table 2: Utilized secondary antibodies

Name	Source	Dilution	Application	Supplier
Alexa Fluor 488 goat α-rabbit IgG	goat, polyclonal	1:300	IF staining	Thermo Fisher Scientific, A-11008
Alexa Fluor 488 goat α-mouse IgG	goat, polyclonal	1:300	IF staining	Thermo Fisher Scientific, A-11001

Alexa Fluor 555 goat α-rabbit IgG	goat, polyclonal	1:300	IF staining	Thermo Fisher Scientific, A-21428
Alexa Fluor 555 goat α-mouse IgG	goat, polyclonal	1:300	IF staining	Thermo Fisher Scientific, A-21422
IRDye 680RD goat α-mouse IgG	goat, polyclonal	1:15,000	WB	LI-COR Biosciences, 926-68070
IRDye 800CW goat α-mouse IgG	goat, polyclonal	1:15,000	WB	LI-COR Biosciences, 926-32210
IRDye 800CW goat α-rabbit IgG	goat, polyclonal	1:15,000	WB	LI-COR Biosciences, 926-32211

6.1.2 Beads

Table 3: Overview of utilized beads

Name	Application	Supplier	Catalogue number
Agencourt AMPure XP beads	ChIRP-Seq, ChIP-Seq	Beckman Coulter	A63880
nProtein A Sepharose 4 Fast Flow	ChIP-Seq	Merck	GE17-5280-04
Sepharose CL-4B beads	ChIP-Seq	Merck	CL4B200

6.2 Buffers and solutions

All buffers and solutions were prepared with deionized H_2O unless stated otherwise.

Table 4: Utilized buffers and solutions

Buffer/Solution	Composition	
10% APS	10% (w/v)	ammonium persulfate in water
2x RNA loading dye	20 mM	MOPS, pH 7.0
	5 mM	sodium acetate
	1 mM	EDTA
	5.9% (v/v)	formaldehyde
	45% (v/v)	formamide
	0.01% (w/v)	bromophenol blue
	5% (v/v)	glycerol
2x SSC	300 mM	sodium chloride
	30 mM	sodium citrate
		pH 7.0
20x SSC	3 M	sodium chloride
	0.3 M	sodium citrate
		pH 7.0
4x Resolving gel buffer	1.5 M	Tris
	0.4% (w/v)	SDS
		pH 8.8
4x Stacking gel buffer	0.5 M	Tris
	0.4% (w/v)	SDS

		pH 6.8
5x laemmli buffer	300 mM	Tris/HCl, pH 6.8
	10% (w/v)	SDS
	62.5% (v/v)	glycerol
	0.1% (w/v)	bromophenol blue
	10% (v/v)	β-mercaptoethanol, added fresh before use
ATAC resuspension buffer	10 mM	Tris/HCl, pH 7.4
	10 mM	NaCl
	3 mM	$MgCl_2$
Coomassie fixative	10% (v/v)	acetic acid
	50% (v/v)	methanol
ChIP-Seq elution buffer	1% (w/v)	SDS
	100 mM	sodium hydrogen carbonate
ChIP RIPA buffer	1% (v/v)	NP-40
	0.5% (w/v)	sodium deoxycholate
	0.1% (w/v)	SDS
	1 mM	EDTA
	add before use:	in PBS, pH 7.8
	1x	protease inhibitor (Roche)
	1 mM	AEBSF
	10 mM	sodium butyrate
ChIP swelling buffer	100 mM	Tris/HCl, pH 7.6
	10 mM	Potassium acetate
	15 mM	magnesium acetate
	1% (v/v)	NP-40
	add before use:	
	1x	protease inhibitor (Roche)
	1 mM	AEBSF
	10 mM	sodium butyrate
ChIP-Seq DB	20 mM	Tris/HCl, pH 7.4
	100 mM	sodium chloride
	2 mM	EDTA
	0.5% (v/v)	Triton X-100
	add before use:	
	1 mM	AEBSF
	10 mM	sodium butyrate
	1x	protease inhibitor (Roche)
ChIP-Seq WB I	20 mM	Tris/HCl, pH 7.4
	150 mM	sodium chloride
	0.1% (w/v)	SDS
	1% (v/v)	Triton X-100
	2 mM	EDTA
ChIP-Seq WB II	20 mM	Tris/HCl, pH 7.4
	500 mM	sodium chloride
	1% (v/v)	Triton X-100
	2 mM	EDTA
ChIP-Seq WB III	10 mM	Tris/HCl, pH 7.4
	250 mM	lithium chloride
	1% (v/v)	NP-40
	1% (w/v)	sodium deoxycholate
	1 mM	EDTA
DNA loading dye	0.25% (w/v)	bromophenol blue
	30% (v/v)	glycerol
Hoechst solution	4 µg/ml	Hoechst 33342

		dissolved in PBS
hybridization solution	750 mM	sodium chloride
	75 mM	sodium citrate
	20 mM	disodium phosphate, pH 7.2
	7% (w/v)	SDS
	0.02% (w/v)	albumin fraction V
	0.02% (w/v)	Ficoll400
	0.02% (w/v)	polyvinylpyrrolidon K30
LB medium	1% (w/v)	sodium chloride
	1% (w/v)	tryptone
	0.5% (w/v)	yeast extract
		pH 7.4, autoclaved before usage
LB-Amp	0.01% (w/v)	ampicillin
		added to LB medium after sterilization
LB-(Amp)agar	1.5% (w/v)	agar
	0.01% (w/v)	ampicillin
		dissolved in LB medium
NB wash I	750 mM	sodium chloride
	75 mM	sodium citrate
	1% (w/v)	SDS
		pH 7.0
NB wash II	150 mM	sodium chloride
	15 mM	sodium citrate
	1% (w/v)	SDS
		pH 7.0
PBS	140 mM	sodium chloride
	2.7 mM	potassium chloride
	10 mM	disodium phosphate
	1.8 mM	monopotassium phosphate
		pH 7.2
protein lysis buffer	25 mM	Tris/HCl, pH 7.5
	150 mM	sodium chloride
	5% (v/v)	glycerol
	2 mM	EDTA
	0.3% (w/v)	NP-40
	1 mM	dithiothreitol, added fresh
	1x	cOmplete, EDTA-free Protease Inhibitor Cocktail (Roche), added fresh
RIPA	50 mM	Tris/HCl, pH 7.5
	150 mM	sodium chloride
	0.1% (w/v)	SDS
	1% (w/v)	sodium deoxycholate
	1% (w/v)	NP-40
	1 mM	dithiothreitol, added fresh
	1x	cOmplete, EDTA-free Protease Inhibitor Cocktail (Roche), added fresh
RNA gel buffer	20 mM	MOPS
	5 mM	sodium acetate
	1 mM	EDTA
	1.9% (v/v)	formaldehyde
		pH 7.0
siRNA annealing buffer	60 mM	HEPES
	4 mM	magnesium acetate
	200 mM	potassium acetate

TAE	8 mM	Tris
	0.2 mM	EDTA
	4 mM	acetic acid
TBS-T	10 mM	Tris
	150 mM	sodium chloride
	0.02 % (w/v)	Tween-20
TE	10 mM	Tris
	1 mM	EDTA
		pH 8.0
TGS	25 mM	Tris
	192 mM	glycine
	0.1% (w/v)	SDS
		pH 8.3
TFBI	30 mM	potassium acetate
	50 mM	manganese chloride
	100 mM	rubidium chloride
	10 mM	calcium chloride
	15% (v/v)	glycerol
		pH 5.8, filtered sterile through 0.2 µm pore filter
TFBII	10 mM	MOPS sodium salt
	75 mM	calcium chloride
	10 mM	rubidium chloride
	15% (v/v)	glycerol
		pH 7.0, filtered sterile through 0.2 µm pore filter
YT-medium	0.8% (w/v)	tryptone
	0.5% (w/v)	yeast extract
	85 mM	sodium chloride
	20 mM	magnesium sulfate
	10mM	potassium chloride
		pH 7.5, autoclaved before usage
western blot transfer buffer	25 mM	Tris
	192 mM	glycine
	20% (v/v)	methanol
		pH 8.6

6.3 Chemicals, enzymes, and peptides

Unless stated otherwise, chemicals were purchased from Applichem (Darmstadt, Germany), Bio-Rad (Hercules, USA), Carl Roth (Karlsruhe, Germany), Merck (Darmstadt, Germany), Roche (Basel, Switzerland), Sigma-Aldrich (St. Louis, USA), Thermo Fisher Scientific (Waltham, USA), VWR International (Radnor, USA) and Weckert Labortechnik (Kitzingen, Germany).

Radiochemicals were purchased from Hartmann Analytics (Braunschweig, Germany), restriction enzymes, enzymes for RNA and DNA modifications (ligases, polymerases etc.) and markers were purchased from Bio-Rad (Hercules, USA), Merck (Darmstadt, Germany), New England Biolabs (Ipswich, USA), Roche (Basel, Switzerland) and Thermo Fisher

Scientific (Waltham, USA).

6.4 Commercial kits

Commercial kits were used according to their included manuals unless stated otherwise.

Table 5: List of commercial kits

Name	Supplier	Catalogue number
Agilent High Sensitivity DNA Kit	Agilent Technologies (Santa Clara, USA)	5067-4626
Agilent RNA 6000 Pico Kit	Agilent Technologies (Santa Clara, USA)	5067-1513
Cytoplasmic and Nuclear RNA Purification Kit	Norgen Biotek (Thorold, Canada)	21000
DNase I, RNase-free	Thermo Fisher Scientific (Waltham, USA)	EN0521
ERCC RNA Spike In Mix	Thermo Fisher Scientific (Waltham, USA)	4456740
Expand Long Template PCR System	Sigma-Aldrich (St. Louis, USA)	11681834001
FirstChoice RLM-RACE Kit	Thermo Fisher Scientific (Waltham, USA)	AM1700
High Sensitivity D1000 ScreenTape and reagents	Agilent Technologies (Santa Clara, USA)	5067- 5584; 5067- 5585
Human Keratinocyte Nucleofector Kit	Lonza (Basel, Switzerland)	VVPD-1002
illustra MicroSpin G-25 Columns	GE Healthcare (Chalfont St Giles, Great Britain)	27532501
iScript cDNA Synthesis Kit	Bio-Rad (Hercules, USA)	170-8890
Lipofectamine 3000	Thermo Fisher Scientific (Waltham, USA)	L3000015
Monarch PCR & DNA Purification Kit	New England Biolabs (Ipswich, USA)	T1030S
NEBNext Multiplex Oligos for Illumina	New England Biolabs (Ipswich, USA)	E7335 (Set1) E7500 (Set 2)
NEBNext Ultra II DNA Library Prep Kit for Illumina	New England Biolabs (Ipswich, USA)	E7645
Nextera DNA Library Preparation Kit	Illumina (San Diego, USA)	FC-121-1030
Nextera Index Kit	Illumina (San Diego, USA)	FC-121-1011
NucleoBond Xtra Maxi EF	Macherey-Nagel (Dueren, Germany)	740424
NucleoBond Xtra Midi Kit	Macherey-Nagel (Dueren, Germany)	740410
NucleoSpin Gel and PCR Clean-up Kit	Macherey-Nagel (Dueren, Germany)	740609
NucleoSpin Plasmid (NoLid)	Macherey-Nagel (Dueren, Germany)	740499
pGEM-T Easy Vector Kit	Promega (Madison, USA)	A1360
Pierce BCA Protein Assay Kit	Thermo Fisher Scientific (Waltham, USA)	23225
PrecisionX Multiplex gRNA Cloning Kit	BioCat (Heidelberg, Germany)	CAS9-GRNA-KIT-SBI
QIAShredder	Qiagen (Hilden, Germany)	79654
QIAquick PCR Purification Kit	Qiagen (Hilden, Germany)	28106
Qubit dsDNA HS Assay Kit	Thermo Fisher Scientific (Waltham, USA)	Q32851
RNeasy Plus Mini Kit	Qiagen (Hilden, Germany)	74136

Roti-Quant	Carl Roth (Karlsruhe, Germany)	K015.1
SsoFast EvaGreen	Bio-Rad (Hercules, USA)	1725200
Takyon No ROX SYBR 2x MasterMix blue dTTP	Eurogentec (Luettich, Belgium)	UF-NSMT-B0701
TURBO DNA-free Kit	Thermo Fisher Scientific (Waltham, USA)	AM1907
TruSeq Stranded mRNA Library Prep	Illumina (San Diego, USA)	20020594

6.5 Consumables, membranes, and screens

Consumables were, unless stated otherwise, purchased from Bio-Rad (Hercules, USA), Carl Roth (Karlsruhe, Germany), Eppendorf (Hamburg, Germany), Eurogentec (Luettich, Belgium), GE Healthcare (Chalfont St Giles, Great Britain), MP Biomedicals (Heidelberg, Germany), NeoLab (Heidelberg, Germany), Sarstedt (Nuembrecht, Germany), Thermo Fisher Scientific (Waltham, USA) or VWR International (Radnor, USA).

Table 6: List of membranes and screens

Name	Supplier	Catalogue number
Amersham Hybond-ECL	GE Healthcare (Chalfont St Giles, Great Britain)	RPN132D
Amersham Hybond-N+	GE Healthcare (Chalfont St Giles, Great Britain)	RPN203B
Storage Phosphor Screen GP	Kodak (Rochester, NY, USA)	1707843

6.6 Eukaryotic cell cultivation

Dermis for regenerated organotypic epidermal tissue cultures was prepared from frozen split-skin obtained from Biopredic International (Saint-Grégoire, France), Tissue Solutions (Glasgow, Great Britain). Utilized primary cells, cell lines, media components and their composition are listed below.

Table 7: Overview of primary eukaryotic cells and cell lines

Name	Details	Supplier
HaCaT cell line	Catalogue number 300493	Cell Lines Service (Eppelheim, Germany)
HEK293T cells	gift from the AG Meister	AG Meister (Regensburg, Germany)
Normal Human Epidermal Keratinocytes (NHEK), adult single donor	isolated from fresh surgical specimens at the University Hospital Regensburg	AG Kretz
Normal Human Epidermal Keratinocytes (NHEK), juvenile foreskin, pooled	Lot numbers: 1020401, 1040101 and 407Z001	PromoCell (Heidelberg, Germany)
NTERT2G	gift from the van den Boogard group	Radboud university (Netherlands)

NTERT1	gift from the van den Boogard group	Radboud university (Netherlands)
3T3-J2	Catalogue number EF3003	Kerafast (Boston, MA)

Table 8: Reagents for eukaryotic cell cultures

Name	Supplier	Catalogue number
3,3',5'-Triiodo-L-thryonine	Sigma-Aldrich (St. Louis, USA)	T0281
Adenine hydrochloride hydrate	Sigma-Aldrich (St. Louis, USA)	A-9795
100x Antibiotic-Antimycotic	Thermo Fisher Scientific (Waltham, USA)	15240-096
Cholera toxin from Vibrio cholerae	Sigma-Aldrich (St. Louis, USA)	C8052
Corning Matrigel	Thermo Fisher Scientific (Waltham, USA)	11543550
DMSO	Carl Roth (Karlsruhe, Germany)	A994.1
Dulbecco's Modified Eagle Medium, high glucose, pyruvate (DMEM)	Thermo Fisher Scientific (Waltham, USA)	41966-029
Dulbecco's Phosphate-Buffered Saline, no calcium, no magnesium (DPBS)	Thermo Fisher Scientific (Waltham, USA)	14190-094
Epidermal Growth Factor human	Sigma-Aldrich (St. Louis, USA)	E9644
Fetal Bovine Serum	Thermo Fisher Scientific (Waltham, USA)	10270-106
Ham's F12	Lonza (Basel, Switzerland)	BE12-615F
Holo-Transferrin human	Sigma-Aldrich (St. Louis, USA)	T0665
Human Keratinocyte Growth Supplement	Thermo Fisher Scientific (Waltham, USA)	S-001-5
HyClone Bovine calf serum	Thermo Fisher Scientific (Waltham, USA)	SH3007303
HyClone Characterized Fetal Bovine serum	Thermo Fisher Scientific (Waltham, USA)	SH3007103
Hydrocortisone	Sigma-Aldrich (St. Louis, USA)	H0396
Insulin solution human	Sigma-Aldrich (St. Louis, USA)	I9278
Keratinocyte-SFM Serum Free Medium	Thermo Fisher Scientific (Waltham, USA)	17005-042
Medium 154	Thermo Fisher Scientific (Waltham, USA)	M-154-500
Opti-MEM Reduced Serum Medium	Thermo Fisher Scientific (Waltham, USA)	31985070
Penicillin-Streptomycin (10000 U/ml)	Thermo Fisher Scientific (Waltham, USA)	15140-122
Puromycin dihydrochloride	Carl Roth (Karlsruhe, Germany)	0240.3
Polybrene	Sigma-Aldrich (St. Louis, USA)	10768910G
Supplements for Keratinocyte-SFM	Thermo Fisher Scientific (Waltham, USA)	37000-015
Trypsin-EDTA 0.05%, phenol red	Thermo Fisher Scientific (Waltham, USA)	25000-054

Trypsin-EDTA 0.25%, phenol red	Thermo Fisher Scientific (Waltham, USA)	25200-056

Table 9: Components and composition of cell culture medium

Medium/Solution	Composition	
50:50 medium	500 ml	Keratinocyte SFM
	500 ml	Medium 154
	5 ml	Human Keratinocyte Growth Supplement
	10 ml	100x Antibiotic-Antimycotic
	1x	Supplements for Keratinocyte-SFM
Adenine stock solution	12 mg	Adenine hydrochloride hydrate
	6.75 ml	DMEM
		adjust pH to 7.5
Basic buffer	0.2 M	sodium chloride
	3 mM	sodium azid
	1 mM	EDTA
		adjust pH to 8.0
Cholera toxin solution	1 mg	Cholera toxin from *Vibrio cholera*
	1 ml	Basic buffer
	99 ml	DMEM
Conditioned 50:50 medium		50:50 medium which was used for cultivation of HaCaT cells for two days and subsequently filtered through a 0.2 µm pore filter
DMEM+BCS	500 ml	DMEM
	50 ml	BCS
	5 ml	Penicillin/Streptomycin
DMEM+FBS	500 ml	DMEM
	50 ml	FBS (Thermo)
	5 ml	Penicillin/Streptomycin
EGF stock solution	100 µg	EGF
	10 ml	ddH_2O
Hydrocortisone stock solution	5 mg	Hydrocortisone
	1 ml	Ethanol
	24 ml	DMEM
Insulin stock solution	5 mg	Insulin solution human
	1 ml	ddH_2O
KGM	330 ml	DMEM
	110 ml	Ham's F12
	5 ml	Penicillin-Streptomycin
	5 ml	100x Antibiotic-Antimycotic
	50 ml	FBS (HyClone)
	1 ml	Adenine stock solution
	0.5 ml	Cholera toxin solution
	1 ml	Hydrocortisone stock solution
	0.5 ml	T/T3 solution
	0.5 ml	EGF stock solution
	0.5 ml	Insulin stock solution
PBS+2x A/A	10 ml	100x Antibiotic-Antimycotic
	500 ml	DPBS
Polybrene solution	1 mg/ml	Polybrene in PBS
T/T3 solution	9.9 ml	Transferrin stock solution

	100 µl	Triiodo-L-thyronine stock solution
Transferrin stock solution	50 mg 10 ml	Holo-Transferrin human DPBS
Triiodo-L-thyronine stock solution	13.6 mg 100 ml	3,3',5'-Triiodo-L-thyronine ddH_2O

6.7 Instruments

General laboratory instruments and devices were purchased from Beckman Coulter (Brea, USA), Bio-Rad (Hercules, USA), Eppendorf (Hamburg, Germany), NeoLab (Heidelberg, Germany) and Thermo Fisher Scientific (Waltham, USA). Particular instruments are listed in the table below.

Table 10: List of instruments

Name	Supplier
2200 TapeStation System	Agilent Technologies (Santa Clara, USA)
Agilent 2100 Bioanalyzer	Agilent Technologies (Santa Clara, USA)
Amersham Ultrospec 3300 pro	GE Healthcare (Chalfont St Giles, Great Britain)
Centrifuge 5424 R	Eppendorf (Hamburg, Germany)
Centrifuge 5810	Eppendorf (Hamburg, Germany)
CO_2-Incubator HERAcell 240i	Thermo Fisher Scientific (Waltham, USA)
Cryostat Microm HM 500 OM	Thermo Fisher Scientific (Waltham, USA)
Electroporation Device Nucleofector II	Lonza (Basel, Switzerland)
FastPrep-24 Instrument	MP Biomedicals (Heidelberg, Germany)
Heraeus Megafuge 40R	Thermo Fisher Scientific (Waltham, USA)
Heraeus Multifuge 1S	Thermo Fisher Scientific (Waltham, USA)
HeraSafe KS	Thermo Fisher Scientific (Waltham, USA)
HiSeq 1000	Illumina (San Diego, USA)
Hybridization oven type T 5042	Heraeus (Hanau, Germany)
IKA MS3	Agilent Technologies (Santa Clara, USA)
Incubator Model B6200	Heraeus (Hanau, Germany)
Inverted microscope Axiovert 200 M	Carl Zeiss (Oberkochen, Germany)
Inverted microscope Diavert	Leitz (Wetzlar, Germany)
IVIS 100 In Vivo Imaging System	PerkinElmer (Waltham, USA)
Leica CM3050 S Cryostat	Leica Biosystems (Nussloch, Germany)
MaXis plus UHR-QTOF	Bruker (Billerica, USA)
MilliQ Q-Pod	Merck (Darmstadt, Germany)
Mx3000P	Agilent Technologies (Santa Clara, USA)
NanoDrop 1000	Thermo Fisher Scientific (Waltham, USA)
Nanophotometer Classic	Implen (Munich, Germany)
New Brunswick Innova 44 Shaker	Eppendorf (Hamburg, Germany)
Odyssey Imaging System	LI-COR Biosciences (Lincoln, USA)
PM1002 mobile anesthesia machine	Parkland Scientific (Coral Springs, USA)
PMI Personal Molecular Imager FX	Bio-Rad (Hercules, USA)
QTRAP 4500	SCIEX (Framingham, USA)
Qubit 2.0 Fluorometer	Thermo Fisher Scientific (Waltham, USA)

Real-Time PCR Cycler CFX96	Bio-Rad (Hercules, USA)
S220 Focused-ultrasonicator	Covaris (Woburn, USA)
Screen Eraser-K	Bio-Rad (Hercules, USA)
Shake 'n' Stack Hybridization Oven	Thermo Fisher Scientific (Waltham, USA)
Thermomixer comfort	Eppendorf (Hamburg, Germany)
Trans-Blot SD Semi-dry transfer cell	Bio-Rad (Hercules, USA)
Transilluminator Quantum ST4	PEQLAB (Erlangen, Germany)
UltiMate 3000 RSLCnano System with Acclaim PepMap100 C18 Nano-Trap column and Acclaim PepMap100 C18 column	Thermo Fisher Scientific (Waltham, USA)
UV Stratalinker 2400	Stratagene (La Jolla, USA)

6.8 Oligonucleotides

DNA oligonucleotides were ordered from Metabion (Martinsried, Germany) or Sigma-Aldrich (St. Louis, USA), siRNA Pools (mixture of 11-30 different siRNAs per target, exact sequences are available from siTools upon request) were designed and ordered from siTools (Munich, Germany) and single siRNAs were obtained from biomers.net (Ulm, Germany).

Table 11: Overview of utilized siRNAs

siRNA	Sequence (5' to 3')
Control_sense	GUAGAUUCAUAUUGUAAGG
Control_antisense	CCUUACAAUAUGAAUCUAC
pan_p63i_sense	CGACAGUCUUGUACAAUUU
pan_p63i_antisense	AAAUUGUACAAGACUGUCG
siCtrl	siPool
siLINC00941	siPool

Table 12: List of sequencing primers

Name	Sequence (5' to 3')
5'Cas9_seq_R	CCGATGCTGTACTTCTTGTC
CMV_F	CGCAAATGGGCGGTAGGCGTG
KO_out_F2	CCAACTCTAAGAGAGGTAAGTATG
KO_out_R2	GTATGCAGTGTTTGCATAGACTGTC
lentiCRISPRv2_seq_F	GGACAGCAGAGATCCAGTTT
lentiCRISPRv2_seq_R	AGCCAATTCCCACTCCTTTC
pLARTA_F5	AGAATCGCAAAACCAGCAAG
PGK_F	TGTTCCGCATTCTGCAAGCC
pLARTA_Ins_F	CGAATCACCGACCTCTCTCC
pLARTA_R1	AAACCGTCTATCAGGGCGAT
pX459_F	TTACGGTTCCTGGCCTTTTG
pX459_R	TGTCTGCAGAATTGGCGCA
SP6	ATTTAGGTGACACTATAG
T7	TAATACGACTCACTATAGGG
WPRE-rev	CATAGCGTAAAAGGAGCAACA

Table 13: List of primer sequences used for qRT-PCR

Name	Forward primer (5' to 3')	Reverse primer (5' to 3')
LINC00941	GACCTTTTCAGGCCAGCATT	ACAATCTGGATAGAGGGCTCA
7SK	CCTGCTAGAACCTCCAAACAAG	GCCTCATTTGGATGTGTCTG
ALOX12B	AGACTGCAATTCCGGATCAC	TGTGGAATGCACTGGAGAAG
β-actin	GGACTTCGAGCAAGAGATGG	AGGAAGGAAGGCTGGAAGAG
CALB1	TGGCTTTGTCGGATGGAGGG	GGTTGCGGCCACCAACTCTA
C1orf68	TTCTGGCCCCCTCTCTGTTA	GGGACTGTACTAACTCTGGC
ELOVL3	TTCGAGGAGTATTGGGCAAC	GAAGATTGCAAGGCAGAAGG
FLG	AAAGAGCTGAAGGAACTTCTGG	AACCATATCTGGGTCATCTGG
GAPDH	GAAGAGAGAGACCCTCACTGCTG	ACTGTGAGGAGGGGAGATTCAGT
preGAPDH	CCACCAACTGCTTAGCACC	CTCCCCACCTTGAAAGGAAAT
KRT1	TGAGCTGAATCGTGTGATCC	CCAGGTCATTCAGCTTGTTC
KRT10	GCAAATTGAGAGCCTGACTG	CAGTGGACACATTTCGAAGG
L32	AGGCATTGACAACAGGGTTC	GTTGCACATCAGCAGCACTT
LacZ	GTGCGGATTGAAAATGGTCT	GACCTGACCATGCAGAGGAT
LCE1A	GAAGCGGACTCTGCACCTAGAA	AGGAGACAGGTGAGGAGGAAATG
LCE1E	TGAAGTGGACCTTGACTTCCTC	CTCCAGGCAAGACTTCAAGC
LCE2A	TGGAGAAACTTGCAACCAGGA	CCTCACAAGGTGTGTCAGCC
LCE2D	GGACGTGTCTGTGCTTTTGC	CTTGGGAGGACATTTGGGAGG
LCE3A	TGTCTGCCTCCAGCTTCCT	AGTTGGAGCTCTGGCAACG
LCE3D	TCTTGATGCATGAGTTCCCAGA	TGGACATCAGACAGGAAGTGC
LCE4A	CCCCCTCCCAAGTGTCCTAT	GAGCCACAGCAGGAAGAGAT
LCE5A	CCCAGGTGCTGAAGATGTGT	ATGGAGTGAACATGGGCAGG
LCE6A	GTCCTGATCTCTCCTCTCGTCT	CAAGATTGCTGCTTCTGCTGT
LOR	CTCTGTCTGCGGCTACTCTG	CACGAGGTCTGAGTGACCTG
Pan-p63	GACAGGAAGGCGGATGAAGATAG	TGTTTCTGAAGTAAGTGCTGGTGC
Puro	CACCAGGGCAAGGGTCTG	GCTCGTAGAAGGGGAGGTTG
SPRR1A	CAGCCCATTCTGCTCCGTAT	GGCTGGCAAGGTTGTTTCAC
SPRR2A	ACACAGGGAGCTTCTTTCTCC	CCAGGACTTCCTTTGCTCAGT
SPRR2D	TCGTTCCACAGCTCCACTTG	CAGGCCACAGGTTAAGGAGA
SPRR3	CCTCGACCTTCTCTGCACAG	GGTTGTTTCACCTGCTGCTG
SPRR4	AGCCTCCAAGAGCAAACAGA	GCAGGAGGAGATGTGAGAGG
SPRR5	AGCAGCTGCAGTTTCCATCT	AAACAGGAGCTGAGGGGAAG
U6	CACATATACTAAAATTGGAACG	CTTCACGAATTTGCGTGTCATC

Table 14: List of ChIRP-Oligos

Name	Sequence (5' to 3')
LINC00941_CHIRP_1	CGCAGTTCAGAGAAGGCTAC
LINC00941_CHIRP_2	CTTGGACACAAAAATCGCGG
LINC00941_CHIRP_3	GTTGGTCTCAGAGGGACTCT
LINC00941_CHIRP_4	AAGGCAGGAAGTCTGTGCTG
LINC00941_CHIRP_5	CTTTAGACACTTCTCGAGGG
LINC00941_CHIRP_6	TTGTTTGGCTATCAACTGTC
LINC00941_CHIRP_7	CATAATCAGTCAGTGAATCC
LINC00941_CHIRP_8	CTGATTCTTGATACCAGTCT
LINC00941_CHIRP_9	GTTTGTATTGTCAGTATGCC
LINC00941_CHIRP_10	ATGCTGGCCTGAAAAGGTCC
LINC00941_CHIRP_11	ATAAGATGGATACATGCTCC
LINC00941_CHIRP_12	ATTGTGAAAGTGATCTCTGC

LINC00941_CHIRP_13	TCTGGATAGAGGGCTCATTA
LINC00941_CHIRP_14	CCAGTCAATTCGCAGAGTAA
LINC00941_CHIRP_15	ATTGATCATGGCAGCAAGAA
LINC00941_CHIRP_16	GGTTATAAGCATAGTTGGTC
U2	CCAAAAGGCCGAGAAGCGAT

Table 15: List of primers used for RACE

Purpose	Name	Sequence (5' to 3')
3´RACE	E5 3´outer	GAATCCTTAGGCTTCCACGT
	E5 3´inner	GAAAGCCTGAGCTAACCTAC
3´RACE	E5 5´ outer	GGATGAGCCATCACCTGGA
	3´E5 UCSC inner	CCCTAGGCCAAGCAACCGTC
5´RACE	Exon 5 Primer 3	GGTCCACTACGTTAGAAGGA TTTCGG
	Exon 5 Primer 2	TGCTTCTGCTACAGAACAAA ACACCA
5´RACE	5´ RACE	GGTTGCTTGGCCTAGGGAGG
	E5 5´ inner	GTAGGTTAGCTCAGGCTTTC

6.9 Plasmids

Table 16: List of plasmids

Plasmid	Properties	Origin
lentiCRISPRv2_complete	*Lentiviral transfer plasmid based on lentiCRISPRv2 from Addgene (#52961). The KO cassette has been inserted via SLIC cloning after BsmBI digest of the vector, encodes Cas9 from S. pyogenes*	*AG Kretz/Julia Junghans (University of Regensburg)*
lentiCRISPRv2_complete_ CMVCas9	*Lentiviral transfer plasmid based on lentiCRISPRv2_complete, with Cas9 under the control of a CMV promotor*	*Christian Ziegler (AG Kretz University of Regensburg)*
pCMV dR8.91	*Packaging plasmid for generation of lentiviral particles, encodes the viral gag, rev, tat and pol proteins under control of the CMV promotor*	*gift from the Khavari laboratory (Stanford University, USA)*
pGEM-T Easy	*vector for TA cloning of PCR products*	*Promega (Madison, USA)*
pLVX-TetOne	*Vector for inducible lentiviral overexpression*	*This work*
pLVX-TetOne_LINC00941	*Vector for inducible lentiviral overexpression*	*This work*
pLVX-TetOne_GFP	*Vector for inducible lentiviral overexpression*	*This work*
pUC-MDG	*Envelope plasmid for generation of lentiviral particles, encodes the viral VSV-G envelope protein under control of the CMV promotor*	*gift from the Khavari laboratory (Stanford University, USA)*
pCMV-sport6-linc00941	*Vector bought from Dharmacon*	

6.10 Prokaryotic cells

Table 17: Overview of utilized *Escherichia coli* strains

Strain	Genotype	Details
DH5α	F^- Φ80*lac*ZΔM15 Δ(*lac*ZYA-*arg*F) U169 *rec*A1 *end*A1 *hsd*R17(r_k^-, m_k^+) *pho*A *sup*E44 *thi*-1 *gyr*A96 *rel*A1 λ^-	Propagation of plasmids

Stbl3	F⁻*mcr*B *mrrhsd*S20(r_B^-, m_B^-) *rec*A13 *sup*E44 *ara*-14 *gal*K2 *lac*Y1 *pro*A2 *rps*L20(Str^R) *xyl*-5 λ⁻*leumtl*-1	Propagation of lentiviral plasmids

6.11 Software

Table 18: List of used software

Name	Source of supply
2200 TapeStation Software	Agilent Technologies (Santa Clara, USA)
Agilent 2100 Expert Software B.02.08SI648	Agilent Technologies (Santa Clara, USA)
AxioVision 4.9.1.0	Carl Zeiss (Oberkochen, Germany)
Bio-Rad CFX Manager 3.1	Bio-Rad (Hercules, USA)
CASAVA1.8.2	https://biogist.wordpress.com/2012/10/23/casava-1-8-2-installation/
Galaxy server tools (indicated individually)	local installation after https://usegalaxy.org/
gRNA design tool	http://crispr.mit.edu/
HOMER (v4.9, 2-20-2017)	http://homer.ucsd.edu/homer/
Integrative Genomics Viewer 2.3.90 (IGV)	https://www.broadinstitute.org/igv/
IrfanView 4.42	http://www.irfanview.de/
Living Image 4.5.2	PerkinElmer (Waltham, USA)
MASCOT 2.5.1	Matrix Science (London, United Kingdom)
Microsoft Office	Microsoft (Redmond, USA)
MxPro QPCR Software	Agilent Technologies (Santa Clara, USA)
ND-1000 3.81	Thermo Fisher Scientific (Waltham, USA)
Odyssey 3.0.30	LI-COR Biosciences (Lincoln, USA)
ProteinScape4 3.1.3 461	Bruker (Billerica, USA)
Quantity One 4.6.9	Bio-Rad (Hercules, USA)
R version 3.3.1	https://www.r-project.org/
Rstudio version 1.0.136	https://www.rstudio.com/
R-packages (several, indicated individually)	Bioconductor
SnapGene Viewer 4.1.4	GSL Biotech LLC (Chicago, USA)
SonoLab Software 7.2	Covaris (Woburn, USA)
Skyline 4.1	University of Washington (McCoss Lab) https://skyline.ms/project/home/software/Skyline/begin.view
Zotero	https://www.zotero.org/

7 Methods

7.1 Bioinformatical data analysis

7.1.1 Analysis of full transcriptome sequencing data

Preprocessing: Quality of sequencing data from the RNA-Seq libraries was examined using FASTQC (http://www.bioinformatics.babraham.ac.uk/projects/fastqc/). Size, adapter and quality trimming was performed using Trimmomatic[347] (ver. 0.32,

ILLUMINACLIP:TruSeq_s tranded_SE.fa:2:30:10 HEADCROP:0 TRAILING:26 LEADING:26 SLIDINGWINDOW:4:15 MINLEN:25). Trimmed reads were aligned to the Homo sapiens genome (ftp://ftp.ensembl.org/pub/release-85/fasta/homo_sapiens/dna/Homo_sapiens.GRCh38.dna.primary_assembly.fa.gz) extended with the ERCC spike in sequence information[348] using STAR[349]. The mapped reads were then assessed on the gene level using featureCounts from the Rsubread R-library[350] based on the annotation information from Ensembl[265] (GRCh38.p7 release-85). Following alignment, further quality control was performed using QoRTs[351] and aligned reads were inspected with the UCSC genome browser[352] or alternative the Integrative Genomics Viewer (IGV)[353,354].

Differential expression analysis: Count data at the gene level was analyzed with DESeq2[355] using ERCC spike ins for library size normalization and all comparisons were corrected for multiple testing using FDR[356]. Genes that met the indicated $\log_2$(fold change) restraint and had a false discovery rate < 0.05 ("padj") were considered significantly differential expressed.

Heatmap generation and functional annotation: Heatmaps for genes with altered expression (adj. p-value < 0.05 and -1 > log2FC > 1) were generated with pheatmap[350] after variance stabilization transformation of count data with DeSeq2. Functional annotation clustering was performed using the David 6.8 database[357,358] as well as the Enrichr tool[359,360] for the GO-Term classes "biological process" and "cellular compartment". Principal component analysis was done in R[361] with the plotPCA function of the DeSeq2 package after variance stabilizing transformation of read counts per gene.

7.1.2 Coding potential analysis for LINC00941

PhyloCSF[362] tracks were imported into the UCSC genome browser[352] by inserting "http://www.broadinstitute.org/compbio1/PhyloCSFtracks/trackHub/hub.txt" into the "my hubs" section and were compared relative to the LINC00941 transcript[363]. Furthermore, the coding potential was assessed by running iSeeRNA[364] with a gtf file of the LINC00941 exons and by inspection of the spliced LINC00941 transcript with the Coding Potential Calculator (CPC)[365] using their default settings.

7.1.3 Data analysis for ChIP-Seq

In general, data analysis with Galaxy[366] and R[361] was performed as described. Peak calling for ChIP-Seq datasets was done against the respective input controls with MACS2[367,368] by "building the shifting model", --mfold 2,5000, --bw 200, --broad, --broad-cutoff=0.1 and

"MergeBed" was run with -d 300. Furthermore, HOMER (v4.9, 2-20-2017)[369] was used for ChIP-Seq data analysis according to the HOMER documentation. Briefly, bedgraphs from filtered and deduplicated bamfiles were generated by "makeUCSCfile" (-res 10) and enriched peaks were identified with "getDifferentialPeaks" (-F 2 or -F 4), using the combined peak files from MACS2[367,368].
Additionally, already published ChIP-Seq datasets were extracted from the GEO data repository[370,371] and processed as described above.

7.1.4 Data analysis for ChIRP-Seq

High-throughput sequencing libraries were constructed from ChIRPed DNA according the ChIP-seq protocol as described, and sequenced on a Next Seq 500/550 High Output Flowcell. Raw reads were uniquely mapped to reference genome using Bowtie[372].

To find peaks, peaks of each sample were called using MACS against its corresponding input with p-value cutoff 1×10^{-5}[367]. For each MACS predicted peak, a window size of ±2 kbp around peak summit or peak width, whichever is smaller, was selected. Motif search was performed according to TFBSTools and mapped against the JASPAR2018 database.

7.2 Cell culture methods

All cell culture methods were performed in a biological safety cabinet under laminar air-flow to obtain sterile conditions. Lentiviral procedures were performed under biosafety level 2 precautions, whereas biosafety level 1 regulations applied to the remaining methods. Cell culture media, trypsin and DPBS (see Table 9) were pre-warmed to 37 °C prior to use. Then, cultivation of cells was performed in a humidified incubator at 37°C and 5% carbon dioxide.

7.2.1 Cultivation of HEK293T cells and fibroblasts

HEK293T cells and fibroblasts were cultivated in DMEM+FBS (see Table 9) and passaged when they reached 80-90% confluency. Therefore, the medium was aspirated, cells were washed once with DPBS and detached using 0.05% trypsin-EDTA. DMEM+FBS was used to quench the trypsin, cells were resuspended to obtain a single cell suspension and after centrifugation (200 rcf, RT, 5 min), cells were resuspended in an appropriate volume of DMEM+FBS and equally distributed onto fresh cell culture dishes.

7.2.2 Cultivation of keratinocytes

Primary keratinocytes and HaCaT cells were cultivated in 50:50 medium (see Table 9) until a maximal confluency of 80% to prevent premature differentiation. For passaging of keratinocytes, cells were washed once with DPBS and detached using 0.05% trypsin-EDTA (4 min, 37 °C). After tapping the plate to lift the cells and adding of at least four volumes of DMEM+BCS, cells were resuspended to obtain a single cell solution and pelleted by centrifugation (200 rcf, RT, 5 min). Cell pellets were resuspended in 50:50 medium and seeded onto appropriate cell culture dishes with at least 5% confluency. Primary keratinocytes were not passaged more than 7 times.

7.2.3 Determination of cell numbers

Cells in suspension were added to a Neubauer Counting Chamber, and the cells in four quadrats were counted. The number of cells per milliliter cell suspension was obtained by:

$$\text{Cells per ml} = \frac{Counted\ number\ of\ cells}{4\ (\#\ of counted\ quadrats)} \text{ x } 10{,}000$$

7.2.4 Electroporation of keratinocytes

Keratinocytes were nucleofected with siRNA pools or annealed siRNAs (see 7.5.1) utilizing the Human Keratinocyte Nucleofector Kit (Lonza). After detaching the cells with trypsin (see 7.2.1), the cell number was determined and six million keratinocytes were pelleted (200 rcf, RT, 5 min) and resuspended in 100 µl electroporation buffer. 95 µl of this suspension were mixed with 10 µl siRNA pool or annealed siRNAs (both 100 µM) and transferred to the electroporation cuvette. Nucleofection was achieved with the Electroporation Device Nucleofector II (Lonza) and its preset program T-018 (Keratinocytes human, neonatal, high efficiency). Following nucleofection, the cells were transferred to 500 µl prewarmed (37°C) 50:50 medium and after recovery at 37°C for 30 minutes, seeded on a 15 cm dish and recovered for at least 24 hours at 37°C with 5% carbon dioxide.

7.2.5 Freezing and thawing of cells

For storage of cells, 1.5 million keratinocytes or 3 million HEK293T cells were resuspended in 1 ml freezing medium (cultivation medium for the cell type supplemented with 10% DMSO) while the temperature was slowly (1°C/min) lowered to -80°C. The next day, cryo-stocks were transferred to the vapor phase of liquid nitrogen for long term storage.

Cryopreserved cells were thawed in a water bath at 37°C, transferred to 10 ml cultivation

medium (see Table 9), and DMSO was removed by aspirating the medium after centrifugation (200 rcf, RT, 5 min). Cells were resuspended in fresh cultivation medium followed by seeding the cells onto appropriate cell culture dishes.

7.2.6 Generation of organotypic epidermal tissue

Setups for organotypic epidermal tissue cultures consisted of an insert with a squared (0.8 cm edge length) cavity that rested on glass beads that had been mounted in a 6 cm cell culture dish. Next, devitalized human dermis was cut, placed with the basement membrane side upwards over the cavity of the insert, and 90 µl matrigel (Thermo Fisher Scientific) were applied to the bottom side of the dermis to seal holes. Finally, KGM was added to the setups until it reached the bottom of the insert, and thus nutrients and fluids could diffuse through the dermis.

Keratinocytes (untreated, nucleofected with siRNA or transduced with lentiviral particles) were detached, counted and pelleted (see 7.2.2 and 7.2.3) and 500,000 cells were resuspended in 20 µl KGM and equally distributed onto the dermis part covering the cavity of the insert. Stratification and differentiation was induced by raising the keratinocytes to the air-liquid interface, and KGM was exchanged every second day.

Organotypic epidermal tissue cultures were harvested by lifting the insert and carefully removing the matrigel and excess of devitalized human dermis. The remaining regenerated organotypic skin tissue was cut in the middle to give rise to two equal triangles. One half was embedded for immunohistological analysis into Tissue-Tek (Weckert Labortechnik), flash frozen on dry-ice and stored at -80°C (see 7.3.1), whereas the other half was used for RNA extraction (see 7.5.14).

7.2.7 Generation of LINC00941 knockout cell lines

Guide RNAs for LINC00941 KO were designed with the gRNA Design tool from the Zhang Lab (http://crispr.mit.edu), and the two gRNAs upstream and two downstream of the LINC00941 sequence with the highest score were chosen and combined into a gRNA expression cassette using the PrecisionX Multiplex gRNA Cloning Kit (BioCat) and subsequently inserted into pX462v2 (Addgene).

For the transient transfection-based approach, 150,000 NTERT2G cells were seeded into a 6-well the day before transfection. The next day, the medium was changed to fresh 50:50 medium, the transfection mix was prepared (according to Table 19) and after combining plasmid and lipofectamine solution and incubation at room temperature for 20 minutes, this

mixture was added dropwise to the cells, followed by a medium change, six hours post transfection.

Table 19: Transfection mix for LINC00941 KO cell line generation

	6-well	Component
Plasmid dilution	125 µl	Opti-MEM
	2.5 µg	pX462vs2
	5 µl	P3000 enhancer reagent
Lipofectamine dilution	125 µl	Opti-MEM
	7,5 µl	Lipofectamine 3000 reagent

Selection of plasmid containing cells was achieved by changing the medium to 50:50 medium supplemented with 5 µg/ml Hygromycin 48 hours and 72 hours post transfection. After selection, medium was exchanged to conditioned 50:50 medium and cells were allowed to recover for one day.

For single cell seeding, cells were detached (7.2.2), counted (7.2.3) and diluted with conditioned 50:50 medium to a concentration of 0.5 cells per 100 µl and then were plated into 96-well plates. Two weeks after seeding, 50 µl of a 1:1 mixture of fresh and conditioned 50:50 medium was added to each well. When a clonal cell would become more than 60% confluent this cell line was expanded by detaching the cells with trypsin (described in 7.2.2), and 60% of the cells were used for further cultivation on a 48-well and 40% for screening purposes.

In order to screen potential KO cell lines, a cell lysate was prepared by pelleting the cells (5 min, RT, 13,000 rcf), resuspending the pellet in 40 µl 1x ThermoPol buffer (New England Biolabs) supplemented with 8 µg Proteinase K (Roche) and incubated at 65°C for one hour followed by 15 minutes at 95°C. This lysate was then used for the PCR-based screening approach (see 7.5.10).

7.2.8 Keratinocyte differentiation cultures

Differentiation of keratinocytes in monolayers was induced by seeding the keratinocytes after detachment and centrifugation (see 7.2.2) at full confluency and addition of 1.2 mM calcium chloride to the 50:50 medium. For differentiation cultures, the medium was renewed every day.

7.2.9 Lentivirus production and transduction of keratinocytes

Transfection of HEK293T cells was performed (according to Table 20) and only endotoxin free plasmid preparations (see 7.5.11) were used for transfection in combination with

Lipofectamine 3000 (Thermo Fisher Scientific). The lentiviral transfer vector was pLVX_TetOne with varying inserts (see Table 16), and the employed amount for transfection was calculated depending on the size of the lentiviral transfer vector to obtain a molar ratio of 1:1:1 for all three plasmids.

Table 20: Transfection reaction mixtures for lentiviral particle generation

	10 cm dish	15 cm dish	Component
Plasmid dilution	1.5 ml	3.5 ml	Opti-MEM
	7.5 µg	17.5 µg	pCMV dR8.91
	3.72 µg	8.68 µg	pUC-MDG
	varied	varied	lentiviral transfer vector
	35 µl	81 µl	P3000 enhancer reagent
Lipofectamine dilution	1.5 ml	3.5 ml	Opti-MEM
	41 µl	95 µl	Lipofectamine 3000 reagent

Plasmid and lipofectamine dilution were mixed and incubated at room temperature for 25 minutes. After that, the transfection reaction was applied to the 10 cm (or 15 cm) dish and 21 million (50 million for 15 cm) HEK293T cells resuspended in 8 ml (or 18 ml for 15 cm) were added for reverse transfection. After six and 24 hours post transfection, the medium was changed to 12 ml (or 25 ml for 15 cm) DMEM+FBS, and viral particles were harvested 48 hours post transfection by filtering the virus containing medium through a 0.45 µm pore-sized polyethersulfone membrane.

For lentiviral transduction, 45,000 (or 250,000 per 10 cm dish) keratinocytes were seeded in a 6-well (or 10 cm dish) the day before infection. The next day, 2.5 ml (or 12 ml per 10 cm dish) transduction mix per 6-well was prepared by diluting the viral particles in DMEM+FBS and addition of polybrene to a final concentration of 5 µg/ml. The optimal dilution was determined in preceding efficiency tests for each batch of lentiviral particles to ensure an adequate overexpression in combination with no cytotoxic effect. The finally employed dilutions can be obtained from Table 21.

Table 21: Overview of employed lentiviral dilutions for keratinocyte transduction

Lentiviral transfer vector	Dilution
pLVX_backbone with varying inserts	1:1.66

Infection of keratinocytes was accomplished by exchanging the growth medium to the transduction mix and centrifugation at room temperature with 250 rcf for one hour. Afterwards, the transduction mix was aspirated, cells were washed twice with DPBS and recovered in 50:50 medium for at least 24 hours.

7.2.10 Preparation of human devitalized dermis

Human split-skin was washed twice in PBS+2x A/A and incubated in PBS+2x A/A at 37°C for 3-7 days until the epidermis could be mechanically detached from the dermis. Until further use, the dermis was stored in PBS+2x A/A at 4°C.

7.3 Histological analysis

7.3.1 Immunofluorescence analysis of cryosections from epidermal tissue

7 µm thick sections from embedded regenerated organotypic epidermal tissue (see 7.2.6) were prepared with the Cryostat Microm HM 500 OM (Thermo Fisher Scientific), transferred onto Polysine slides (Carl Roth) and dried for one hour at room temperature and stored at -20°C until staining.

Depending on the differentiation protein to be analyzed, skin sections were fixed in methanol, ethanol or acetone (see Table 1) for 10 min at -20°C, and after gradually replacing the fixative with PBS, slides were blocked for 20 min at room temperature in PBS with 10% BCS (Thermo Fisher Scientific). Primary antibody solution in 1% BCS in PBS was applied and incubated on the sections for one hour at room temperature or overnight at 4°C in a humidified chamber (double staining of differentiation protein and collagen VII, dilutions are given in Table 1). Next, sections were washed with 1% BCS in PBS (three times, 5 min each), and fluorescently labeled secondary antibodies (see Table 2) diluted in 1% BCS in PBS were applied in a dark humidified chamber for one hour at room temperature. The differentiation protein was labeled with Alexa 555 and collagen VII with Alexa 488. Following this step, slides were briefly rinsed in PBS and nuclei were stained by incubating the sections with Hoechst solution for 5 min at room temperature. Slides were washed three times with PBS (5 min, RT), air dried, mounted using ProLong Gold Antifade Mountant (Thermo Fisher Scientific) and stored at 4°C.

Pictures from representative areas for each section were taken with the Inverted microscope Axiovert 200 M (Carl Zeiss) in combination with the AxioVision software (Carl Zeiss) by overlaying pictures from the DAPI, GFP and Cy5 channel taken at 20x magnification.

7.3.2 RNAScope

RNA Scope was performed accordingly to manufacturer´s manual. In short, cells were fixed for 30 min in 4% formaldehyde followed by protease digestion. The cells were then

incubated 2 hours at 40°C with hybridization solution containing 100µl probe mix. For amplifying, three steps were performed. After each hybridization step, slides were washed with wash buffer three times at room temperature. For signal development, TSA Plus fluorophores (Perkin Elmer, TSA kit) were used accordingly to manufacturers standards. For mounting, ProLong Gold Antifade mountant (Thermo Fisher Scientific) was used and the slides were stored at 4°C.

7.4 Microbiological techniques

7.4.1 Cultivation of Escherichia coli

All cultures were incubated at a suitable temperature, that is 37 °C for DH5α bacteria and 30 °C for One Shot® Stbl3™ bacteria, liquid cultures in appropriate volume of Lysogenia Broth (LB) medium shaking at 180 rpm. Cultures on plates were incubated on LB - agar containing adequate antibiotics.

7.4.2 Preparation of chemically competent *Escherichia coli*

5 ml YT-medium were inoculated with a single colony of the selected *Escherichia coli* strain and grown overnight at 37°C and 220 rpm. The next day, 50 µl from this starter culture were mixed with 5 ml fresh YT-medium and incubated at 37°C and 220 rpm until an OD_{600} of 0.8 was reached. 100 ml YT-medium were added and the culture was grown to an OD_{600} of 0.5. Cells were spun down (2,000 rcf, 5 min, 4°C), resuspended in 20 ml ice-cold TFBI and incubated on ice for 10 minutes. After sedimentation (2,000 rcf, 5 min, 4°C), cells were resuspended in 4 ml ice-cold TFBII, divided in 100 µl aliquots, snap-frozen in liquid nitrogen and stored at -80°C.

7.4.3 Transformation of chemically competent *Escherichia coli*

The chemical competent cells (Table 17) were thawed on ice. An amount of 10 µl (50 ng/µl) plasmid solution was added to 100 µl cell suspension, carefully mixed and incubated for 30 min on ice. After the heat shock (90 sec for DH5α, 45 sec for One Shot® Stbl3™ at 42 °C), the cells were incubated for 2 min on ice. 900 µl LB-media were added and the cell solution was incubated on a thermomixer for one hour at the suitable temperature at 650 rpm. 70 - 100 µl of the suspension were plated on LB-selection plates and incubated at the specific temperature.

7.5 Molecular biological methods

7.5.1 Annealing of siRNAs

To anneal of siRNAs, 1 nmol of sense and antisense single siRNAs (for sequences see Table 11) were mixed with 5 µl siRNA annealing buffer in a 10 µl reaction and heated to 95°C for 3 min, followed by one hour at 37°C.

7.5.2 cDNA synthesis

For cDNA synthesis, 500-1000 ng of TRIzol purified RNA (7.5.15) was first subjected to a DNase digest with either DNaseI or the TURBO DNA-free Kit (both Thermo), according to the manufacturer's instructions, followed by cDNA synthesis with the iScript cDNA Synthesis Kit (Bio-Rad, following the manufacturer's instructions). In contrast to this, RNA obtained with the RNeasy Plus Mini Kit was directly used for cDNA synthesis without prior DNase digest.

After cDNA synthesis, H_2O was added to give a final volume of 200 µl, and the cDNA was stored at -20°C.

7.5.3 Quantification of RNA molecules per cell

An artificial RNA control was generated with the SP6 RNA Polymerase in vitro transcription system (NEB, M0207) according to manufacturer's instructions and quantified by NanoDrop. The reaction was carried out at 37°C for two hours. Residual plasmid DNA was removed using DNAse I (Thermo Fisher Scientific) prior to cDNA synthesis. In vitro transcribed RNA was subjected to reverse transcription with the iScript cDNA synthesis kit (Bio-Rad). The cDNA products were diluted in series to generate a standard curve ranging 103 –106 copies. qPCR data analysis was performed essentially as described before with total RNA extracted from 1–5 × 10^6 keratinocytes and recalculated to reflect single-cell analysis.

7.5.4 Cellular fractionation of keratinocytes

Cell fractionation was performed as described with modifications described below[373]. All subsequent steps had been conducted on ice or at 4°C and in the presence of 50 units RiboLock RNase Inhibitor (ThermoFisher, EO0381) and Protease inhibitors cOmplete (Roche, 11873580001) according to manufacturer's instructions using RNase-free equipment. After incubation with cytoplasmic lysis buffer for 10 min on ice, the cell pellet

was layered onto 500 ll sucrose buffer and centrifuged at 16,000 g for 10 min. The supernatant corresponding to the cytoplasmic fraction was carefully removed. The nuclei pellet was gently resuspended in nuclei wash buffer and centrifuged at 1,500 g for 1 min. The RNA was extracted as described before.

7.5.5 Chromatin Immunoprecipitation by RNA purification (ChIRP)

DNA-ChIRP was performed as described with following changes[374]. Undifferentiated keratinocytes were harvested as described above (7.2.2 and 7.2.3), and formaldehyde crosslink was achieved by resuspending 10 million cells in 10 ml 3% (v/v) formaldehyde solution and incubation at room temperature for 10 minutes under constant rotation. Next, excess formaldehyde was quenched by addition of 1/10 volume 1.25 M glycine (5 min, RT, rotation), and crosslinked cells were pelleted (2,000 rcf, 4°C, 10 min), washed once with 10 ml ice-cold PBS supplemented with 1 mM AEBSF and 10 mM sodium butyrate (2,000 rcf, 4°C, 10 min) and transferred to a 1.5 ml reaction tube with 750 µl ice-cold PBS supplemented with 1 mM AEBSF and 10 mM sodium butyrate. Following centrifugation (6,000 rcf, 5 min, 4°C), the liquid was removed completely, the weight of the cell pellet was determined, samples were flash frozen in liquid nitrogen and stored at -80°C.

For chromatin sonication, crosslinked cells were thawed on ice and resuspended in 10 times excess of supplemented CHIRP lysis buffer per mg crosslinked pellet. Following the crosslinked DNA was sheared to fragments between 150 bp to 250 bp by sonication with the S220 Focused-ultrasonicator (Covaris) in combination with 12 ml tubes (Covaris PN 52086) and the indicated settings (Table 22).

Table 22: Settings for sonication of chromatin

Duty cycle	20%
Mode	Freq sweeping
Intensity	6
Cycles of burst	400
Water level	12
Time	5 hours

After centrifugation (15,870 rcf, 5 min, 4°C), 20 µl of the supernatant were set aside, while the remaining supernatant was transferred to a fresh reaction tube. A 5% (v/v) input sample was taken, and input and chromatin were flash-frozen and stored at -80°C. Next, the chromatin corresponding to 120 million (equals 40 million cells for odd, even and negative control probe) cells was thawed on ice, 2 volumes of supplemented ChIRP hybridization buffer were added. Additionally, 200 pmol ChIRP probe was added and incubated for 4h at

37°C. With 20 min hybridization remaining, 200 µl C-1 streptavidin coupled magnetic beads per reaction were washed three times with unsupplemented Lysis buffer. Subsequently, beads were added to the reaction and incubated for 30 min at 37°C. The reaction was washed five times in ChIRP wash buffer. Finally, elution was performed with a DynaMag-2 magnetic strip to remove all wash buffer. 10% of it was saved for RNA extraction which was performed as described (7.5.15). To extract DNA from ChIRP samples, they were resuspended in 150µl DNA elution buffer with added RNaseA and H and incubated for 30 min at 37°C. This step was performed twice. The whole supernatant (300µl) was incubated with Proteinase K and finally cleaned up using PhOH:Chloroform:Isoamyl and eluted in 30µl water. Library preparation for ChIRP-Seq was performed with the NEBNext Ultra II DNA Library Prep Kit for Illumina (New England Biolabs) in combination with the Index Primer Set 1+2 of the NEBNext Multiplex Oligos for Illumina (New England Biolabs). In general, the manufacturer's instructions were followed, however for adapter ligation a 1:10 dilution of the NEBNext adapter was used, and Agencourt AMPure XP beads (Beckman Coulter) were used for PCR clean-up as well as for size selection of DNA inserts of approximately 200 bp. Finally, the obtained libraries were quantified on the Qubit 2.0 Fluorometer in combination with the Qubit dsDNA HS Assay Kit (both Thermo Fisher Scientific) according to the manufacturer´s instruction. The size distribution was analyzed on the TapeStation in combination with the High Sensitivity D1000 ScreenTape and its corresponding reagents (Agilent), and libraries were pooled in an equimolar ratio.

7.5.6 DNA agarose gel electrophoresis

Depending on the expected DNA size, horizontal agarose gel electrophoresis was performed with 0.8 - 1.4% (w/v) agarose gels (dissolved in TAE buffer, supplemented with a final concentration of 0.5 µg/ml ethidium bromide). To this end, samples were mixed with 1/6 volume of DNA loading dye, loaded next to 5 µl of 1 kb Plus DNA Ladder (Thermo Fisher Scientific), and separation of DNA fragments was achieved by applying 90 V in gel chambers filled with TAE buffer. Gel documentation was done with the Transilluminator Quantum ST4 (PEQLAB).

7.5.7 Full transcriptome RNA sequencing

Library preparation and sequencing were performed by the "Kompetenzzentrum fuer Fluoreszente Bioanalytik" Regensburg with RNAs, being isolated from regenerated organotypic epidermal tissue (7.5.14). In general, library preparation and mRNA sequencing

were carried out according to the Illumina TruSeq Stranded mRNA Sample Preparation Guide, the Illumina HiSeq 1000 System User Guide (Illumina), and the KAPA Library Quantification Kit - Illumina/ABI Prism User Guide (Kapa Biosystems), with minor modifications. In brief, mRNA molecules were purified using oligo-dT probes immobilized on magnetic beads starting with 250 ng of total RNA, supplied with ERCC spike ins[348]. Chemical fragmentation of the mRNA to an average insert size of 200-400 bases was performed using divalent cations under elevated temperature (94°C, 4 minutes). First strand cDNA was produced by reverse transcription with random primers. Actinomycin D was added to improve strand specificity by preventing spurious DNA-dependent synthesis. Blunt-ended second strand cDNA was synthesized using DNA Polymerase I, RNase H and dUTP nucleotides. The resulting cDNA fragments were adenylated at the 3' ends, the indexing adapters were ligated and subsequently specific cDNA libraries were created by PCR enrichment. The libraries were quantified using the KAPA SYBR FAST ABI Prism Library Quantification Kit. Equimolar amounts of each library were used for cluster generation on the cBot (TruSeq SR Cluster Kit v3). The sequencing run was performed on a HiSeq 1000 instrument using the indexed, 1x50 cycles single end protocol and TruSeq SBS v3 Reagents according to the Illumina HiSeq 1000 System User Guide. Image analysis and base calling resulted in .bcl files which were converted into .fastq files by the CASAVA1.8.2 software (Bio Gist).

7.5.8 Generation of plasmids

The concentration of digested and purified vector and insert (see 7.5.13) was determined using the NanoDrop 1000 device (Thermo Fisher Scientific), and 50 ng vector were mixed with the designated insert in a 1:3 molar ratio with 1x T4 DNA ligase buffer (New England Biolabs) and 400 units T4 DNA ligase (New England Biolabs) in a 20 µl reaction. Ligation was achieved by incubation at room temperature for one hour or overnight at 4°C. Following heat inactivation (10 min, 65°C), the obtained plasmids were used for transformation of competent *Escherichia coli* cells (7.4.3).

7.5.9 Northern blot analysis

15 to 25 µg TRIzol purified RNA from keratinocytes at varying timepoints of differentiation as well as 5 µl RiboRuler High Range or Low Range RNA Ladder (Thermo Fisher Scientific) were mixed with the same amount of 2x RNA loading dye, incubated at 65°C for 10 min, and subsequently placed on ice. Ethidium bromide was added to a final concentration of 40

µg/ml, and the samples were loaded onto a formaldehyde agarose gel (1.2% agarose dissolved in RNA gel buffer) and separated by horizontal gel electrophoresis (running buffer: RNA gel buffer, 70 V) until the blue dye was 3 cm above the end of the gel. After shaking the gel for 30 min in 20x SSC, the RNA was transferred onto a trimmed piece of Amersham Hybond-N+ membrane (GE Healthcare) by upward capillary transfer using 20x SSC as transfer buffer and incubation overnight (detailed description of the setup can be found here[375]).

The next day, the RNA was crosslinked to the membrane with UV-light at 254 nm (auto crosslink function of the UV Stratalinker 2400 (Stratagene)), and successful RNA transfer as well as migration pattern of the RNA ladder was captured with the Transilluminator Quantum ST4 (PEQLAB). After prehybridization (one hour at 40-50°C with hybridization solution supplemented with 1 mg heat denaturated hering sperm DNA (Promega)), specific transcripts were detected by adding 20 pmol antisense DNA-oligos (see Table 14) that have been labeled in a T4 PNK reaction (Thermo Fisher Scientific) with 20 µCi ^{32}P (20 µl total reaction volume, according to the manufacturer's instructions), purified with a G-25 column (GE Healthcare, according to the manufacturer's instructions) and incubated overnight at 40-50°C under constant rotation.
The next day, excess radioactivity was washed away (10 min each, 40-50°C, twice with NB wash I and once with NB wash II) and a phosphorimager screen (Kodak) was used to accumulate the radioactive signal. The resulting radioactive signals were read with the Personal Molecular Imager (Bio-Rad) and analyzed with the Quantity One software (Bio-Rad). Sizes for the detected transcripts were determined by superimposing the ethidium bromide picture with the obtained phosphorimager signals.

7.5.10 PCR-based screening of potential LINC00941 knockout cell lines

Screening PCRs for potential LINC00941 knockout cell lines (7.2.7) were performed utilizing the Taq DNA polymerase (New England Biolabs) to detect genomic alterations (KO allele PCR) and remaining WT alleles (WT allele PCR). For the PCR, 12.5 µl cell lysate (see 7.2.7) was brought to a final concentration of 200 µM dNTPs, 0.2 µM forward and reverse primer (see Table 23 and Table 24), 1x ThermoPol buffer (New England Biolabs) and 1.25 units Taq DNA polymerase in a 25 µl reaction. 15 µl from the PCR were analyzed by DNA gel electrophoresis (7.5.6), and selected PCR products were purified with the NucleoSpin Gel and PCR Clean-up Kit (Macherey-Nagel) according to the manufacturer's instructions and their sequence was determined by Sanger sequencing

(Macrogen) to ensure specificity of the employed screening approach as well as to detect genomic alterations.

Utilized PCR primers and gRNAs can be seen in Table 24, and the PCR conditions and utilized primers are listed below.

Table 23:Thermal cycling conditions for KO allele PCRs and WT allele PCRs

Step	Time	
95°C	5 min	
95°C	30 s	35 x
60°C	30 s	35 x
68°C	5 min	35 x
68°C	7 min	
10°C	∞	

Table 24: Expected sizes of various PCR approaches

Primer 1	Primer 2	expected size
00941_5GT_ex_F1	00941_5GT_int_R1	3223
00941_5GT_ex_F1	009941_3GT_ex_R1	7917
00941_5GT_int_F1	00941_5GT_int_R1	2121
00941_5GT_int_F1	00941_3GT_ex_R1	6869

7.5.11 Plasmid purification

Depending on the required amount of DNA vectors, plasmid purification was done with the NucleoBond Xtra Maxi EF (for endotoxin-free plasmid preparations), NucleoBond Xtra Midi or the NucleoSpin Plasmid Kit (Macherey-Nagel) following the manufacturer's instructions. The obtained DNA was dissolved in a suitable amount of H_2O, the concentration was determined with the NanoDrop 1000 (Thermo Fisher Scientific). The sequence integrity was verified by restriction enzyme digestion as well as by Sanger sequencing of the included inserts (Macrogen, sequencing primers are listed in Table 12).

7.5.12 Polymerase chain reaction (PCR)

For PCR amplification of DNA fragments designated for the generation of new plasmids, PCR was performed in a 50 µl scale using Phusion High-Fidelity DNA Polymerase (New England Biolabs) with 50 ng of DNA template and a final concentration of 1x HF buffer, 200 µM dNTPs, 0.5 µM of each primer (sequences are given in Table 15), 3% DMSO and one unit of Phusion DNA Polymerase in combination with the thermal cycling program given in Table 25.

Table 25: Thermal cycling program for PCR with the Phusion High-Fidelity DNA Polymerase

Step	Time	
98°C	30 s	
98°C	10 s	35 x
55-60°C	30 s	35 x
72°C	30 s/kbp	35 x
72°C	10 min	
4°C	∞	

Successful PCR amplification was verified by DNA agarose gel electrophoresis (7.5.6) and the desired PCR product was purified by either PCR clean-up (in case of only one PCR amplicon) or gel extraction, both done with the NucleoSpin Gel and PCR Clean-up Kit (Macherey-Nagel) according to the manufacturer's instructions.

7.5.13 Restriction enzyme digest

For preparative restriction enzyme digests, 5 to 8 µg DNA vector (1 µg for analytical purposes) or the complete amount of purified PCR product was entirely digested with suitable restriction enzymes in the designated buffer according to the New England Biolabs guidelines. In case of vector backbone preparation for molecular cloning, a dephosphorylation step with Antarctic phosphatase (New England Biolabs) was done according to the manufacturer's instructions. Following heat inactivation of the enzymes, the obtained DNA fragments were analyzed by DNA agarose gel electrophoresis (7.5.6), and desired fragments for molecular cloning were purified via gel extraction with the NucleoSpin Gel and PCR Clean-up Kit (Macherey-Nagel) according to the manufacturer's instructions.

7.5.14 RNA extraction from organotypic tissue

The portion of organotypic tissue (7.2.6) was minced and transferred into a Lysing Matrix D tube (MP Biomedicals) that contained 800 µl RLT Plus buffer (from the RNeasy Plus Mini Kit, Qiagen) supplemented with 1% β-mercaptoethanol. Cell lysis and homogenization were performed with the FastPrep-24 Instrument (MP Biomedicals) for 45 s at 6.5 m/s. After centrifugation (2 min, 4°C, 13,000 rcf), the supernatant was transferred to a QIAShredder tube (Qiagen) and additionally homogenized by centrifugation (2 min, 4°C, 13,000 rcf). The flow-through from this step was then subjected to RNA purification with the RNeasy Plus Mini Kit (Qiagen) following the manufacturer's instructions, except all centrifugation steps were done at 4°C. The RNA was eluted in 30 µl H_2O, quantified with the NanoDrop 1000 (Thermo Fisher Scientific) and stored at -80°C until further usage.

7.5.15 RNA extraction with TRIzol

Keratinocytes were washed with DPBS and directly lysed in a suitable volume of TRIzol Reagent (Thermo Fisher Scientific), then RNA purification was performed according to the manufacturer's instructions but with an additional chloroform extraction step. The obtained RNA pellet was dissolved in an appropriate amount of H_2O (55°C, 900 rpm, 5 min), quantified with the NanoDrop 1000 (Thermo Fisher Scientific), and stored at -80°C.

7.5.16 RT-qPCR analysis

For RT-qPCR analysis, 7.5 µl of SsoFast EvaGreen Mix (Bio-Rad) or Takyon Mix (Eurogentec) were mixed with 4.5 µl H_2O, 1 µl Primermix (5 µM each primer, for sequences see Table 13), 2 µl cDNA and analyzed in a 96-well format using the Real-Time PCR Cycler CFX96 (Bio-Rad) in combination with the Bio-Rad CFX Manager 3.1 (Bio-Rad). Samples were at least run in duplicates, and specificity of each reaction was monitored using a melt curve analysis for each PCR product, whereas the linear amplification for each Primermix was ensured by testing their amplification range with a serial cDNA dilution series in preliminary experiments.

Table 26: Thermal cycling program for RT-qPCR analysis

Step	Time	
95°C	3 min	
95°C	15 s	40 x
60°C	30 s	40 x
72°C	30 s	40 x
plate read		40 x
95°C	10 s	
65°C to 95°C +0.5°C/step	5s	melt curve
plate read		melt curve

Sample wise fold changes were calculated for each gene of interest (goi) in reference to the control from the exported C_q-values using the $2^{-\Delta\Delta Cq}$ method[376] and L32 (where applicable) for normalization according to the following formula:

$$\text{Fold change} = 2^{-[(Cq\ sample(goi)\ -Cq\ control(goi))-(Cq\ sample(L32)-Cq\ control\ (L32))]}$$

7.6 Protein biochemistry

7.6.1 BCA assay for protein quantification

Protein concentration was determined using the Pierce BCA protein assay kit (Thermo Fisher Scientific) according to the manufacturer's instructions in a 96-well format. Samples were measured in duplicates, analyzed at 562 nm, and the protein concentration was determined using the standard curve obtained by plotting the blank-corrected A_{562} for the protein standards against their concentration.

7.6.2 Bradford assay for protein quantification

5x Roti-Quant (Carl Roth) was diluted 1:5 with water and 900 µl of this dilution were mixed with 100 µl prepared bovine serum albumin standard ranging from 0 to 150 µg/ml. 1 to 10 µl of protein sample were brought to a final volume of 10 µl with the respective protein lysis buffer and mixed with 990 µl 1x Roti-Quant. After 5 min at room temperature, the absorption at 595 nm was measured with a Nanophotometer (Implen), and the total protein amount for each sample was determined using the standard curve obtained by plotting the blank-corrected A_{595} for the protein standards against their total protein amount. The concentration of the protein lysate was obtained by dividing the total protein amount through the utilized volume of protein sample.

7.6.3 Mass spectrometry

The edges of the SDS-gel were removed and divided horizontally into stripes based on the coomassie staining. Each stripe was further divided into equally sized pieces. Each gel piece was minced and transferred into a 2 ml micro tube (Eppendorf), washed for 30 min each with 950 µl 50 mM NH_4HCO_3, 50 mM NH_4HCO_3/acetonitrile (3/1), 10 mM NH_4HCO_3/acetonitrile (3/1), 10 mM NH_4HCO_3/ acetonitrile (1/1), and lyophilized. After reduction with 300 µl 1 mg/ml DTT dissolved in 100 mM NH_4HCO_3 (50°C, 1 hour), cysteines were alkylated with 200 µl. 5 mg/ml Iodoacetamide in 50 mM NH_4HCO_3 (35 min, RT), followed by another washes and lyophilization of the gel pieces (see above). Next, proteins were subjected to an *in gel* tryptic digest overnight at 37°C with 1 µg Trypsin Gold mass spectrometry grade (Promega) in 50 mM NH_4HCO_3. Peptides were extracted twice with 150 µl 100 mM NH_4HCO_3, followed by one elution with 150 µl 100 mM NH_4HCO_3/ acetonitrile (2/1), and the obtained eluates were combined and lyophilized. Further processing of samples, mass spectrometry measurements and protein identification was done

by Dr. Astrid Bruckmann and Eduard Hochmuth at the mass spectrometry facility of Biochemistry I, University of Regensburg. Data obtained from these samples, analyzed on the MaXiS mass spectrometer and were transferred to MASCOT 2.5.1 using the Protein-Scape software 3.1.3 (Bruker Daltonics). MASCOT aligned the obtained data to the annotated proteins of the SWISS-PROT database.

7.6.4 Preparation of protein lysates from keratinocytes

Protein lysates were prepared by collecting the cells in RIPA buffer, followed by incubation on ice for 15 minutes and centrifugation for 15 minutes at 4°C and full speed. The obtained supernatant was transferred into a new tube, and this protein lysate was stored at -80°C until further use.

7.6.5 SDS-PAGE analysis and Coomassie staining

Depending on the size of the protein of interest, proteins were separated on 10% or 15% SDS-polyacrylamide gels (composition see Table 27). To this end, protein samples were mixed with 1/5 volume of 5x laemmli buffer and denaturated at 95°C for 5 min. To determine size, 5 µl pre-stained Precision Plus Protein Standard Dual Color (Bio-Rad) was used and electrophoresis was performed with TGS at 100 V until the dye front reached the bottom of the gel.

Gels for mass spectrometry analysis were fixed with coomassie fixative (30 min, RT) washed with water (5 min, RT, 3 times) and stained with Bio-Safe Coomassie Stain (Bio-Rad) at 4°C overnight. Destaining with water was done until protein bands became visible, and pictures were captured with the Odyssey Imaging System (LI-COR Biosciences) and analyzed with the Odyssey software (LI-COR Biosciences).

Table 27: Composition of SDS-PAGE gels

Stacking gel (4%)	Resolving gel (10%)	Resolving gel (15%)	Component
2.25 ml	3.2 ml	1.9 ml	Water
-	1.9 ml	1.9 ml	4x Resolving gel buffer
0.95 ml	-	-	4x Stacking gel buffer
0.5 ml	2.6 ml	3.9 ml	Acrylamid/Bis-solution 30% (37.5:1)
5 µl	4.5 µl	4.5 µl	TEMED
22.5 µl	45 µl	45 µl	10% APS

7.6.6 Western Blot analysis

7.5 to 30 µg total protein (7.6.4) from keratinocytes was separated via SDS-PAGE (7.6.5) and subsequently transferred onto the Amersham Hybond-ECL membrane (GE Healthcare) by semi-dry blot (Bio-Rad system) using western blot transfer buffer and 13 V for one hour. Blocking was done in 5% milk powder in TBS-T for one hour at room temperature and primary antibodies (Table 1) were diluted in 5% milk powder in TBS-T and applied for 1 hour at room temperature or overnight at 4°C. After washing the membrane three times with TBS-T (5 min each, RT), secondary antibodies were diluted in TBS-T supplemented with 5% milk powder, added to the membrane, and incubated for 1 hour at room temperature. Following three washing steps with TBS-T (5 min, RT), the signal was captured with the Odyssey Imaging System (LI-COR Biosciences) and analyzed with the Odyssey software (LI-COR Biosciences).

8 Publications

Ziegler C & Graf J, Faderl S, Schedlbauer J, Strieder N, Förstl B, Spang R, Bruckmann A, Merkl R, Hombach S, Kretz M. The long non-coding RNA LINC00941 and SPRR5 are novel regulators of human epidermal homeostasis. EMBO Rep. 2019 Feb;20(2):e46612.

Graf J., Kretz M., From structure to function: route to understanding lncRNA mechanism (BioEssays Volume 42, Issue 12, December 2020)

9 Appendix

9.1 Supplementary figures

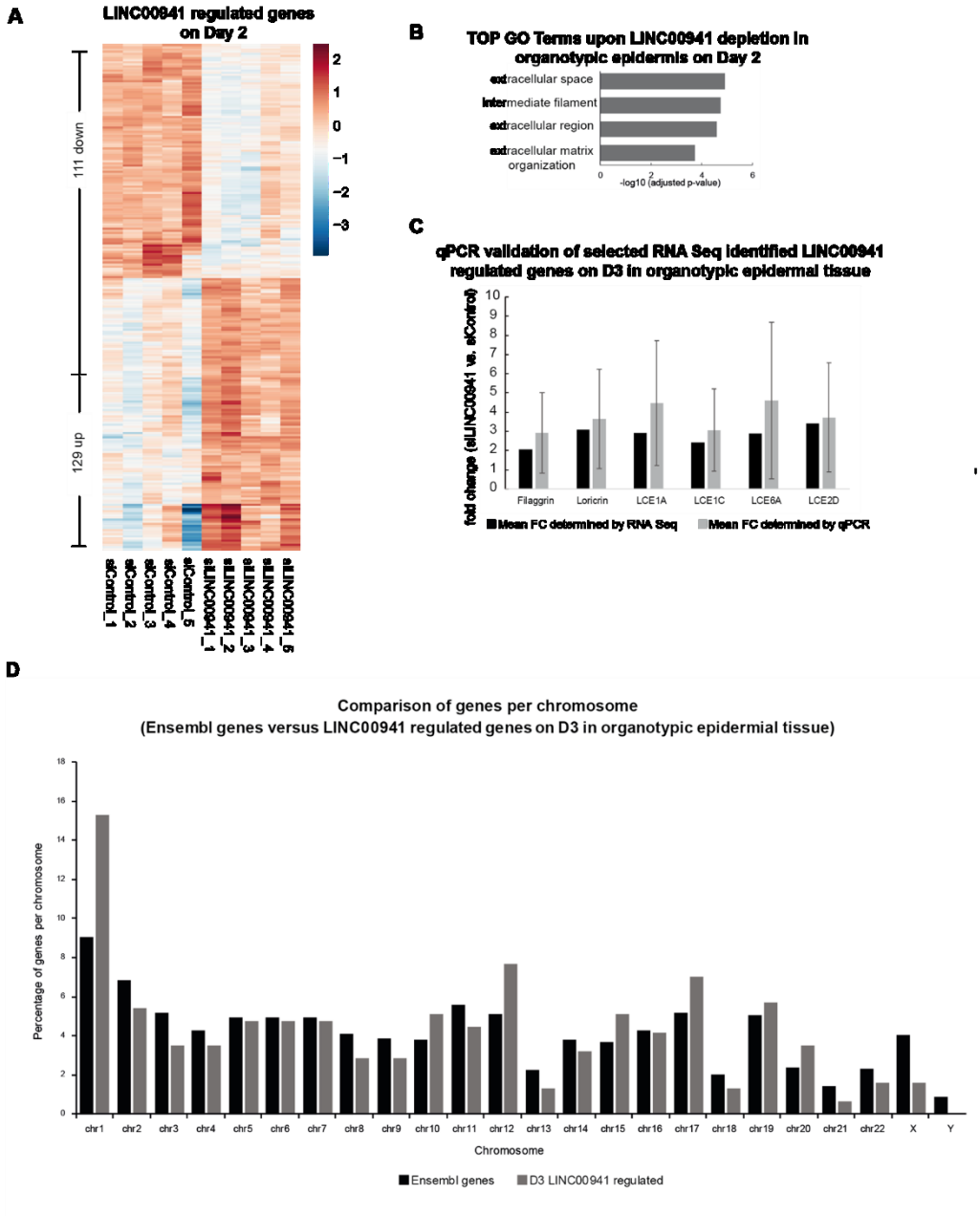

Figure 30: RNA-Seq validation of the LINC00941 depletion
(A) Heatmap of regulated genes upon knockdown of LINC00941 in d2 organotypic epidermis (B) Top GO Terms regulated upon knockdown of LINC00941 in d2 organotypic epidermis (C) q-RT-PCR validation of selected mRNAs (D) Comparison of the genomic localization of LINC00941-regulated genes ($P_{adj} < 0.05$ and $-1 > \log_2 FC > 1$) on day 3 (D3) and distribution of Ensembl genes per chromosome (n = 4–5 epidermal tissue cultures/knockdown group).

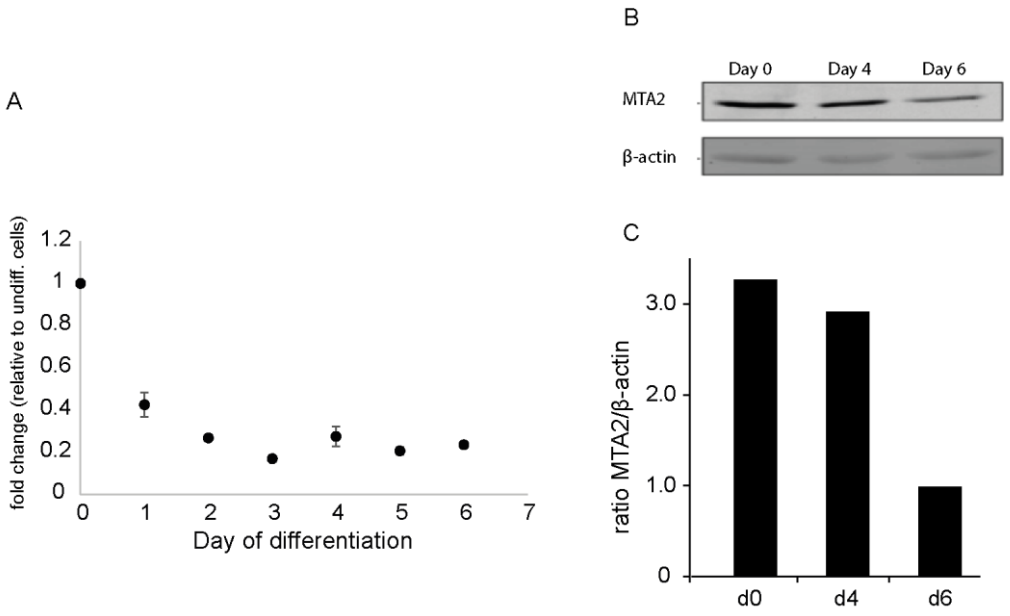

Figure 31: Expression analysis of MTA2
(A) expression of MTA2 in Ca2+ induced keratinocytes during differentiation (B) Western Blot of MTA2 in cell lysates of Ca 2+ induced keratinocytes (C) Quantification of protein levels relative to β-actin.

9.2 LINC00941 transcript sequence and genomic localization

5´-

CCTTTTCTCCCGGGTCCACACCGCAGTTCCCACCGCTCCGGGTGTCCTCCCCAG
TGCGCCGCGATTTTTGTGTCCAAGCCCCAGAGTCCCTCTGAGACCAACCCCCA
GCCAGCACAGACTTCCTGCCTTCCCAGCTCGGAAGCGCCCTCGAGAAGTGTCT
AAAGGAGACAGTTGATAGCCAAACAACAGTTTTGGATTCACTGACTGATTATG
AAAGAAGCAGTAGACTGGTATCAAGAATCAGTCAGCAAGGAGGCCCTCACCA
GACGCCAGTGCCATGTTCTTGGACTTCTCAGCCTCCATATTCATGAACTAAGTT
TTTGGAATCCTTAGGCTTCCACGTGTGGAAAGCCTGAGCTAACCTACTGGAGG
ATGAGCCATCACCTGGAGCAGATTCAGGCCATCCTAGTTGAAGCCTCCCTAGG
CCAAGCAACCGTCCAACTACCAGACATTGACCATTCAGCCTTGAACATTCAGC
ACAAAGACAAAACAGACCAGACCAGAAGAGTCCCACAGAATAGGGGAAACTA
TTCAGAGAAAACTTAAGCCACTAAGTTTTATGGTGTTTTGTTCTGTAGCAGAAG
CATAGGCATACTGACAATACAAACCGAAATCCTTCTAACGTAGTGGACCTTTT
CAGGCCAGCATTTTTTCCTTGAAAACCTGGAGCATGTATCCATCTTATAGCAGA
GATCACTTTCACAATGTTTGGGCTCTTGATTTGAATTGATGATGTAATGAGCCC
TCTATCCAGATTGTAACTAATTACTCTGCGAATTGACTGGATTCCACACCCTTC
TAATATTTTACTTTTCCTCTTTTATCAACTCTCATTCTTGCTGCCATGATCAATG
GACCAACTATGCTTATAACCACAAATTTTGATATGCTTAAACAAATGAACAAA

TATATTTAATAATTTCTTTTTTTTTTTTGAAATAGTATCTTGCTCTGTCACCCAG
GCTGCAGTGCAGCAGCGTGATCTCAGCTCACTATAACCTCCACCTCCCGGGTTC
AAGTGATTCTCCTGCCTCAGCCTCCCAAGTAGCTGGGACTACAGGCGCCCACC
ACCATACCTGGCTAATTTTTTGTATTTTTAGTAGAGACAGGGTTTATCCATGTT
GGCCAGGCTGGTCTCAAACTCCTGACCTCAAGTGATCCTCCTGCCTCGGCCTCC
CAAAGTGCTGGGATTACAGGTGTGAGCCACCATGCCCAGCCAATAATTTCCTG
ATATAATAAAAATGCCAATACTATACAATTAAATAGTAAAGTGATAAAAAATA
GGATAACATGATAACCACTAATTAATATATACTACATAATCATC-3´

Table 28: Genomic localization of LINC00941 (hg38)

	Chromosome	Strand	Start	End
Exon1	12	+	30796078	30796216
Intron 1	12	+	30796217	30799912
Exon3	121	+	30799913	30800021
Intron 3	2	+	30800022	30800532
Exon4	12	+	30800533	30800601
Intron 4	12	+	30800602	30801700
Exon5	12	+	30801701	30802711

Table 29: Genomic localization of LINC00941 isoforms including exon 2 (hg38)

	Chromosome	Strand	Start	End
Exon1	12	+	30796078	30796216
Intron 1	12	+	30796217	30798145
Exon2	12	+	30798146	30798316
Intron 2	12	+	30798317	30799912
Exon3	121	+	30799913	30800021
Intron 3	2	+	30800022	30800532
Exon4	12	+	30800533	30800601
Intron 4	12	+	30800602	30801700
Exon5	12	+	30801701	30802711

9.3 RNA-Sequencing mapping efficiency

Table 30: Mapping efficiency of RNA-Sequencing Counts

sample	total reads	mapped reads
si00941_d2_1	33.892.681	30601616
si00941_d2_2	26.842.525	24359161
si00941_d2_3	33.167.377	29948392
si00941_d2_4	32.613.896	29746375
si00941_d2_5	26.842.525	19298239
si00941_d3_1	22.297.678	20143556
si00941_d3_2	32.334.467	29209526
si00941_d3_3	38.500.823	34074479
si00941_d3_4	35.774.557	32365768
siNgCtrl_d2_1	39.826.307	35960376
siNgCtrl_d2_2	31.287.850	28462568
siNgCtrl_d2_3	37.955.219	34536058
siNgCtrl_d2_4	35.420.446	32325014
siNgCtrl_d2_5	36.637.765	32781647
siNgCtrl_d3_1	39.644.340	36185952
siNgCtrl_d3_2	38.445.656	34851876
siNgCtrl_d3_3	35.832.311	32286579
siNgCtrl_d3_4	34.830.650	31589776
siNgCtrl_d3_5	34.919.998	31997190

9.4 List of figures

9.5 List of tables

9.6 Lists of significantly altered genes upon LINC00941 depletion

Only those genes with -1 > $\log_2$(fold change) > 1 and an adjusted p-value < 0.05 are shown here.

9.6.1 LINC00941 regulated genes on day 2 in organotypic epidermis

Identifier	Gene name	Chr	baseMean	log2FoldChange	pvalue	padj
ENSG00000006059	KRT33A	17	45,365	1,125	7,98E-04	3,62E-02
ENSG00000026025	VIM	10	4246,439	-1,524	2,73E-09	3,05E-06
ENSG00000038295	TLL1	4	43,087	-1,082	1,06E-03	4,17E-02
ENSG00000038427	VCAN	5	60,765	-1,135	6,16E-04	3,12E-02
ENSG00000046604	DSG2	18	3653,672	-1,046	1,74E-04	1,46E-02
ENSG00000047936	ROS1	6	22,897	-1,708	4,79E-06	1,06E-03
ENSG00000050438	SLC4A8	12	37,615	-1,207	2,11E-04	1,68E-02
ENSG00000050628	PTGER3	1	132,320	1,759	1,20E-03	4,40E-02
ENSG00000055163	CYFIP2	5	145,561	1,076	2,55E-04	1,84E-02
ENSG00000064270	ATP2C2	16	892,680	1,689	4,36E-05	5,63E-03
ENSG00000067715	SYT1	12	22,975	-1,720	2,97E-05	4,19E-03
ENSG00000073067	CYP2W1	7	171,328	1,604	3,39E-10	4,76E-07
ENSG00000073670	ADAM11	17	48,825	1,356	3,90E-05	5,16E-03
ENSG00000078687	TNRC6C	17	70,124	-1,172	3,71E-04	2,31E-02
ENSG00000084110	HAL	12	3190,502	2,241	2,76E-05	4,03E-03
ENSG00000086548	CEACAM6	19	3032,895	-1,034	9,54E-05	9,53E-03
ENSG00000090512	FETUB	3	292,077	2,171	9,98E-07	3,38E-04
ENSG00000091128	LAMB4	7	23,411	-1,439	1,06E-04	1,01E-02
ENSG00000091129	NRCAM	7	120,523	-1,208	1,39E-05	2,44E-03
ENSG00000094796	KRT31	17	1254,880	1,151	1,41E-05	2,44E-03
ENSG00000096006	CRISP3	6	91,320	1,904	2,48E-10	4,63E-07
ENSG00000099840	IZUMO4	19	105,310	1,254	3,79E-06	9,08E-04
ENSG00000099960	SLC7A4	22	144,563	1,640	1,87E-10	3,93E-07
ENSG00000100341	PNPLA5	22	45,964	2,853	3,26E-04	2,13E-02
ENSG00000101210	EEF1A2	20	312,724	1,206	1,93E-06	5,50E-04
ENSG00000101311	FERMT1	20	12297,017	-1,476	1,76E-08	1,28E-05
ENSG00000101445	PPP1R16B	20	18,783	1,814	5,57E-05	6,82E-03
ENSG00000101751	POLI	18	111,826	-1,136	7,17E-05	8,02E-03
ENSG00000102098	SCML2	X	20,989	-1,302	9,49E-04	3,94E-02
ENSG00000104267	CA2	8	2180,107	1,353	5,33E-08	2,98E-05
ENSG00000105357	MYH14	19	1075,941	1,195	2,07E-05	3,30E-03
ENSG00000106302	HYAL4	7	76,234	1,760	5,86E-06	1,23E-03
ENSG00000106692	FKTN	9	413,987	-1,040	4,82E-04	2,72E-02
ENSG00000106701	FSD1L	9	46,543	-1,020	7,16E-04	3,41E-02
ENSG00000107249	GLIS3	9	20,938	-1,422	1,80E-04	1,50E-02
ENSG00000108242	CYP2C18	10	68,577	1,175	7,51E-06	1,46E-03
ENSG00000108244	KRT23	17	5959,095	1,923	4,15E-06	9,55E-04

ENSG00000108309	RUNDC3A	17	536,830	1,147	3,41E-06	8,64E-04
ENSG00000108852	MPP2	17	84,324	1,914	4,96E-09	4,54E-06
ENSG00000109099	PMP22	17	45,063	-1,542	2,85E-06	7,48E-04
ENSG00000109943	CRTAM	11	86,255	-1,548	8,37E-09	6,69E-06
ENSG00000112293	GPLD1	6	171,033	2,416	1,16E-06	3,68E-04
ENSG00000112294	ALDH5A1	6	363,428	1,412	2,62E-06	6,99E-04
ENSG00000113300	CNOT6	5	1420,471	-1,008	2,56E-06	6,94E-04
ENSG00000114374	USP9Y	Y	656,880	-1,006	5,23E-04	2,84E-02
ENSG00000114854	TNNC1	3	36,266	2,621	3,13E-05	4,31E-03
ENSG00000115221	ITGB6	2	1561,227	-1,008	4,59E-06	1,03E-03
ENSG00000115414	FN1	2	4227,978	-1,889	1,92E-04	1,56E-02
ENSG00000116984	MTR	1	509,359	-1,032	3,64E-04	2,29E-02
ENSG00000117020	AKT3	1	65,373	-1,287	2,48E-05	3,79E-03
ENSG00000117152	RGS4	1	44,288	-1,311	4,38E-04	2,56E-02
ENSG00000117984	CTSD	11	16630,139	1,017	1,34E-05	2,40E-03
ENSG00000118785	SPP1	4	12,700	-2,132	5,80E-06	1,23E-03
ENSG00000118849	RARRES1	3	313,612	1,346	2,78E-04	1,95E-02
ENSG00000119915	ELOVL3	10	70,922	1,562	3,91E-06	9,12E-04
ENSG00000122641	INHBA	7	999,747	-1,066	1,02E-05	1,86E-03
ENSG00000122870	BICC1	10	47,636	-1,104	9,46E-05	9,53E-03
ENSG00000128268	MGAT3	22	33,048	2,104	3,50E-07	1,43E-04
ENSG00000129990	SYT5	19	69,555	1,010	1,66E-04	1,41E-02
ENSG00000129991	TNNI3	19	38,319	1,276	6,15E-06	1,26E-03
ENSG00000130427	EPO	7	17,513	2,543	2,42E-04	1,80E-02
ENSG00000130600	H19	11	7004,987	2,041	1,07E-04	1,01E-02
ENSG00000131711	MAP1B	5	193,900	-1,816	1,94E-09	2,32E-06
ENSG00000131737	KRT34	17	135,021	1,078	4,21E-04	2,50E-02
ENSG00000131738	KRT33B	17	56,730	1,254	3,03E-04	2,03E-02
ENSG00000131771	PPP1R1B	17	31,745	1,121	1,03E-03	4,13E-02
ENSG00000132677	RHBG	1	174,508	1,925	1,77E-05	2,94E-03
ENSG00000133110	POSTN	13	47,498	-2,154	2,43E-08	1,70E-05
ENSG00000133134	BEX2	X	140,873	1,107	6,62E-05	7,67E-03
ENSG00000133216	EPHB2	1	110,296	1,108	6,11E-04	3,12E-02
ENSG00000133710	SPINK5	5	75611,802	1,266	5,27E-04	2,85E-02
ENSG00000133739	LRRCC1	8	97,356	-1,075	1,17E-04	1,07E-02
ENSG00000135074	ADAM19	5	1271,135	-1,364	2,70E-08	1,81E-05
ENSG00000135253	KCP	7	54,927	-1,053	2,56E-04	1,84E-02
ENSG00000135374	ELF5	11	485,736	2,285	4,18E-04	2,50E-02
ENSG00000135678	CPM	12	1622,254	1,037	1,97E-04	1,59E-02
ENSG00000135917	SLC19A3	2	64,854	1,666	8,29E-04	3,65E-02
ENSG00000136603	SKIL	3	704,185	-1,092	1,11E-06	3,59E-04
ENSG00000136696	IL36B	2	151,607	1,269	8,04E-06	1,55E-03
ENSG00000136697	IL1F10	2	174,775	1,351	3,63E-06	8,82E-04
ENSG00000137628	DDX60	4	1426,624	-1,288	3,41E-10	4,76E-07
ENSG00000137868	STRA6	15	306,288	-1,760	1,15E-08	8,79E-06

ENSG00000137959	IFI44L	1	745,449	-1,009	1,03E-07	5,41E-05
ENSG00000138685	FGF2	4	18,477	-1,445	7,61E-05	8,19E-03
ENSG00000138735	PDE5A	4	36,031	-1,120	1,11E-03	4,24E-02
ENSG00000139364	TMEM132B	12	30,155	-1,277	1,26E-03	4,46E-02
ENSG00000140297	GCNT3	15	107,217	1,605	2,50E-06	6,88E-04
ENSG00000140481	CCDC33	15	42,791	-1,750	6,72E-04	3,27E-02
ENSG00000141485	SLC13A5	17	138,505	-1,442	9,40E-07	3,36E-04
ENSG00000142973	CYP4B1	1	758,466	2,079	1,44E-07	7,31E-05
ENSG00000143412	ANXA9	1	1219,648	1,774	2,98E-10	4,76E-07
ENSG00000143882	ATP6V1C2	2	1740,283	1,744	8,06E-04	3,62E-02
ENSG00000144331	ZNF385B	2	18,604	-1,343	1,25E-03	4,45E-02
ENSG00000144810	COL8A1	3	98,212	-1,320	4,34E-08	2,51E-05
ENSG00000149311	ATM	11	427,834	-1,034	2,25E-04	1,75E-02
ENSG00000149809	TM7SF2	11	4330,167	1,158	2,66E-05	3,95E-03
ENSG00000150764	DIXDC1	11	98,475	-1,185	2,79E-04	1,95E-02
ENSG00000151320	AKAP6	14	61,217	-1,159	7,38E-05	8,19E-03
ENSG00000151414	NEK7	1	696,271	-1,093	1,83E-07	8,31E-05
ENSG00000153140	CETN3	5	184,111	-1,051	9,89E-07	3,38E-04
ENSG00000153162	BMP6	6	554,192	-1,496	3,46E-07	1,43E-04
ENSG00000154874	CCDC144B	17	12,442	-2,263	2,29E-04	1,76E-02
ENSG00000157368	IL34	16	168,679	1,024	1,42E-03	4,73E-02
ENSG00000158352	SHROOM4	X	80,276	-1,205	1,38E-04	1,21E-02
ENSG00000158517	NCF1	7	46,985	1,050	2,39E-04	1,80E-02
ENSG00000161031	PGLYRP2	19	49,684	1,759	3,45E-06	8,64E-04
ENSG00000162078	ZG16B	16	44,002	1,230	2,35E-04	1,79E-02
ENSG00000163221	S100A12	1	1082,370	1,530	2,72E-05	4,00E-03
ENSG00000163464	CXCR1	2	42,282	-1,006	5,99E-04	3,08E-02
ENSG00000163687	DNASE1L3	3	45,211	1,969	1,47E-10	3,53E-07
ENSG00000165029	ABCA1	9	612,471	-1,103	8,22E-05	8,57E-03
ENSG00000165178	NCF1C	7	32,006	1,487	1,77E-05	2,94E-03
ENSG00000165410	CFL2	14	286,214	-1,003	5,31E-05	6,56E-03
ENSG00000165874	FAM35BP	10	79,949	-1,025	9,08E-04	3,83E-02
ENSG00000166250	CLMP	11	535,086	-1,009	4,56E-05	5,85E-03
ENSG00000166825	ANPEP	15	427,822	-1,126	1,70E-06	5,01E-04
ENSG00000167779	IGFBP6	12	3895,036	1,011	5,76E-07	2,20E-04
ENSG00000167968	DNASE1L2	16	914,716	2,072	9,67E-06	1,82E-03
ENSG00000168447	SCNN1B	16	1730,275	1,555	1,46E-03	4,77E-02
ENSG00000168952	STXBP6	14	19,179	2,323	1,19E-03	4,40E-02
ENSG00000169026	MFSD7	4	64,558	1,106	4,73E-04	2,70E-02
ENSG00000169245	CXCL10	4	41,575	-1,878	3,13E-08	1,95E-05
ENSG00000169248	CXCL11	4	15,605	-1,718	1,08E-04	1,02E-02
ENSG00000169435	RASSF6	4	155,847	-1,044	8,04E-05	8,54E-03
ENSG00000169509	CRCT1	1	6537,672	1,291	5,95E-04	3,08E-02
ENSG00000170477	KRT4	12	26284,325	1,852	4,19E-11	1,17E-07
ENSG00000170482	SLC23A1	5	44,353	1,717	1,69E-06	5,01E-04

ENSG00000171401	KRT13	17	191262,031	1,571	1,68E-09	2,17E-06
ENSG00000171617	ENC1	5	2612,799	-1,023	2,48E-05	3,79E-03
ENSG00000171766	GATM	15	50,495	1,177	1,82E-04	1,50E-02
ENSG00000171827	ZNF570	19	62,976	-1,061	5,10E-04	2,79E-02
ENSG00000172137	CALB2	16	1530,728	1,121	3,06E-07	1,33E-04
ENSG00000172164	SNTB1	8	66,311	1,901	7,17E-06	1,42E-03
ENSG00000172782	FADS6	17	101,360	1,577	2,09E-04	1,67E-02
ENSG00000172927	MYEOV	11	28,018	1,315	2,36E-04	1,79E-02
ENSG00000173227	SYT12	11	54,808	1,047	1,20E-03	4,40E-02
ENSG00000173239	LIPM	10	564,358	1,825	2,41E-04	1,80E-02
ENSG00000173275	ZNF449	X	67,395	-1,040	9,28E-04	3,88E-02
ENSG00000173338	KCNK7	11	360,576	1,268	1,58E-07	7,79E-05
ENSG00000174640	SLCO2A1	3	726,930	-1,751	1,54E-04	1,32E-02
ENSG00000175121	WFDC5	20	2630,257	1,918	1,45E-05	2,49E-03
ENSG00000176194	CIDEA	18	847,368	1,195	1,08E-06	3,57E-04
ENSG00000177409	SAMD9L	7	461,064	-1,046	1,01E-06	3,38E-04
ENSG00000177694	NAALADL2	3	18,664	-1,136	9,93E-04	4,01E-02
ENSG00000177707	NECTIN3	3	85,134	-1,026	2,17E-05	3,41E-03
ENSG00000177888	ZBTB41	1	181,886	-1,024	3,10E-04	2,07E-02
ENSG00000178033	CALHM5	6	94,449	-1,097	1,28E-04	1,14E-02
ENSG00000178172	SPINK6	5	541,859	-1,206	6,96E-06	1,39E-03
ENSG00000180488	MIGA1	1	268,930	-1,090	2,63E-05	3,94E-03
ENSG00000180673	EXOC5P1	4	30,503	-1,170	6,07E-04	3,11E-02
ENSG00000180730	SHISA2	13	25,988	-1,220	3,64E-04	2,29E-02
ENSG00000181218	HIST3H2A	1	95,494	1,032	1,33E-05	2,40E-03
ENSG00000181381	DDX60L	4	816,481	-1,180	4,50E-09	4,54E-06
ENSG00000181458	TMEM45A	3	11934,203	1,204	9,75E-04	3,97E-02
ENSG00000182253	SYNM	15	64,480	-1,308	2,23E-05	3,47E-03
ENSG00000182687	GALR2	17	18,602	1,598	4,22E-04	2,50E-02
ENSG00000183091	NEB	2	122,508	1,337	1,59E-04	1,36E-02
ENSG00000183734	ASCL2	11	57,542	1,029	5,27E-04	2,85E-02
ENSG00000184060	ADAP2	17	422,089	1,261	1,99E-05	3,24E-03
ENSG00000184148	SPRR4	1	3301,205	3,185	4,42E-12	1,86E-08
ENSG00000184261	KCNK12	2	68,006	-1,249	1,03E-04	1,00E-02
ENSG00000184613	NELL2	12	118,244	-1,011	9,71E-04	3,97E-02
ENSG00000185168	LINC00482	17	107,659	1,678	5,63E-07	2,20E-04
ENSG00000185332	TMEM105	17	92,657	1,019	1,03E-04	1,00E-02
ENSG00000187796	CARD9	9	99,883	1,706	1,82E-07	8,31E-05
ENSG00000188613	NANOS1	10	100,379	1,348	6,86E-06	1,39E-03
ENSG00000188647	PTAR1	9	426,731	-1,080	1,80E-05	2,96E-03
ENSG00000188921	HACD4	9	215,253	-1,054	1,41E-05	2,44E-03
ENSG00000189014	FAM35DP	10	40,964	-1,246	8,95E-04	3,80E-02
ENSG00000189108	IL1RAPL2	X	15,560	-2,631	8,07E-07	3,01E-04
ENSG00000189377	CXCL17	19	31,249	1,277	9,02E-04	3,81E-02
ENSG00000196437	ZNF569	19	38,330	-1,041	8,05E-04	3,62E-02

ENSG00000197191	CYSRT1	9	1869,651	1,195	3,78E-05	5,07E-03
ENSG00000197353	LYPD2	8	222,782	2,691	1,71E-07	8,19E-05
ENSG00000197580	BCO2	11	109,598	1,202	3,05E-05	4,27E-03
ENSG00000197603	C5orf42	5	252,106	-1,165	1,10E-04	1,03E-02
ENSG00000197766	CFD	19	96,107	1,689	4,78E-09	4,54E-06
ENSG00000197930	ERO1A	14	1924,172	-1,065	3,01E-08	1,94E-05
ENSG00000198707	CEP290	12	161,518	-1,111	1,17E-04	1,07E-02
ENSG00000198732	SMOC1	14	232,162	-1,419	2,17E-06	6,07E-04
ENSG00000198734	F5	1	35,004	-1,242	4,63E-04	2,67E-02
ENSG00000203782	LOR	1	8474,252	2,247	9,41E-05	9,53E-03
ENSG00000204020	LIPN	10	247,347	1,234	9,64E-04	3,97E-02
ENSG00000204421	LY6G6C	6	3364,269	1,583	4,39E-06	9,95E-04
ENSG00000204538	PSORS1C2	6	573,305	2,263	8,32E-14	9,59E-10
ENSG00000204542	C6orf15	6	762,452	1,836	1,72E-05	2,92E-03
ENSG00000204767	FAM196B	5	36,315	-1,332	7,20E-04	3,41E-02
ENSG00000205363	C15orf59	15	359,693	1,776	3,00E-12	1,68E-08
ENSG00000212864	RNF208	9	186,905	1,032	7,95E-04	3,62E-02
ENSG00000213085	CFAP45	1	116,099	1,476	3,09E-07	1,33E-04
ENSG00000213949	ITGA1	5	261,714	-1,099	5,93E-06	1,23E-03
ENSG00000218416	PP14571	2	140,071	1,663	7,21E-09	6,05E-06
ENSG00000221972	C3orf36	3	34,240	-2,257	7,53E-04	3,51E-02
ENSG00000224721	AC007182.1	14	51,318	1,526	5,31E-05	6,56E-03
ENSG00000225191	AL136455.1	1	17,256	-1,344	1,36E-03	4,64E-02
ENSG00000229807	XIST	X	88,981	-1,022	8,18E-05	8,57E-03
ENSG00000230606	AC092683.1	2	105,622	-1,157	2,02E-05	3,26E-03
ENSG00000230650	AC140479.2	2	35,101	-1,142	7,63E-04	3,54E-02
ENSG00000230662	TNPO1P2	17	66,452	-1,046	9,52E-04	3,95E-02
ENSG00000230836	LINC01293	2	27,550	-1,419	1,42E-03	4,73E-02
ENSG00000231826	LINC01819	2	155,937	1,058	1,43E-04	1,25E-02
ENSG00000232267	ACTR3P2	X	27,752	-1,303	8,04E-04	3,62E-02
ENSG00000233441	CYP2AB1P	3	13,363	2,386	3,34E-06	8,62E-04
ENSG00000234323	LINC01505	9	27,608	-2,445	4,30E-08	2,51E-05
ENSG00000234478	ACBD3-AS1	1	30,663	1,394	8,75E-04	3,76E-02
ENSG00000235008	AL023775.1	6	97,687	-1,029	1,22E-03	4,40E-02
ENSG00000235721	AC013268.3	2	27,588	-1,369	1,23E-03	4,43E-02
ENSG00000235884	LINC00941	12	48,550	-2,748	1,14E-13	9,59E-10
ENSG00000242435	UPK3BP1	7	16,208	1,514	8,30E-04	3,65E-02
ENSG00000243566	UPK3B	7	142,987	1,143	1,12E-04	1,04E-02
ENSG00000244242	IFITM10	11	135,079	1,281	7,52E-05	8,19E-03
ENSG00000248485	PCP4L1	1	45,306	1,705	2,09E-05	3,30E-03
ENSG00000250091	DNAH10OS	12	19,675	-1,731	2,83E-05	4,09E-03
ENSG00000250742	LINC02381	12	103,303	-1,574	5,14E-09	4,54E-06
ENSG00000253125	AC055854.1	8	92,911	1,448	1,33E-03	4,61E-02
ENSG00000253159	PCDHGA12	5	144,897	-1,042	4,90E-04	2,76E-02
ENSG00000254024	AP001207.3	8	34,558	1,766	3,55E-06	8,77E-04

ENSG00000255173	AP003068.3	11	46,770	1,221	8,77E-04	3,76E-02
ENSG00000255501	CARD18	11	1401,339	1,484	2,29E-11	7,70E-08
ENSG00000259803	SLC22A31	16	39,601	2,050	3,85E-07	1,54E-04
ENSG00000260581	AC011374.1	5	235,205	1,070	9,82E-06	1,83E-03
ENSG00000260673	AL034376.2	6	25,389	2,738	3,63E-04	2,29E-02
ENSG00000261040	WFDC21P	17	500,966	1,421	9,90E-05	9,83E-03
ENSG00000261268	AC112236.1	4	39,570	1,129	8,64E-04	3,74E-02
ENSG00000261468	AC096921.2	3	14,621	-1,504	5,37E-04	2,87E-02
ENSG00000261556	SMG1P7	16	99,629	-1,061	2,22E-04	1,74E-02
ENSG00000261786	AC006058.1	3	137,767	-1,197	1,29E-06	3,93E-04
ENSG00000263740	RN7SL4P	3	23,043	1,953	1,81E-06	5,25E-04
ENSG00000265735	RN7SL5P	9	46,453	1,540	8,18E-05	8,57E-03
ENSG00000267156	TPMTP1	18	29,077	-1,187	4,81E-04	2,72E-02
ENSG00000267368	UPK3BL1	7	73,241	1,217	8,94E-08	4,84E-05
ENSG00000267416	AC025048.4	17	16,735	1,852	3,76E-04	2,31E-02
ENSG00000268307	LINC02560	19	320,129	1,089	1,91E-04	1,56E-02
ENSG00000269729	AC006262.2	19	99,076	1,094	3,72E-04	2,31E-02
ENSG00000269741	AC011473.4	19	2169,575	1,072	1,03E-04	1,00E-02
ENSG00000274012	RN7SL2	14	150,730	1,297	1,01E-05	1,86E-03
ENSG00000278192	AL118505.1	20	21,011	-1,077	1,10E-03	4,24E-02
ENSG00000278771	RN7SL3	14	195,388	1,365	5,48E-06	1,19E-03
ENSG00000283142	AL049767.1	20	40,758	1,091	1,07E-03	4,19E-02
ENSG00000283227	SPRR5	1	1720,770	1,347	9,12E-07	3,33E-04

9.6.2 LINC00941 regulated genes on day 3 in organotypic epidermis

Identifier	Gene name	Chr	baseMean	log2FoldChange	pvalue	padj
ENSG00000070388	FGF22	19	24,345	4,697	1,00E-06	2,52E-04
ENSG00000242950	ERVW-1	7	23,855	4,232	8,00E-05	7,61E-03
ENSG00000133063	CHIT1	1	60,853	4,193	2,25E-07	8,21E-05
ENSG00000117594	HSD11B1	1	29,987	4,071	1,28E-08	8,59E-06
ENSG00000214456	PLIN5	19	24,711	4,028	3,54E-05	4,13E-03
ENSG00000100341	PNPLA5	22	45,964	3,616	2,68E-06	5,27E-04
ENSG00000165495	PKNOX2	11	44,647	3,550	2,19E-07	8,19E-05
ENSG00000197915	HRNR	1	2307,741	3,456	1,06E-05	1,63E-03
ENSG00000161798	AQP5	12	59,268	3,455	1,05E-04	9,17E-03
ENSG00000187223	LCE2D	1	844,677	3,415	3,98E-05	4,57E-03
ENSG00000159455	LCE2B	1	2261,590	3,376	1,53E-07	6,01E-05
ENSG00000244057	LCE3C	1	553,142	3,363	2,20E-04	1,51E-02
ENSG00000185962	LCE3A	1	384,888	3,256	2,65E-05	3,31E-03
ENSG00000106178	CCL24	7	21,423	3,252	1,63E-09	1,87E-06
ENSG00000187173	LCE2A	1	857,886	3,200	4,78E-05	5,16E-03
ENSG00000165953	SERPINA12	14	31,266	3,186	1,11E-03	3,53E-02
ENSG00000198854	C1orf68	1	294,692	3,149	7,60E-09	5,83E-06

ENSG00000203782	LOR	1	8474,252	3,094	3,14E-07	1,03E-04
ENSG00000187180	LCE2C	1	1373,617	3,087	4,79E-06	8,29E-04
ENSG00000172155	LCE1D	1	351,205	3,007	7,55E-08	3,68E-05
ENSG00000184148	SPRR4	1	3301,205	3,000	1,32E-09	1,63E-06
ENSG00000244617	ASPRV1	2	14631,421	2,992	1,53E-05	2,12E-03
ENSG00000118520	ARG1	6	920,462	2,985	3,00E-04	1,92E-02
ENSG00000260673	AL034376.2	6	25,389	2,972	9,26E-07	2,40E-04
ENSG00000173578	XCR1	3	25,876	2,955	1,02E-09	1,50E-06
ENSG00000176075	LINC00302	1	92,543	2,941	3,01E-04	1,92E-02
ENSG00000283646	LINC02009	3	38,147	2,930	1,48E-12	5,94E-09
ENSG00000203786	KPRP	1	4383,131	2,927	1,29E-05	1,91E-03
ENSG00000186844	LCE1A	1	1113,631	2,927	8,13E-07	2,26E-04
ENSG00000183638	RP1L1	8	58,252	2,914	2,85E-07	9,76E-05
ENSG00000140600	SH3GL3	15	21,667	2,896	3,09E-04	1,93E-02
ENSG00000235942	LCE6A	1	377,031	2,883	2,46E-07	8,80E-05
ENSG00000237512	UNC5B-AS1	10	55,092	2,839	7,52E-07	2,17E-04
ENSG00000167968	DNASE1L2	16	914,716	2,834	1,24E-08	8,59E-06
ENSG00000125780	TGM3	20	440,351	2,804	2,77E-03	4,88E-02
ENSG00000240386	LCE1F	1	803,687	2,787	5,18E-08	2,62E-05
ENSG00000125571	IL37	2	112,315	2,777	2,59E-03	4,79E-02
ENSG00000183479	TREX2	X	546,111	2,688	2,57E-07	8,99E-05
ENSG00000196734	LCE1B	1	1482,888	2,632	1,49E-06	3,43E-04
ENSG00000174343	CHRNA9	4	149,907	2,615	2,00E-08	1,24E-05
ENSG00000186226	LCE1E	1	621,957	2,613	3,49E-09	3,30E-06
ENSG00000211448	DIO2	14	279,336	2,597	1,13E-03	3,54E-02
ENSG00000204538	PSORS1C2	6	573,305	2,514	9,11E-16	1,47E-11
ENSG00000160862	AZGP1	7	2818,541	2,504	1,16E-06	2,87E-04
ENSG00000084110	HAL	12	3190,502	2,499	1,28E-05	1,91E-03
ENSG00000070601	FRMPD1	9	326,154	2,480	9,43E-08	4,34E-05
ENSG00000110675	ELMOD1	11	166,190	2,464	4,08E-08	2,19E-05
ENSG00000178597	PSAPL1	4	464,465	2,421	1,09E-07	4,62E-05
ENSG00000197084	LCE1C	1	1889,971	2,415	6,97E-15	5,61E-11
ENSG00000180332	KCTD4	13	70,462	2,411	1,23E-05	1,84E-03
ENSG00000204542	C6orf15	6	762,452	2,400	1,43E-07	5,76E-05
ENSG00000274213	AC015912.3	17	17,030	2,399	4,79E-06	8,29E-04
ENSG00000186207	LCE5A	1	20,270	2,379	1,73E-07	6,63E-05
ENSG00000115488	NEU2	2	56,281	2,372	1,71E-05	2,32E-03
ENSG00000183760	ACP7	19	921,131	2,342	5,20E-06	8,89E-04
ENSG00000140678	ITGAX	16	41,733	2,332	6,43E-09	5,17E-06
ENSG00000084674	APOB	2	117,375	2,327	8,94E-06	1,40E-03
ENSG00000214313	AZGP1P1	7	138,805	2,325	2,55E-05	3,21E-03
ENSG00000170255	MRGPRX1	11	16,351	2,289	4,20E-05	4,69E-03
ENSG00000232679	LINC01705	1	23,621	2,285	9,78E-07	2,50E-04
ENSG00000131969	ABHD12B	14	170,279	2,268	5,35E-06	9,06E-04
ENSG00000100292	HMOX1	22	2193,630	2,225	1,99E-06	4,37E-04

ENSG00000163202	LCE3D	1	10002,389	2,219	2,83E-04	1,86E-02
ENSG00000231672	DIRC3	2	36,555	2,217	8,52E-08	4,03E-05
ENSG00000042062	RIPOR3	20	23,696	2,194	1,59E-03	4,14E-02
ENSG00000241479	AC074033.2	3	23,504	2,184	2,16E-03	4,53E-02
ENSG00000165799	RNASE7	14	1331,373	2,176	1,44E-06	3,43E-04
ENSG00000185966	LCE3E	1	3554,523	2,171	1,82E-03	4,36E-02
ENSG00000257878	AC007298.2	12	16,345	2,167	4,49E-06	7,93E-04
ENSG00000277496	AL357033.4	20	106,480	2,165	1,49E-10	2,40E-07
ENSG00000198691	ABCA4	1	29,808	2,159	4,27E-07	1,37E-04
ENSG00000224614	TNK2-AS1	3	45,240	2,152	3,75E-04	2,19E-02
ENSG00000276317	AL357033.3	20	21,119	2,133	8,66E-07	2,32E-04
ENSG00000124920	MYRF	11	112,965	2,131	1,82E-05	2,44E-03
ENSG00000102962	CCL22	16	21,163	2,128	3,30E-06	6,32E-04
ENSG00000158220	ESYT3	3	457,878	2,123	7,07E-12	2,28E-08
ENSG00000171360	KRT38	17	16,605	2,120	1,23E-04	1,04E-02
ENSG00000283227	SPRR5	1	1720,770	2,116	2,78E-13	1,49E-09
ENSG00000114854	TNNC1	3	36,266	2,082	6,72E-04	2,85E-02
ENSG00000173221	GLRX	5	391,456	2,062	1,21E-10	2,16E-07
ENSG00000143520	FLG2	1	27017,707	2,047	1,11E-03	3,54E-02
ENSG00000172164	SNTB1	8	66,311	2,044	2,92E-08	1,68E-05
ENSG00000179761	PIPOX	17	16,340	2,044	3,38E-05	4,03E-03
ENSG00000050628	PTGER3	1	132,320	1,997	3,81E-04	2,19E-02
ENSG00000172349	IL16	15	20,942	1,993	8,87E-07	2,34E-04
ENSG00000224307	AL161785.1	9	64,849	1,986	3,93E-08	2,18E-05
ENSG00000204539	CDSN	6	10440,017	1,982	1,45E-05	2,04E-03
ENSG00000158786	PLA2G2F	1	523,482	1,969	1,39E-05	1,97E-03
ENSG00000119457	SLC46A2	9	116,177	1,964	3,49E-06	6,45E-04
ENSG00000165238	WNK2	9	20,934	1,959	3,77E-06	6,89E-04
ENSG00000173926	MARCH3	5	268,192	1,929	3,37E-04	2,04E-02
ENSG00000258279	LINC00592	12	48,920	1,927	4,51E-07	1,42E-04
ENSG00000131738	KRT33B	17	56,730	1,908	1,06E-07	4,60E-05
ENSG00000168952	STXBP6	14	19,179	1,895	1,85E-05	2,46E-03
ENSG00000108578	BLMH	17	1723,777	1,834	1,87E-06	4,18E-04
ENSG00000103740	ACSBG1	15	190,957	1,827	2,29E-03	4,61E-02
ENSG00000261026	AC105046.1	8	44,414	1,769	2,02E-03	4,44E-02
ENSG00000204618	RNF39	6	897,098	1,756	1,21E-04	1,03E-02
ENSG00000187185	AC092118.1	16	24,212	1,738	2,41E-05	3,05E-03
ENSG00000159450	TCHH	1	792,171	1,734	9,01E-11	1,81E-07
ENSG00000229980	TOB1-AS1	17	23,111	1,731	1,79E-05	2,42E-03
ENSG00000213904	LIPE-AS1	19	80,860	1,723	6,69E-07	1,99E-04
ENSG00000161031	PGLYRP2	19	49,684	1,721	3,48E-06	6,45E-04
ENSG00000164120	HPGD	4	1652,388	1,719	5,36E-11	1,44E-07
ENSG00000279693	AC099521.3	16	65,134	1,718	3,06E-04	1,93E-02
ENSG00000157368	IL34	16	168,679	1,702	3,05E-07	1,02E-04
ENSG00000130600	H19	11	7004,987	1,698	2,84E-03	4,91E-02

ENSG00000197948	FCHSD1	5	2443,277	1,691	3,15E-09	3,16E-06
ENSG00000276900	AC023157.3	12	52,516	1,688	1,32E-05	1,93E-03
ENSG00000234996	AC098934.2	1	16,724	1,681	4,82E-04	2,53E-02
ENSG00000253125	AC055854.1	8	92,911	1,671	2,72E-04	1,79E-02
ENSG00000132677	RHBG	1	174,508	1,666	4,47E-04	2,43E-02
ENSG00000187796	CARD9	9	99,883	1,664	7,80E-07	2,20E-04
ENSG00000143882	ATP6V1C2	2	1740,283	1,663	2,99E-03	4,99E-02
ENSG00000136697	IL1F10	2	174,775	1,661	4,01E-09	3,58E-06
ENSG00000166920	C15orf48	15	165,895	1,640	1,03E-03	3,44E-02
ENSG00000130475	FCHO1	19	208,518	1,636	5,89E-09	4,99E-06
ENSG00000165091	TMC1	9	18,446	1,634	1,21E-04	1,03E-02
ENSG00000108417	KRT37	17	103,219	1,610	2,10E-06	4,51E-04
ENSG00000106302	HYAL4	7	76,234	1,610	6,63E-06	1,09E-03
ENSG00000075673	ATP12A	13	10529,121	1,609	8,54E-04	3,19E-02
ENSG00000269985	AL021328.1	6	29,931	1,607	1,57E-04	1,23E-02
ENSG00000108556	CHRNE	17	23,370	1,603	6,04E-04	2,76E-02
ENSG00000261572	AC097639.1	3	25,121	1,601	7,65E-05	7,46E-03
ENSG00000197353	LYPD2	8	222,782	1,588	2,95E-03	4,97E-02
ENSG00000036672	USP2	11	418,375	1,579	5,21E-08	2,62E-05
ENSG00000143412	ANXA9	1	1219,648	1,578	1,34E-07	5,54E-05
ENSG00000185168	LINC00482	17	107,659	1,570	2,22E-06	4,69E-04
ENSG00000188277	C15orf62	15	364,916	1,568	1,62E-04	1,24E-02
ENSG00000103811	CTSH	15	2304,900	1,551	2,63E-08	1,57E-05
ENSG00000162040	HS3ST6	16	140,532	1,542	9,10E-04	3,27E-02
ENSG00000177363	LRRN4CL	11	18,979	1,538	7,45E-04	3,02E-02
ENSG00000172551	MUCL1	12	147,835	1,535	1,09E-03	3,52E-02
ENSG00000168703	WFDC12	20	1939,436	1,494	1,87E-04	1,38E-02
ENSG00000259803	SLC22A31	16	39,601	1,479	5,01E-05	5,31E-03
ENSG00000221878	PSG7	19	16,799	1,476	1,23E-03	3,70E-02
ENSG00000140297	GCNT3	15	107,217	1,473	1,91E-05	2,48E-03
ENSG00000006059	KRT33A	17	45,365	1,471	2,96E-05	3,61E-03
ENSG00000243137	PSG4	19	299,541	1,466	1,47E-06	3,43E-04
ENSG00000108852	MPP2	17	84,324	1,466	5,80E-06	9,72E-04
ENSG00000138623	SEMA7A	15	574,880	1,465	3,46E-06	6,45E-04
ENSG00000254966	AC103974.1	11	56,368	1,454	2,68E-06	5,27E-04
ENSG00000108244	KRT23	17	5959,095	1,451	1,28E-03	3,76E-02
ENSG00000256462	AL732437.1	10	19,089	1,446	1,95E-03	4,36E-02
ENSG00000129437	KLK14	19	302,792	1,446	4,42E-06	7,90E-04
ENSG00000263823	AC009831.1	18	71,633	1,440	1,48E-06	3,43E-04
ENSG00000150471	ADGRL3	4	89,571	1,440	1,65E-03	4,22E-02
ENSG00000148734	NPFFR1	10	32,725	1,435	1,75E-04	1,32E-02
ENSG00000101445	PPP1R16B	20	18,783	1,422	8,43E-04	3,18E-02
ENSG00000167046	AL357033.1	20	21,529	1,413	3,43E-04	2,05E-02
ENSG00000163803	PLB1	2	209,789	1,412	8,52E-07	2,32E-04
ENSG00000188100	FAM25A	10	127,454	1,396	1,90E-05	2,48E-03

ENSG00000152137	HSPB8	12	3089,031	1,389	4,04E-04	2,28E-02
ENSG00000172731	LRRC20	10	1028,504	1,385	2,57E-06	5,27E-04
ENSG00000224721	AC007182.1	14	51,318	1,385	6,30E-05	6,42E-03
ENSG00000171711	DEFB4A	8	51,551	1,378	5,70E-04	2,73E-02
ENSG00000178776	C5orf46	5	291,022	1,377	2,05E-05	2,64E-03
ENSG00000273132	AL355312.3	6	22,739	1,369	8,66E-04	3,21E-02
ENSG00000088386	SLC15A1	13	840,146	1,366	1,67E-06	3,78E-04
ENSG00000166105	GLB1L3	11	124,072	1,364	1,16E-05	1,76E-03
ENSG00000110799	VWF	12	158,331	1,361	4,59E-05	4,99E-03
ENSG00000101460	MAP1LC3A	20	443,984	1,348	8,92E-04	3,25E-02
ENSG00000130751	NPAS1	19	130,954	1,347	3,50E-05	4,12E-03
ENSG00000236263	AC234582.2	1	30,613	1,344	5,88E-04	2,75E-02
ENSG00000197249	SERPINA1	14	43,639	1,333	1,61E-04	1,24E-02
ENSG00000187210	GCNT1	9	285,317	1,332	4,09E-05	4,66E-03
ENSG00000204941	PSG5	19	34,571	1,320	7,99E-04	3,14E-02
ENSG00000180667	YOD1	1	790,541	1,315	5,49E-07	1,70E-04
ENSG00000119915	ELOVL3	10	70,922	1,314	1,29E-04	1,07E-02
ENSG00000131737	KRT34	17	135,021	1,313	5,09E-05	5,35E-03
ENSG00000134830	C5AR2	19	20,897	1,309	8,67E-04	3,21E-02
ENSG00000248485	PCP4L1	1	45,306	1,309	1,29E-03	3,77E-02
ENSG00000205269	TMEM170B	6	35,355	1,306	5,80E-04	2,74E-02
ENSG00000119125	GDA	9	373,958	1,297	1,32E-09	1,63E-06
ENSG00000136696	IL36B	2	151,607	1,284	2,03E-06	4,40E-04
ENSG00000204421	LY6G6C	6	3364,269	1,281	5,63E-04	2,73E-02
ENSG00000154274	C4orf19	4	69,788	1,280	1,34E-05	1,94E-03
ENSG00000179859	LINC02581	17	262,186	1,264	2,70E-05	3,34E-03
ENSG00000234478	ACBD3-AS1	1	30,663	1,259	2,99E-04	1,92E-02
ENSG00000256751	PLBD1-AS1	12	19,936	1,224	2,68E-03	4,84E-02
ENSG00000169026	MFSD7	4	64,558	1,211	2,40E-04	1,62E-02
ENSG00000010030	ETV7	6	81,051	1,200	4,13E-04	2,32E-02
ENSG00000174950	CD164L2	1	155,043	1,195	2,27E-04	1,55E-02
ENSG00000177406	AC021054.1	12	129,250	1,192	1,65E-05	2,27E-03
ENSG00000099954	CECR2	22	44,334	1,186	1,33E-03	3,82E-02
ENSG00000128268	MGAT3	22	33,048	1,180	7,75E-04	3,10E-02
ENSG00000123154	WDR83	19	302,390	1,177	2,49E-04	1,65E-02
ENSG00000160766	GBAP1	1	793,365	1,176	8,28E-06	1,32E-03
ENSG00000006625	GGCT	7	3190,004	1,174	2,57E-06	5,27E-04
ENSG00000111344	RASAL1	12	546,883	1,163	7,98E-05	7,61E-03
ENSG00000280587	LINC01348	1	61,479	1,150	7,43E-04	3,02E-02
ENSG00000255501	CARD18	11	1401,339	1,149	1,31E-06	3,19E-04
ENSG00000182218	HHIPL1	14	39,951	1,138	9,05E-04	3,26E-02
ENSG00000158486	DNAH3	16	42,592	1,132	4,66E-04	2,48E-02
ENSG00000159516	SPRR2G	1	3920,118	1,123	1,33E-04	1,09E-02
ENSG00000177628	GBA	1	3012,472	1,119	2,67E-06	5,27E-04
ENSG00000197580	BCO2	11	109,598	1,117	1,04E-04	9,11E-03

ENSG00000169896	ITGAM	16	51,604	1,115	1,27E-03	3,75E-02
ENSG00000187098	MITF	3	56,624	1,109	1,03E-04	9,11E-03
ENSG00000213462	ERV3-1	7	450,047	1,109	3,27E-04	2,00E-02
ENSG00000255173	AP003068.3	11	46,770	1,105	2,29E-03	4,61E-02
ENSG00000122877	EGR2	10	244,622	1,082	9,39E-04	3,32E-02
ENSG00000088826	SMOX	20	651,694	1,080	4,33E-05	4,81E-03
ENSG00000138639	ARHGAP24	4	163,077	1,077	8,07E-05	7,64E-03
ENSG00000135678	CPM	12	1622,254	1,064	3,80E-04	2,19E-02
ENSG00000069667	RORA	15	769,679	1,059	1,69E-04	1,29E-02
ENSG00000078804	TP53INP2	20	943,163	1,058	1,07E-04	9,27E-03
ENSG00000108309	RUNDC3A	17	536,830	1,057	5,91E-05	6,09E-03
ENSG00000164442	CITED2	6	1368,982	1,056	1,51E-04	1,21E-02
ENSG00000122042	UBL3	13	594,071	1,052	6,04E-06	1,00E-03
ENSG00000167914	GSDMA	17	4393,787	1,049	3,10E-04	1,93E-02
ENSG00000188613	NANOS1	10	100,379	1,044	1,00E-03	3,40E-02
ENSG00000108830	RND2	17	44,349	1,036	1,46E-03	4,01E-02
ENSG00000179148	ALOXE3	17	2541,632	1,036	4,49E-04	2,43E-02
ENSG00000182489	XKRX	X	440,414	1,034	1,35E-04	1,10E-02
ENSG00000231122	FAM25E	10	38,260	1,032	7,95E-04	3,13E-02
ENSG00000100867	DHRS2	14	98,824	1,031	1,87E-03	4,36E-02
ENSG00000166046	TCP11L2	12	275,329	1,027	7,45E-04	3,02E-02
ENSG00000119986	AVPI1	10	1127,676	1,021	2,22E-05	2,84E-03
ENSG00000158050	DUSP2	2	153,501	1,017	1,02E-04	9,11E-03
ENSG00000149328	GLB1L2	11	156,708	1,009	6,08E-04	2,76E-02
ENSG00000133401	PDZD2	5	1060,250	1,005	1,90E-04	1,38E-02
ENSG00000205363	C15orf59	15	359,693	1,001	2,00E-04	1,42E-02
ENSG00000151491	EPS8	12	52,925	-1,003	1,48E-03	4,04E-02
ENSG00000256223	ZNF10	12	49,407	-1,007	2,07E-03	4,48E-02
ENSG00000103202	NME4	16	1385,528	-1,010	7,92E-05	7,61E-03
ENSG00000184378	ACTRT3	3	60,985	-1,010	2,24E-03	4,60E-02
ENSG00000277586	NEFL	8	381,186	-1,010	5,48E-04	2,73E-02
ENSG00000228203	RNF144A-AS1	2	30,072	-1,014	2,48E-03	4,69E-02
ENSG00000234115	AL138878.2	6	66,501	-1,017	9,57E-04	3,35E-02
ENSG00000253159	PCDHGA12	5	144,897	-1,022	1,40E-03	3,92E-02
ENSG00000178033	CALHM5	6	94,449	-1,023	6,10E-04	2,76E-02
ENSG00000117472	TSPAN1	1	1794,589	-1,025	3,06E-06	5,93E-04
ENSG00000188321	ZNF559	19	68,513	-1,036	5,00E-04	2,60E-02
ENSG00000073849	ST6GAL1	3	317,625	-1,037	3,99E-04	2,26E-02
ENSG00000272602	ZNF595	4	92,775	-1,039	4,16E-04	2,32E-02
ENSG00000267652	AC011712.1	18	226,886	-1,040	1,16E-03	3,61E-02
ENSG00000146530	VWDE	7	30,876	-1,042	1,94E-03	4,36E-02
ENSG00000163328	GPR155	2	96,719	-1,061	3,28E-05	3,94E-03
ENSG00000225973	PIGBOS1	15	43,068	-1,061	8,85E-04	3,24E-02
ENSG00000156113	KCNMA1	10	154,705	-1,066	2,18E-04	1,51E-02
ENSG00000224078	SNHG14	15	663,487	-1,066	2,05E-04	1,44E-02

ENSG00000137868	STRA6	15	306,288	-1,068	1,24E-03	3,70E-02
ENSG00000213104	NPM1P46	2	435,186	-1,070	6,48E-05	6,51E-03
ENSG00000197653	DNAH10	12	112,894	-1,073	1,80E-03	4,33E-02
ENSG00000197467	COL13A1	10	77,862	-1,074	1,46E-04	1,17E-02
ENSG00000104332	SFRP1	8	941,270	-1,078	1,03E-04	9,11E-03
ENSG00000138439	FAM117B	2	111,279	-1,079	1,57E-04	1,23E-02
ENSG00000232391	RANP2	7	62,017	-1,084	5,37E-04	2,71E-02
ENSG00000184613	NELL2	12	118,244	-1,091	8,46E-04	3,18E-02
ENSG00000174130	TLR6	4	52,760	-1,097	3,10E-04	1,93E-02
ENSG00000164509	IL31RA	5	35,676	-1,097	2,35E-03	4,62E-02
ENSG00000106070	GRB10	7	190,541	-1,105	8,51E-05	7,96E-03
ENSG00000214357	NEURL1B	5	95,695	-1,109	2,42E-04	1,62E-02
ENSG00000257513	NPIPB1P	18	40,642	-1,110	1,09E-03	3,52E-02
ENSG00000013588	GPRC5A	12	1377,291	-1,111	1,98E-04	1,41E-02
ENSG00000231245	C1DP1	10	40,874	-1,113	1,94E-03	4,36E-02
ENSG00000232801	SDCBPP3	X	37,139	-1,116	2,42E-03	4,65E-02
ENSG00000119922	IFIT2	10	76,846	-1,119	4,40E-05	4,84E-03
ENSG00000258778	AL161670.2	14	32,345	-1,120	1,35E-03	3,84E-02
ENSG00000120327	PCDHB14	5	25,331	-1,121	2,89E-03	4,93E-02
ENSG00000123095	BHLHE41	12	60,143	-1,129	2,86E-03	4,93E-02
ENSG00000161912	ADCY10P1	6	37,113	-1,129	9,27E-04	3,28E-02
ENSG00000168916	ZNF608	5	107,735	-1,138	8,58E-05	7,98E-03
ENSG00000224785	AC006026.1	7	34,889	-1,138	5,72E-04	2,73E-02
ENSG00000196371	FUT4	11	40,119	-1,140	5,19E-04	2,63E-02
ENSG00000156284	CLDN8	21	22,746	-1,142	2,65E-03	4,83E-02
ENSG00000267336	EIF4A2P1	18	49,255	-1,152	8,75E-04	3,22E-02
ENSG00000166265	CYYR1	21	58,561	-1,157	3,50E-04	2,08E-02
ENSG00000050438	SLC4A8	12	37,615	-1,157	8,94E-04	3,25E-02
ENSG00000166780	C16orf45	16	55,784	-1,163	1,56E-04	1,23E-02
ENSG00000038427	VCAN	5	60,765	-1,164	9,96E-04	3,40E-02
ENSG00000161132	AC007663.1	22	28,711	-1,165	2,93E-03	4,96E-02
ENSG00000198910	L1CAM	X	515,857	-1,167	7,57E-07	2,17E-04
ENSG00000257219	LINC02407	12	26,890	-1,169	1,76E-03	4,30E-02
ENSG00000124469	CEACAM8	19	51,659	-1,175	1,31E-03	3,80E-02
ENSG00000166825	ANPEP	15	427,822	-1,187	4,03E-06	7,28E-04
ENSG00000231638	LUARIS	7	30,934	-1,189	2,44E-03	4,66E-02
ENSG00000231205	ZNF826P	19	37,516	-1,190	1,04E-03	3,45E-02
ENSG00000091129	NRCAM	7	120,523	-1,192	9,17E-05	8,43E-03
ENSG00000138061	CYP1B1	2	308,211	-1,195	1,16E-04	9,91E-03
ENSG00000103599	IQCH	15	32,762	-1,203	5,76E-04	2,74E-02
ENSG00000142920	AZIN2	1	33,007	-1,212	2,08E-04	1,45E-02
ENSG00000198046	ZNF667	19	78,455	-1,221	8,42E-06	1,33E-03
ENSG00000250722	SELENOP	5	142,505	-1,239	7,31E-06	1,19E-03
ENSG00000123096	SSPN	12	27,971	-1,240	6,50E-04	2,83E-02
ENSG00000236811	GAPDHP2	20	38,976	-1,243	9,49E-04	3,34E-02

ENSG00000105419	MEIS3	19	57,632	-1,248	1,85E-04	1,37E-02
ENSG00000107719	PALD1	10	330,940	-1,257	3,51E-05	4,12E-03
ENSG00000076351	SLC46A1	17	126,346	-1,262	1,38E-05	1,97E-03
ENSG00000141485	SLC13A5	17	138,505	-1,301	4,48E-05	4,91E-03
ENSG00000164125	FAM198B	4	87,323	-1,307	6,56E-05	6,56E-03
ENSG00000108602	ALDH3A1	17	81,348	-1,327	7,85E-05	7,61E-03
ENSG00000230439	MIG7	1	87,244	-1,334	6,30E-05	6,42E-03
ENSG00000247570	SDCBPP2	8	22,425	-1,335	2,24E-03	4,60E-02
ENSG00000241014	AC114490.1	1	18,571	-1,341	1,94E-03	4,36E-02
ENSG00000166669	ATF7IP2	16	25,745	-1,360	1,82E-04	1,36E-02
ENSG00000230006	ANKRD36BP2	2	30,485	-1,377	2,98E-04	1,92E-02
ENSG00000026025	VIM	10	4246,439	-1,385	5,72E-07	1,74E-04
ENSG00000269983	AC146944.4	5	39,572	-1,404	1,48E-03	4,04E-02
ENSG00000131711	MAP1B	5	193,900	-1,441	1,08E-05	1,66E-03
ENSG00000115461	IGFBP5	2	43,062	-1,454	6,48E-05	6,51E-03
ENSG00000171004	HS6ST2	X	38,181	-1,482	5,79E-04	2,74E-02
ENSG00000178172	SPINK6	5	541,859	-1,535	1,06E-07	4,60E-05
ENSG00000161544	CYGB	17	124,857	-1,538	1,55E-08	9,94E-06
ENSG00000259781	HMGB1P6	15	30,058	-1,557	9,65E-05	8,73E-03
ENSG00000169245	CXCL10	4	41,575	-1,568	1,40E-05	1,97E-03
ENSG00000234297	AL592293.2	9	29,444	-1,571	4,93E-05	5,28E-03
ENSG00000091128	LAMB4	7	23,411	-1,662	5,29E-05	5,53E-03
ENSG00000144810	COL8A1	3	98,212	-1,667	2,11E-09	2,26E-06
ENSG00000250742	LINC02381	12	103,303	-1,696	9,04E-09	6,61E-06
ENSG00000000971	CFH	1	34,895	-1,772	1,91E-05	2,48E-03
ENSG00000171243	SOSTDC1	7	21,196	-1,850	2,59E-06	5,27E-04
ENSG00000235884	LINC00941	12	48,550	-2,517	7,94E-11	1,81E-07

10 References

1. Martin, M. T., Vulin, A. & Hendry, J. H. Human epidermal stem cells: Role in adverse skin reactions and carcinogenesis from radiation. *Mutat. Res. Mutat. Res.* **770**, 349–368 (2016).
2. Gonzales, K. A. U. & Fuchs, E. Skin and Its Regenerative Powers: An Alliance between Stem Cells and Their Niche. *Dev. Cell* **43**, 387–401 (2017).
3. Proksch, E., Brandner, J. M. & Jensen, J.-M. The skin: an indispensable barrier. *Exp. Dermatol.* **17**, 1063–1072 (2008).

4. Blanpain, C. & Fuchs, E. Epidermal Stem Cells of the Skin. *Annu. Rev. Cell Dev. Biol.* **22**, 339–373 (2006).

5. Abe, Y. & Tanaka, N. Roles of the Hedgehog Signaling Pathway in Epidermal and Hair Follicle Development, Homeostasis, and Cancer. *J. Dev. Biol.* **5**, 12 (2017).

6. Baroni, A. *et al.* Structure and function of the epidermis related to barrier properties. *Clin. Dermatol.* **30**, 257–262 (2012).

7. Kanitakis, J. Anatomy, histology and immunohistochemistry of normal human skin. *Eur. J. Dermatol. EJD* **12**, 390–399; quiz 400–401 (2002).

8. MacNeil, S. Progress and opportunities for tissue-engineered skin. *Nature* **445**, 874–880 (2007).

9. Baroni, A. *et al.* Structure and function of the epidermis related to barrier properties. *Clin. Dermatol.* **30**, 257–262 (2012).

10. Webb, A., Li, A. & Kaur, P. Location and phenotype of human adult keratinocyte stem cells of the skin. *Differentiation* **72**, 387–395 (2004).

11. Baroni, A. *et al.* Structure and function of the epidermis related to barrier properties. *Clin. Dermatol.* **30**, 257–262 (2012).

12. Cooper, S. The Biology of the Skin. *J. R. Soc. Med.* **95**, 109–109 (2002).

13. Millington, P. F. & Wilkinson, R. *Skin*. (Cambridge University Press, 2009).

14. Solanas, G. & Benitah, S. A. Regenerating the skin: a task for the heterogeneous stem cell pool and surrounding niche. *Nat. Rev. Mol. Cell Biol.* **14**, 737–748 (2013).

15. Jones, P. H., Harper, S. & Watt, F. M. Stem cell patterning and fate in human epidermis. *Cell* **80**, 83–93 (1995).

16. Fuchs, E. Skin stem cells: rising to the surface. *J. Cell Biol.* **180**, 273–284 (2008).

17. Candi, E., Schmidt, R. & Melino, G. The cornified envelope: a model of cell death in the skin. *Nat. Rev. Mol. Cell Biol.* **6**, 328–340 (2005).

18. Potten, C. S. & Morris, R. J. Epithelial stem cells in vivo. *J. Cell Sci.* **1988**, 45–62 (1988).

19. Doupé, D. P. & Jones, P. H. Interfollicular epidermal homeostasis: dicing with differentiation: Interfollicular epidermal homeostasis. *Exp. Dermatol.* **21**, 249–253 (2012).

20. Clayton, E. *et al.* A single type of progenitor cell maintains normal epidermis. *Nature* **446**, 185–189 (2007).

21. Alcolea, M. P. & Jones, P. H. Lineage Analysis of Epidermal Stem Cells. *Cold Spring Harb. Perspect. Med.* **4**, a015206–a015206 (2014).

22. Alonso, L. & Fuchs, E. Stem cells of the skin epithelium. *Proc. Natl. Acad. Sci. U. S. A.* **100 Suppl 1**, 11830–11835 (2003).

23. Presland, R. B. & Dale, B. A. Epithelial Structural Proteins of the Skin and Oral Cavity: Function in Health and Disease. *Crit. Rev. Oral Biol. Med.* **11**, 383–408 (2000).

24. Sahle, F. F., Gebre-Mariam, T., Dobner, B., Wohlrab, J. & Neubert, R. H. H. Skin Diseases Associated with the Depletion of Stratum Corneum Lipids and Stratum Corneum Lipid Substitution Therapy. *Skin Pharmacol. Physiol.* **28**, 42–55 (2015).

25. Watt, F. M. Involucrin and Other Markers of Keratinocyte Terminal Differentiation. *J. Invest. Dermatol.* **81**, S100–S103 (1983).

26. Mehrel, T. *et al.* Identification of a major keratinocyte cell envelope protein, loricrin. *Cell* **61**, 1103–1112 (1990).

27. Denecker, G., Ovaere, P., Vandenabeele, P. & Declercq, W. Caspase-14 reveals its secrets. *J. Cell Biol.* **180**, 451–458 (2008).

28. Candi, E. *et al.* Biochemical, Structural, and Transglutaminase Substrate Properties Of Human Loricrin, the Major Epidermal Cornified Cell Envelope Protein. *J. Biol. Chem.* **270**, 26382–26390 (1995).

29. Gan, S. Q., McBride, O. W., Idler, W. W., Markova, N. & Steinert, P. M. Organization, structure, and polymorphisms of the human profilaggrin gene. *Biochemistry* **29**, 9432–9440 (1990).

30. Presland, R. B., Haydock, P. V., Fleckman, P., Nirunsuksiri, W. & Dale, B. A. Characterization of the human epidermal profilaggrin gene. Genomic organization and identification of an S-100-like calcium binding domain at the amino terminus. *J. Biol. Chem.* **267**, 23772–23781 (1992).

31. McGrath, J. A. & Uitto, J. The filaggrin story: novel insights into skin-barrier function and disease. *Trends Mol. Med.* **14**, 20–27 (2008).

32. Candi, E., Schmidt, R. & Melino, G. The cornified envelope: a model of cell death in the skin. *Nat. Rev. Mol. Cell Biol.* **6**, 328–340 (2005).

33. Steinert, P. M., Cantieri, J. S., Teller, D. C., Lonsdale-Eccles, J. D. & Dale, B. A. Characterization of a class of cationic proteins that specifically interact with intermediate filaments. *Proc. Natl. Acad. Sci. U. S. A.* **78**, 4097–4101 (1981).

34. Presland, R. B. & Dale, B. A. Epithelial Structural Proteins of the Skin and Oral Cavity: Function in Health and Disease. *Crit. Rev. Oral Biol. Med.* **11**, 383–408 (2000).

35. Presland, R. B., Haydock, P. V., Fleckman, P., Nirunsuksiri, W. & Dale, B. A. Characterization of the human epidermal profilaggrin gene. Genomic organization and identification of an S-100-like calcium binding domain at the amino terminus. *J. Biol. Chem.* **267**, 23772–23781 (1992).

36. Fuchs, E. Epidermal differentiation: the bare essentials. *J. Cell Biol.* **111**, 2807–2814 (1990).

37. Kalinin, A., Marekov, L. N. & Steinert, P. M. Assembly of the epidermal cornified cell envelope. *J. Cell Sci.* **114**, 3069–3070 (2001).

38. Hitomi, K. Transglutaminases in skin epidermis. *Eur. J. Dermatol. EJD* **15**, 313–319 (2005).

39. Nemes, Z. & Steinert, P. M. Bricks and mortar of the epidermal barrier. *Exp. Mol. Med.* **31**, 5–19 (1999).

40. Kosak, S. T. *et al.* Coordinate Gene Regulation during Hematopoiesis Is Related to Genomic Organization. *PLoS Biol.* **5**, e309 (2007).

41. Neems, D. S., Garza-Gongora, A. G., Smith, E. D. & Kosak, S. T. Topologically associated domains enriched for lineage-specific genes reveal expression-dependent nuclear topologies during myogenesis. *Proc. Natl. Acad. Sci.* **113**, E1691–E1700 (2016).

42. Mischke, D., Korge, B. P., Marenholz, I., Volz, A. & Ziegler, A. Genes encoding structural proteins of epidermal cornification and S100 calcium-binding proteins form a gene complex ('epidermal differentiation complex') on human chromosome 1q21. *J. Invest. Dermatol.* **106**, 989–992 (1996).

43. Kypriotou, M., Huber, M. & Hohl, D. The human epidermal differentiation complex: cornified envelope precursors, S100 proteins and the 'fused genes' family. *Exp. Dermatol.* **21**, 643–649 (2012).

44. de Guzman Strong, C. *et al.* A milieu of regulatory elements in the epidermal differentiation complex syntenic block: implications for atopic dermatitis and psoriasis. *Hum. Mol. Genet.* **19**, 1453–1460 (2010).

45. Eckert, R. L. *et al.* S100 proteins in the epidermis. *J. Invest. Dermatol.* **123**, 23–33 (2004).

46. Kizawa, K., Takahara, H., Unno, M. & Heizmann, C. W. S100 and S100 fused-type protein families in epidermal maturation with special focus on S100A3 in mammalian hair cuticles. *Biochimie* **93**, 2038–2047 (2011).

47. Zimmer, D. B., Cornwall, E. H., Landar, A. & Song, W. The S100 protein family: History, function, and expression. *Brain Res. Bull.* **37**, 417–429 (1995).

48. Abtin, A. *et al.* The Antimicrobial Heterodimer S100A8/S100A9 (Calprotectin) Is Upregulated by Bacterial Flagellin in Human Epidermal Keratinocytes. *J. Invest. Dermatol.* **130**, 2423–2430 (2010).

49. Wolf, R., Ruzicka, T. & Yuspa, S. H. Novel S100A7 (psoriasin)/S100A15 (koebnerisin) subfamily: highly homologous but distinct in regulation and function. *Amino Acids* **41**, 789–796 (2011).

50. Backendorf, C. & Hohl, D. A common origin for cornified envelope proteins? *Nat. Genet.* **2**, 91–91 (1992).

51. Gibbs, S. *et al.* Molecular characterization and evolution of the SPRR family of keratinocyte differentiation markers encoding small proline-rich proteins. *Genomics* **16**, 630–637 (1993).

52. Yoneda, K. & Steinert, P. M. Overexpression of human loricrin in transgenic mice produces a normal phenotype. *Proc. Natl. Acad. Sci.* **90**, 10754–10758 (1993).

53. Steven, A. C. & Steinert, P. M. Protein composition of cornified cell envelopes of epidermal keratinocytes. *J. Cell Sci.* **107**, 693 (1994).

54. Hennings, H. & Holbrook, K. A. Calcium regulation of cell-cell contact and differentiation of epidermal cells in culture. An ultrastructural study. *Exp. Cell Res.* **143**, 127–142 (1983).

55. Hennings, H. *et al.* Calcium regulation of growth and differentiation of mouse epidermal cells in culture. *Cell* **19**, 245–254 (1980).

56. Bikle, D. D., Xie, Z. & Tu, C.-L. Calcium regulation of keratinocyte differentiation. *Expert Rev. Endocrinol. Metab.* **7**, 461–472 (2012).

57. Lee, S. E. & Lee, S. H. Skin Barrier and Calcium. *Ann. Dermatol.* **30**, 265–275 (2018).

58. Charest, J. L., Jennings, J. M., King, W. P., Kowalczyk, A. P. & García, A. J. Cadherin-Mediated Cell–Cell Contact Regulates Keratinocyte Differentiation. *J. Invest. Dermatol.* **129**, 564–572 (2009).

59. Blanpain, C. & Fuchs, E. Epidermal stem cells of the skin. *Annu. Rev. Cell Dev. Biol.* **22**, 339–373 (2006).

60. Pillai, S., Bikle, D. D. & Elias, P. M. 1,25-Dihydroxyvitamin D production and receptor binding in human keratinocytes varies with differentiation. *J. Biol. Chem.* **263**, 5390–5395 (1988).

61. Bikle, D. D. Vitamin D regulated keratinocyte differentiation. *J. Cell. Biochem.* **92**, 436–444 (2004).

62. Pillai, S., Bikle, D. D., Su, M. J., Ratnam, A. & Abe, J. 1,25-Dihydroxyvitamin D3 upregulates the phosphatidylinositol signaling pathway in human keratinocytes by increasing phospholipase C levels. *J. Clin. Invest.* **96**, 602–609 (1995).

63. Bikle, D. D., Xie, Z. & Tu, C.-L. Calcium regulation of keratinocyte differentiation. *Expert Rev. Endocrinol. Metab.* **7**, 461–472 (2012).

64. Eckert, R. L. *et al.* AP1 Transcription Factors in Epidermal Differentiation and Skin Cancer. *J. Skin Cancer* **2013**, 1–9 (2013).

65. Botchkarev, V. A. Integration of the Transcription Factor-Regulated and Epigenetic Mechanisms in the Control of Keratinocyte Differentiation. *J. Investig. Dermatol. Symp. Proc.* **17**, 30–32 (2015).

66. Lopez-Pajares, V., Yan, K., Zarnegar, B. J., Jameson, K. L. & Khavari, P. A. Genetic Pathways in Disorders of Epidermal Differentiation. *Trends Genet. TIG* **29**, 31–40 (2013).

67. Eckert, R. L. *et al.* AP1 Transcription Factors in Epidermal Differentiation and Skin Cancer. *J. Skin Cancer* **2013**, 1–9 (2013).

68. Bikle, D. D., Xie, Z. & Tu, C.-L. Calcium regulation of keratinocyte differentiation. *Expert Rev. Endocrinol. Metab.* **7**, 461–472 (2012).

69. Botchkarev, V. A. Integration of the Transcription Factor-Regulated and Epigenetic Mechanisms in the Control of Keratinocyte Differentiation. *J. Investig. Dermatol. Symp. Proc.* **17**, 30–32 (2015).

70. Lowell, S., Jones, P., Le Roux, I., Dunne, J. & Watt, F. M. Stimulation of human epidermal differentiation by Delta–Notch signalling at the boundaries of stem-cell clusters. *Curr. Biol.* **10**, 491–500 (2000).

71. Rangarajan, A. Notch signaling is a direct determinant of keratinocyte growth arrest and entry into differentiation. *EMBO J.* **20**, 3427–3436 (2001).

72. Sen, G. L. *et al.* ZNF750 is a p63 target gene that induces KLF4 to drive terminal epidermal differentiation. *Dev. Cell* **22**, 669–677 (2012).

73. Lopez-Pajares, V. *et al.* A LncRNA-MAF:MAFB transcription factor network regulates epidermal differentiation. *Dev. Cell* **32**, 693–706 (2015).

74. Teng, A., Nair, M., Wells, J., Segre, J. A. & Dai, X. Strain-dependent perinatal lethality of Ovol1-deficient mice and identification of Ovol2 as a downstream target of Ovol1 in skin epidermis. *Biochim. Biophys. Acta* **1772**, 89–95 (2007).

75. Yu, Z. *et al.* The Grainyhead-like epithelial transactivator Get-1/Grhl3 regulates epidermal terminal differentiation and interacts functionally with LMO4. *Dev. Biol.* **299**, 122–136 (2006).

76. Romano, R.-A. *et al.* ΔNp63 knockout mice reveal its indispensable role as a master regulator of epithelial development and differentiation. *Dev. Camb. Engl.* **139**, 772–782 (2012).

77. Blanpain, C., Horsley, V. & Fuchs, E. Epithelial Stem Cells: Turning over New Leaves. *Cell* **128**, 445–458 (2007).

78. Yang, A. *et al.* p63 is essential for regenerative proliferation in limb, craniofacial and epithelial development. *Nature* **398**, 714–718 (1999).

79. Pellegrini, G. *et al.* p63 identifies keratinocyte stem cells. *Proc. Natl. Acad. Sci.* **98**, 3156–3161 (2001).

80. Truong, A. B., Kretz, M., Ridky, T. W., Kimmel, R. & Khavari, P. A. p63 regulates proliferation and differentiation of developmentally mature keratinocytes. *Genes Dev.* **20**, 3185–3197 (2006).

81. Soares, E. & Zhou, H. Master regulatory role of p63 in epidermal development and disease. *Cell. Mol. Life Sci.* **75**, 1179–1190 (2018).

82. Koster, M. I. p63 in skin development and ectodermal dysplasias. *J. Invest. Dermatol.* **130**, 2352–2358 (2010).

83. Bao, X. *et al.* A novel ATAC-seq approach reveals lineage-specific reinforcement of the open chromatin landscape via cooperation between BAF and p63. *Genome Biol.* **16**, (2015).

84. LeBoeuf, M. *et al.* Hdac1 and Hdac2 act redundantly to control p63 and p53 functions in epidermal progenitor cells. *Dev. Cell* **19**, 807–818 (2010).

85. Perdigoto, C. N., Valdes, V. J., Bardot, E. S. & Ezhkova, E. Epigenetic Regulation of Epidermal Differentiation. *Cell. Mol. Life Sci. CMLS* **69**, 2161–2172 (2012).

86. Ho, L. & Crabtree, G. R. Chromatin remodelling during development. *Nature* **463**, 474–484 (2010).

87. Margueron, R. *et al.* Ezh1 and Ezh2 Maintain Repressive Chromatin through Different Mechanisms. *Mol. Cell* **32**, 503–518 (2008).

88. Ezhkova, E. *et al.* Ezh2 Orchestrates Gene Expression for the Stepwise Differentiation of Tissue-Specific Stem Cells. *Cell* **136**, 1122–1135 (2009).

89. Agger, K. *et al.* UTX and JMJD3 are histone H3K27 demethylases involved in HOX gene regulation and development. *Nature* **449**, 731–734 (2007).

90. Cavazza, A. *et al.* Dynamic Transcriptional and Epigenetic Regulation of Human Epidermal Keratinocyte Differentiation. *Stem Cell Rep.* **6**, 618–632 (2016).

91. Sen, G. L., Webster, D. E., Barragan, D. I., Chang, H. Y. & Khavari, P. A. Control of differentiation in a self-renewing mammalian tissue by the histone demethylase JMJD3. *Genes Dev.* **22**, 1865–1870 (2008).

92. Driskell, I. *et al.* The histone methyltransferase Setd8 acts in concert with c-Myc and is required to maintain skin. *EMBO J.* **31**, 616–629 (2012).

93. Gdula, M. R. *et al.* Remodeling of three-dimensional organization of the nucleus during terminal keratinocyte differentiation in the epidermis. *J. Invest. Dermatol.* **133**, 2191–2201 (2013).

94. Fessing, M. Y. *et al.* p63 regulates Satb1 to control tissue-specific chromatin remodeling during development of the epidermis. *J. Cell Biol.* **194**, 825–839 (2011).

95. Blanpain, C., Lowry, W., Pasolli, H. & Fuchs, E. Canonical notch signaling functions as a commitment switch in the epidermal lineage. *Genes Dev.* **20**, 3022–35 (2006).

96. Green, C. L. & Khavari, P. A. Targets for molecular therapy of skin cancer. *Semin. Cancer Biol.* **14**, 63–69 (2004).

97. Skin Cancer Treatment. *National Cancer Institute* https://www.cancer.gov/types/skin/hp/skin-treatment-pdq#section/all.

98. Nehal, K. S. & Bichakjian, C. K. Update on Keratinocyte Carcinomas. *N. Engl. J. Med.* **379**, 363–374 (2018).

99. Saladi, R. N. & Persaud, A. N. The causes of skin cancer: A comprehensive review. *Drugs Today* **41**, 37 (2005).

100. Nagarajan, P. *et al.* Keratinocyte Carcinomas: Current Concepts and Future Research Priorities. *Clin. Cancer Res.* **25**, 2379–2391 (2019).

101. Riihilä, P. *et al.* Complement System in Cutaneous Squamous Cell Carcinoma. *Int. J. Mol. Sci.* **20**, 3550 (2019).

102. *World cancer report 2014*. (International Agency for Research on Cancer, 2014).

103. Swetter, S. M. Dermatological perspectives of malignant melanoma. *Surg. Clin. North Am.* **83**, 77–95 (2003).

104. Lomas, A., Leonardi-Bee, J. & Bath-Hextall, F. A systematic review of worldwide incidence of nonmelanoma skin cancer. *Br. J. Dermatol.* **166**, 1069–1080 (2012).

105. Burton, K. A., Ashack, K. A. & Khachemoune, A. Cutaneous Squamous Cell Carcinoma: A Review of High-Risk and Metastatic Disease. *Am. J. Clin. Dermatol.* **17**, 491–508 (2016).

106. South, A. P. *et al.* NOTCH1 Mutations Occur Early during Cutaneous Squamous Cell Carcinogenesis. *J. Invest. Dermatol.* **134**, 2630–2638 (2014).

107. Pellegrini, C. *et al.* Understanding the Molecular Genetics of Basal Cell Carcinoma. *Int. J. Mol. Sci.* **18**, 2485 (2017).

108. Bonilla, X. *et al.* Genomic analysis identifies new drivers and progression pathways in skin basal cell carcinoma. *Nat. Genet.* **48**, 398–406 (2016).

109. Nissinen, L., Farshchian, M., Riihilä, P. & Kähäri, V.-M. New perspectives on role of tumor microenvironment in progression of cutaneous squamous cell carcinoma. *Cell Tissue Res.* **365**, 691–702 (2016).

110. Rognoni, E. & Watt, F. M. Skin Cell Heterogeneity in Development, Wound Healing, and Cancer. *Trends Cell Biol.* **28**, 709–722 (2018).

111. Rodríguez-Paredes, M. *et al.* Methylation profiling identifies two subclasses of squamous cell carcinoma related to distinct cells of origin. *Nat. Commun.* **9**, 577 (2018).

112. Rao, R. C., Chan, M. P., Andrews, C. A. & Kahana, A. Epigenetic markers in basal cell carcinoma: universal themes in oncogenesis and tumor stratification? - a short report. *Cell. Oncol.* **41**, 693–698 (2018).

113. Didona, D., Paolino, G., Bottoni, U. & Cantisani, C. Non Melanoma Skin Cancer Pathogenesis Overview. *Biomedicines* **6**, (2018).

114. Jayaraman, S. S., Rayhan, D. J., Hazany, S. & Kolodney, M. S. Mutational Landscape of Basal Cell Carcinomas by Whole-Exome Sequencing. *J. Invest. Dermatol.* **134**, 213–220 (2014).

115. Jayaraman, S. S., Rayhan, D. J., Hazany, S. & Kolodney, M. S. Mutational Landscape of Basal Cell Carcinomas by Whole-Exome Sequencing. *J. Invest. Dermatol.* **134**, 213–220 (2014).

116. Green, C. L. & Khavari, P. A. Targets for molecular therapy of skin cancer. *Semin. Cancer Biol.* **14**, 63–69 (2004).

117. Xie, J. *et al.* A role of PDGFRα in basal cell carcinoma proliferation. *Proc. Natl. Acad. Sci.* **98**, 9255–9259 (2001).

118. Yanagi, T., Kitamura, S. & Hata, H. Novel Therapeutic Targets in Cutaneous Squamous Cell Carcinoma. *Front. Oncol.* **8**, (2018).

119. Ashford, B. G. *et al.* Reviewing the genetic alterations in high-risk cutaneous squamous cell carcinoma: A search for prognostic markers and therapeutic targets. *Head Neck* **39**, 1462–1469 (2017).

120. Kamb, A. *et al.* A cell cycle regulator potentially involved in genesis of many tumor types. *Science* **264**, 436–440 (1994).

121. Sasaki, S. *et al.* Molecular processes of chromosome 9p21 deletions in human cancers. *Oncogene* **22**, 3792–3798 (2003).

122. Nobori, T. *et al.* Deletions of the cyclin-dependent kinase-4 inhibitor gene in multiple human cancers. *Nature* **368**, 753–756 (1994).

123. Miliani de Marval, P. L., Macias, E., Conti, C. J. & Rodriguez-Puebla, M. L. Enhanced malignant tumorigenesis in Cdk4 transgenic mice. *Oncogene* **23**, 1863–1873 (2004).

124. Lazarov, M. *et al.* CDK4 coexpression with Ras generates malignant human epidermal tumorigenesis. *Nat. Med.* **8**, 1105–1114 (2002).

125. Dajee, M. *et al.* NF-κB blockade and oncogenic Ras trigger invasive human epidermal neoplasia. *Nature* **421**, 639–643 (2003).

126. Maurelli, R. *et al.* The role of oncogenic Ras in human skin tumorigenesis depends on the clonogenic potential of the founding keratinocytes. *J. Cell Sci.* **129**, 1003–1017 (2016).

127. Takaoka, M. *et al.* Ha-Ras(G12V) induces senescence in primary and immortalized human esophageal keratinocytes with p53 dysfunction. *Oncogene* **23**, 6760–6768 (2004).

128. Seitz, C. S., Lin, Q., Deng, H. & Khavari, P. A. Alterations in NF-kappaB function in transgenic epithelial tissue demonstrate a growth inhibitory role for NF-kappaB. *Proc. Natl. Acad. Sci. U. S. A.* **95**, 2307–2312 (1998).

129. Green, C. L. & Khavari, P. A. Targets for molecular therapy of skin cancer. *Semin. Cancer Biol.* **14**, 63–69 (2004).

130. Ashford, B. G. *et al.* Reviewing the genetic alterations in high-risk cutaneous squamous cell carcinoma: A search for prognostic markers and therapeutic targets. *Head Neck* **39**, 1462–1469 (2017).

131. Pierceall, W. E., Goldberg, L. H., Tainsky, M. A., Mukhopadhyay, T. & Ananthaswamy, H. N. Ras gene mutation and amplification in human nonmelanoma skin cancers. *Mol. Carcinog.* **4**, 196–202 (1991).

132. Tufaro, A. P. *et al.* Molecular Markers in Cutaneous Squamous Cell Carcinoma. *Int. J. Surg. Oncol.* **2011**, 1–5 (2011).

133. Gannon, O. M., Merida de Long, L., Endo-Munoz, L., Hazar-Rethinam, M. & Saunders, N. A. Dysregulation of the repressive H3K27 trimethylation mark in head and neck squamous cell carcinoma contributes to dysregulated squamous differentiation. *Clin. Cancer Res. Off. J. Am. Assoc. Cancer Res.* **19**, 428–441 (2013).

134. Scott, R. E. *et al.* Human squamous carcinoma cells express complex defects in the control of proliferation and differentiation. *Am. J. Pathol.* **133**, 374–380 (1988).

135. Ratushny, V., Gober, M. D., Hick, R., Ridky, T. W. & Seykora, J. T. From keratinocyte to cancer: the pathogenesis and modeling of cutaneous squamous cell carcinoma. *J. Clin. Invest.* **122**, 464–472 (2012).

136. Fatica, A. & Bozzoni, I. Long non-coding RNAs: new players in cell differentiation and development. *Nat. Rev. Genet.* **15**, 7–21 (2013).

137. Kretz, M. *et al.* Control of somatic tissue differentiation by the long non-coding RNA TINCR. *Nature* **493**, 231–235 (2012).

138. Lee, C. S. *et al.* Cancer-Associated Long Noncoding RNA SMRT-2 Controls Epidermal Differentiation. *J. Invest. Dermatol.* (2018) doi:10.1016/j.jid.2018.01.003.

139. Piipponen, M. *et al.* Long Noncoding RNA PICSAR Promotes Growth of Cutaneous Squamous Cell Carcinoma by Regulating ERK1/2 Activity. *J. Invest. Dermatol.* **136**, 1701–1710 (2016).

140. Yildirim, E. *et al.* Xist RNA Is a Potent Suppressor of Hematologic Cancer in Mice. *Cell* **152**, 727–742 (2013).

141. Sand, M. *et al.* Expression profiles of long noncoding RNAs in cutaneous squamous cell carcinoma. *Epigenomics* **8**, 501–518 (2016).

142. Crick, F. H. On protein synthesis. *Symp. Soc. Exp. Biol.* **12**, 138–163 (1958).

143. Crick, F. Central Dogma of Molecular Biology. *Nature* **227**, 561–563 (1970).

144. Mattick, J. S. Non-coding RNAs: the architects of eukaryotic complexity. *EMBO Rep.* **2**, 986–991 (2001).

145. Djebali, S. *et al.* Landscape of transcription in human cells. *Nature* **489**, 101–108 (2012).

146. International Human Genome Sequencing Consortium. Finishing the euchromatic sequence of the human genome. *Nature* **431**, 931–945 (2004).

147. Farazi, T. A., Juranek, S. A. & Tuschl, T. The growing catalog of small RNAs and their association with distinct Argonaute/Piwi family members. *Development* **135**, 1201–1214 (2008).

148. Matera, A. G., Terns, R. M. & Terns, M. P. Non-coding RNAs: lessons from the small nuclear and small nucleolar RNAs. *Nat. Rev. Mol. Cell Biol.* **8**, 209–220 (2007).

149. Okamura, K. & Lai, E. C. Endogenous small interfering RNAs in animals. *Nat. Rev. Mol. Cell Biol.* **9**, 673–678 (2008).

150. Bartel, D. P. MicroRNAs: Target Recognition and Regulatory Functions. *Cell* **136**, 215–233 (2009).

151. Derrien, T. *et al.* The GENCODE v7 catalog of human long noncoding RNAs: Analysis of their gene structure, evolution, and expression. *Genome Res.* **22**, 1775–1789 (2012).

152. Jia, H. *et al.* Genome-wide computational identification and manual annotation of human long noncoding RNA genes. *RNA* **16**, 1478–1487 (2010).

153. Cabili, M. N. *et al.* Integrative annotation of human large intergenic noncoding RNAs reveals global properties and specific subclasses. *Genes Dev.* **25**, 1915–1927 (2011).

154. Pang, K. C., Frith, M. C. & Mattick, J. S. Rapid evolution of noncoding RNAs: lack of conservation does not mean lack of function. *Trends Genet.* **22**, 1–5 (2006).

155. Ransohoff, J. D., Wei, Y. & Khavari, P. A. The functions and unique features of long intergenic non-coding RNA. *Nat. Rev. Mol. Cell Biol.* **19**, 143–157 (2018).

156. Rinn, J. L. & Chang, H. Y. Genome Regulation by Long Noncoding RNAs. *Annu. Rev. Biochem.* **81**, 145–166 (2012).

157. Rinn, J. L. *et al.* Functional Demarcation of Active and Silent Chromatin Domains in Human HOX Loci by Noncoding RNAs. *Cell* **129**, 1311–1323 (2007).

158. Wang, K. C. & Chang, H. Y. Molecular Mechanisms of Long Noncoding RNAs. *Mol. Cell* **43**, 904–914 (2011).

159. Dinger, M. E., Pang, K. C., Mercer, T. R. & Mattick, J. S. Differentiating protein-coding and noncoding RNA: challenges and ambiguities. *PLoS Comput. Biol.* **4**, e1000176 (2008).

160. Quinn, J. J. & Chang, H. Y. Unique features of long non-coding RNA biogenesis and function. *Nat. Rev. Genet.* **17**, 47–62 (2015).

161. Lai, W.-J. C. *et al.* mRNAs and lncRNAs intrinsically form secondary structures with short end-to-end distances. *Nat. Commun.* **9**, 4328 (2018).

162. Guo, X. *et al.* Advances in long noncoding RNAs: identification, structure prediction and function annotation. *Brief. Funct. Genomics* **15**, 38–46 (2016).

163. Nelson, B. R. *et al.* A peptide encoded by a transcript annotated as long noncoding RNA enhances SERCA activity in muscle. *Science* **351**, 271–275 (2016).

164. Anderson, D. M. *et al.* A Micropeptide Encoded by a Putative Long Noncoding RNA Regulates Muscle Performance. *Cell* **160**, 595–606 (2015).

165. Ingolia, N. T., Lareau, L. F. & Weissman, J. S. Ribosome Profiling of Mouse Embryonic Stem Cells Reveals the Complexity and Dynamics of Mammalian Proteomes. *Cell* **147**, 789–802 (2011).

166. Guttman, M. *et al.* lincRNAs act in the circuitry controlling pluripotency and differentiation. *Nature* **477**, 295–300 (2011).

167. Clark, M. B. *et al.* Genome-wide analysis of long noncoding RNA stability. *Genome Res.* **22**, 885–898 (2012).

168. Ayupe, A. C. *et al.* Global analysis of biogenesis, stability and sub-cellular localization of lncRNAs mapping to intragenic regions of the human genome. *RNA Biol.* **12**, 877–892 (2015).

169. Carpenter, S. *et al.* A Long Noncoding RNA Mediates Both Activation and Repression of Immune Response Genes. *Science* **341**, 789–792 (2013).

170. Sánchez, Y. *et al.* Genome-wide analysis of the human p53 transcriptional network unveils a lncRNA tumour suppressor signature. *Nat. Commun.* **5**, 5812 (2014).

171. Fico, A., Fiorenzano, A., Pascale, E., Patriarca, E. J. & Minchiotti, G. Long non-coding RNA in stem cell pluripotency and lineage commitment: functions and evolutionary conservation. *Cell. Mol. Life Sci.* **76**, 1459–1471 (2019).

172. Ma, L., Bajic, V. B. & Zhang, Z. On the classification of long non-coding RNAs. *RNA Biol.* **10**, 924–933 (2013).

173. Kung, J. T. Y., Colognori, D. & Lee, J. T. Long Noncoding RNAs: Past, Present, and Future. *Genetics* **193**, 651–669 (2013).

174. Chakraborty, S., Deb, A., Maji, R. K., Saha, S. & Ghosh, Z. LncRBase: An Enriched Resource for lncRNA Information. *PLoS ONE* **9**, e108010 (2014).

175. Rinn, J. L. & Chang, H. Y. Genome Regulation by Long Noncoding RNAs. *Annu. Rev. Biochem.* **81**, 145–166 (2012).

176. Barrett, S. P. & Salzman, J. Circular RNAs: analysis, expression and potential functions. *Development* **143**, 1838–1847 (2016).

177. Stein, J. M. The effect of adrenaline and of alpha- and beta-adrenergic blocking agents on ATP concentration and on incorporation of 32Pi into ATP in rat fat cells. *Biochem. Pharmacol.* **24**, 1659–1662 (1975).

178. Yin, Q.-F. *et al.* Long Noncoding RNAs with snoRNA Ends. *Mol. Cell* **48**, 219–230 (2012).

179. Derrien, T. *et al.* The GENCODE v7 catalog of human long noncoding RNAs: Analysis of their gene structure, evolution, and expression. *Genome Res.* **22**, 1775–1789 (2012).

180. Amaral, P. P. *et al.* Complex architecture and regulated expression of the Sox2ot locus during vertebrate development. *RNA* **15**, 2013–2027 (2009).

181. Niemczyk, M. *et al.* Imprinted Chromatin around DIRAS3 Regulates Alternative Splicing of GNG12-AS1, a Long Noncoding RNA. *Am. J. Hum. Genet.* **93**, 224–235 (2013).

182. Kornienko, A. E. *et al.* Long non-coding RNAs display higher natural expression variation than protein-coding genes in healthy humans. *Genome Biol.* **17**, (2016).

183. Schmitt, A. M. & Chang, H. Y. Long Noncoding RNAs in Cancer Pathways. *Cancer Cell* **29**, 452–463 (2016).

184. Gupta, R. A. *et al.* Long non-coding RNA HOTAIR reprograms chromatin state to promote cancer metastasis. *Nature* **464**, 1071–1076 (2010).

185. Tsai, M.-C. *et al.* Long Noncoding RNA as Modular Scaffold of Histone Modification Complexes. *Science* **329**, 689–693 (2010).

186. Martianov, I., Ramadass, A., Serra Barros, A., Chow, N. & Akoulitchev, A. Repression of the human dihydrofolate reductase gene by a non-coding interfering transcript. *Nature* **445**, 666–670 (2007).

187. Feng, J. The Evf-2 noncoding RNA is transcribed from the Dlx-5/6 ultraconserved region and functions as a Dlx-2 transcriptional coactivator. *Genes Dev.* **20**, 1470–1484 (2006).

188. Lee, J. T. Lessons from X-chromosome inactivation: long ncRNA as guides and tethers to the epigenome. *Genes Dev.* **23**, 1831–1842 (2009).

189. Bartolomei, M. S., Zemel, S. & Tilghman, S. M. Parental imprinting of the mouse H19 gene. *Nature* **351**, 153–155 (1991).

190. Sleutels, F., Zwart, R. & Barlow, D. P. The non-coding Air RNA is required for silencing autosomal imprinted genes. *Nature* **415**, 810–813 (2002).

191. Flynn, R. A. & Chang, H. Y. Long Noncoding RNAs in Cell-Fate Programming and Reprogramming. *Cell Stem Cell* **14**, 752–761 (2014).

192. Wang, K. C. & Chang, H. Y. Molecular mechanisms of long noncoding RNAs. *Mol. Cell* **43**, 904–914 (2011).

193. Quinn, J. J. & Chang, H. Y. Unique features of long non-coding RNA biogenesis and function. *Nat. Rev. Genet.* **17**, 47–62 (2016).

194. Blythe, A. J., Fox, A. H. & Bond, C. S. The ins and outs of lncRNA structure: How, why and what comes next? *Biochim. Biophys. Acta BBA - Gene Regul. Mech.* **1859**, 46–58 (2016).

195. Amin, V. *et al.* Epigenomic footprints across 111 reference epigenomes reveal tissue-specific epigenetic regulation of lincRNAs. *Nat. Commun.* **6**, 6370 (2015).

196. Yuan, T. *et al.* Plasma extracellular RNA profiles in healthy and cancer patients. *Sci. Rep.* **6**, 19413 (2016).

197. Umu, S. U. *et al.* A comprehensive profile of circulating RNAs in human serum. *RNA Biol.* **15**, 242–250 (2018).

198. Sun, Q., Hao, Q. & Prasanth, K. V. Nuclear Long Noncoding RNAs: Key Regulators of Gene Expression. *Trends Genet.* **34**, 142–157 (2018).

199. Noh, J. H., Kim, K. M., McClusky, W. G., Abdelmohsen, K. & Gorospe, M. Cytoplasmic functions of long noncoding RNAs. *Wiley Interdiscip. Rev. RNA* **9**, e1471 (2018).

200. Kopp, F. & Mendell, J. T. Functional Classification and Experimental Dissection of Long Noncoding RNAs. *Cell* **172**, 393–407 (2018).

201. Piipponen, M., Nissinen, L. & Kähäri, V.-M. Long non-coding RNAs in cutaneous biology and keratinocyte carcinomas. *Cell. Mol. Life Sci.* (2020) doi:10.1007/s00018-020-03554-3.

202. Simon, M. D. *et al.* High-resolution Xist binding maps reveal two-step spreading during X-chromosome inactivation. *Nature* **504**, 465–469 (2013).

203. Brown, C. J. *et al.* A gene from the region of the human X inactivation centre is expressed exclusively from the inactive X chromosome. *Nature* **349**, 38–44 (1991).

204. da Rocha, S. T. & Heard, E. Novel players in X inactivation: insights into Xist-mediated gene silencing and chromosome conformation. *Nat. Struct. Mol. Biol.* **24**, 197–204 (2017).

205. Chu, C. *et al.* Systematic Discovery of Xist RNA Binding Proteins. *Cell* **161**, 404–416 (2015).

206. Pintacuda, G., Young, A. N. & Cerase, A. Function by Structure: Spotlights on Xist Long Non-coding RNA. *Front. Mol. Biosci.* **4**, 90 (2017).

207. McHugh, C. A. *et al.* The Xist lncRNA interacts directly with SHARP to silence transcription through HDAC3. *Nature* **521**, 232–236 (2015).

208. Bonasio, R. & Shiekhattar, R. Regulation of Transcription by Long Noncoding RNAs. *Annu. Rev. Genet.* **48**, 433–455 (2014).

209. Hamada, F. N. Global regulation of X chromosomal genes by the MSL complex in Drosophila melanogaster. *Genes Dev.* **19**, 2289–2294 (2005).

210. Guo, X. *et al.* Long Non-coding RNA–mRNA Correlation Analysis Reveals the Potential Role of HOTAIR in Pathogenesis of Sporadic Thoracic Aortic Aneurysm. *Eur. J. Vasc. Endovasc. Surg.* **54**, 303–314 (2017).

211. Willingham, A. T. A Strategy for Probing the Function of Noncoding RNAs Finds a Repressor of NFAT. *Science* **309**, 1570–1573 (2005).

212. Lanz, R. B. *et al.* A Steroid Receptor Coactivator, SRA, Functions as an RNA and Is Present in an SRC-1 Complex. *Cell* **97**, 17–27 (1999).

213. Hung, T. *et al.* Extensive and coordinated transcription of noncoding RNAs within cell-cycle promoters. *Nat. Genet.* **43**, 621–629 (2011).

214. Yang, G., Lu, X. & Yuan, L. LncRNA: A link between RNA and cancer. *Biochim. Biophys. Acta BBA - Gene Regul. Mech.* **1839**, 1097–1109 (2014).

215. Bernard, D. *et al.* A long nuclear-retained non-coding RNA regulates synaptogenesis by modulating gene expression. *EMBO J.* **29**, 3082–3093 (2010).

216. Faghihi, M. A. *et al.* Evidence for natural antisense transcript-mediated inhibition of microRNA function. *Genome Biol.* **11**, R56 (2010).

217. Cesana, M. *et al.* A Long Noncoding RNA Controls Muscle Differentiation by Functioning as a Competing Endogenous RNA. *Cell* **147**, 358–369 (2011).

218. Salviano-Silva, A., Lobo-Alves, S. C., Almeida, R. C. de, Malheiros, D. & Petzl-Erler, M. L. Besides Pathology: Long Non-Coding RNA in Cell and Tissue Homeostasis. *Non-Coding RNA* **4**, 3 (2018).

219. Mueller, A. C. *et al.* MUNC, a Long Noncoding RNA That Facilitates the Function of MyoD in Skeletal Myogenesis. *Mol. Cell. Biol.* **35**, 498–513 (2015).

220. Lyu, Q. *et al. SENCR* stabilizes vascular endothelial cell adherens junctions through interaction with CKAP4. *Proc. Natl. Acad. Sci.* **116**, 546–555 (2019).

221. Geng, T. *et al.* H19 lncRNA Promotes Skeletal Muscle Insulin Sensitivity in Part by Targeting AMPK. *Diabetes* **67**, 2183–2198 (2018).

222. Zhu, M. *et al.* Lnc-mg is a long non-coding RNA that promotes myogenesis. *Nat. Commun.* **8**, 14718 (2017).

223. Klattenhoff, C. A. *et al.* Braveheart, a long noncoding RNA required for cardiovascular lineage commitment. *Cell* **152**, 570–583 (2013).

224. Grote, P. *et al.* The tissue-specific lncRNA Fendrr is an essential regulator of heart and body wall development in the mouse. *Dev. Cell* **24**, 206–214 (2013).

225. Ounzain, S. *et al.* CARMEN, a human super enhancer-associated long noncoding RNA controlling cardiac specification, differentiation and homeostasis. *J. Mol. Cell. Cardiol.* **89**, 98–112 (2015).

226. Ramos, A. D. *et al.* The Long Noncoding RNA Pnky Regulates Neuronal Differentiation of Embryonic and Postnatal Neural Stem Cells. *Cell Stem Cell* **16**, 439–447 (2015).

227. Kretz, M. *et al.* Suppression of progenitor differentiation requires the long noncoding RNA ANCR. *Genes Dev.* **26**, 338–343 (2012).

228. Cai, P. *et al.* A genome-wide long noncoding RNA CRISPRi screen identifies *PRANCR* as a novel regulator of epidermal homeostasis. *Genome Res.* **30**, 22–34 (2020).

229. Sen, G. L. *et al.* ZNF750 Is a p63 Target Gene that Induces KLF4 to Drive Terminal Epidermal Differentiation. *Dev. Cell* **22**, 669–677 (2012).

230. Hazawa, M. *et al.* ZNF750 is a lineage-specific tumour suppressor in squamous cell carcinoma. *Oncogene* **36**, 2243–2254 (2017).

231. Thieu, K., Ruiz, M. E. & Owens, D. M. Cells of origin and tumor-initiating cells for nonmelanoma skin cancers. *Cancer Lett.* **338**, 82–88 (2013).

232. Kuri, P. & Rompolas, P. Differentiation keeps skin cancer at bay. *Nat. Cell Biol.* **20**, 1237–1239 (2018).

233. Ponzio, G. *et al.* A new long noncoding RNA (lncRNA) is induced in cutaneous squamous cell carcinoma and down-regulates several anticancer and cell differentiation genes in mouse. *J. Biol. Chem.* **292**, 12483–12495 (2017).

234. Tanis, S. E. J., Köksal, E. S., van Buggenum, J. A. G. L. & Mulder, K. W. BLNCR is a long non-coding RNA adjacent to integrin beta-1 that is rapidly lost during epidermal progenitor cell differentiation. *Sci. Rep.* **9**, 31 (2019).

235. Jones, P. H. & Watt, F. M. Separation of human epidermal stem cells from transit amplifying cells on the basis of differences in integrin function and expression. *Cell* **73**, 713–724 (1993).

236. Piipponen, M., Heino, J., Kähäri, V.-M. & Nissinen, L. Long non-coding RNA PICSAR decreases adhesion and promotes migration of squamous carcinoma cells by downregulating α2β1 and α5β1 integrin expression. *Biol. Open* **7**, bio037044 (2018).

237. Piipponen, M. *et al.* p53-Regulated Long Noncoding RNA PRECSIT Promotes Progression of Cutaneous Squamous Cell Carcinoma via STAT3 Signaling. *Am. J. Pathol.* **190**, 503–517 (2020).

238. Ponzio, G. *et al.* A new long noncoding RNA (lncRNA) is induced in cutaneous squamous cell carcinoma and down-regulates several anticancer and cell differentiation genes in mouse. *J. Biol. Chem.* **292**, 12483–12495 (2017).

239. Nassar, D., Latil, M., Boeckx, B., Lambrechts, D. & Blanpain, C. Genomic landscape of carcinogen-induced and genetically induced mouse skin squamous cell carcinoma. *Nat. Med.* **21**, 946–954 (2015).

240. Casanova, M. L. *et al.* A critical role for ras-mediated, epidermal growth factor receptor-dependent angiogenesis in mouse skin carcinogenesis. *Cancer Res.* **62**, 3402–3407 (2002).

241. Dlugosz, A. A. *et al.* Autocrine transforming growth factor alpha is dispensible for v-rasHa-induced epidermal neoplasia: potential involvement of alternate epidermal growth factor receptor ligands. *Cancer Res.* **55**, 1883–1893 (1995).

242. Peng, Y., Song, X., Zheng, Y., Wang, X. & Lai, W. Circular RNA profiling reveals that circCOL3A1-859267 regulate type I collagen expression in photoaged human dermal fibroblasts. *Biochem. Biophys. Res. Commun.* **486**, 277–284 (2017).

243. Lei, L. *et al.* MALAT1 participates in ultraviolet B-induced photo-aging via regulation of the ERK/MAPK signaling pathway. *Mol. Med. Rep.* **15**, 3977–3982 (2017).

244. Sonkoly, E. *et al.* Identification and characterization of a novel, psoriasis susceptibility-related noncoding RNA gene, PRINS. *J. Biol. Chem.* **280**, 24159–24167 (2005).

245. Hall, J. R. *et al.* Long noncoding RNA lincRNA-p21 is the major mediator of UVB-induced and p53-dependent apoptosis in keratinocytes. *Cell Death Dis.* **6**, e1700–e1700 (2015).

246. Jin, S. *et al.* p53-targeted lincRNA-p21 acts as a tumor suppressor by inhibiting JAK2/STAT3 signaling pathways in head and neck squamous cell carcinoma. *Mol. Cancer* **18**, 38 (2019).

247. Danis, J., Göblös, A., Bata-Csörgő, Z., Kemény, L. & Széll, M. PRINS Non-Coding RNA Regulates Nucleic Acid-Induced Innate Immune Responses of Human Keratinocytes. *Front. Immunol.* **8**, (2017).

248. Leucci, E., Coe, E. A., Marine, J.-C. & Vance, K. W. The emerging role of long non-coding RNAs in cutaneous melanoma. *Pigment Cell Melanoma Res.* **29**, 619–626 (2016).

249. Hombach, S. & Kretz, M. The non-coding skin: Exploring the roles of long non-coding RNAs in epidermal homeostasis and disease: Review essay. *BioEssays* **35**, 1093–1100 (2013).

250. Flockhart, R. J. *et al.* BRAFV600E remodels the melanocyte transcriptome and induces BANCR to regulate melanoma cell migration. *Genome Res.* **22**, 1006–1014 (2012).

251. Sun, M. *et al.* Downregulation of BRAF activated non-coding RNA is associated with poor prognosis for non-small cell lung cancer and promotes metastasis by affecting epithelial-mesenchymal transition. *Mol. Cancer* **13**, 68 (2014).

252. Cai, B. *et al.* BANCR contributes to the growth and invasion of melanoma by functioning as a competing endogenous RNA to upregulate Notch2 expression by sponging miR-204. *Int. J. Oncol.* **51**, 1941–1951 (2017).

253. Li, R. *et al.* Long non-coding RNA BANCR promotes proliferation in malignant melanoma by regulating MAPK pathway activation. *PloS One* **9**, e100893 (2014).

254. Yu, X., Zheng, H., Chan, M. T. & Wu, W. K. K. BANCR: a cancer-related long non-coding RNA. *Am. J. Cancer Res.* **7**, 1779–1787 (2017).

255. Lee, C. S. *et al.* Cancer-Associated Long Noncoding RNA SMRT-2 Controls Epidermal Differentiation. *J. Invest. Dermatol.* **138**, 1445–1449 (2018).

256. Yan, X. *et al.* Mesenchymal Stem Cells Promote Hepatocarcinogenesis via lncRNA–MUF Interaction with ANXA2 and miR-34a. *Cancer Res.* **77**, 6704–6716 (2017).

257. Wang, F. *et al.* RNAscope. *J. Mol. Diagn.* **14**, 22–29 (2012).

258. Raj, A., van den Bogaard, P., Rifkin, S. A., van Oudenaarden, A. & Tyagi, S. Imaging individual mRNA molecules using multiple singly labeled probes. *Nat. Methods* **5**, 877–879 (2008).

259. Orjalo, A. V. & Johansson, H. E. Stellaris® RNA Fluorescence In Situ Hybridization for the Simultaneous Detection of Immature and Mature Long Noncoding RNAs in Adherent Cells. in *Long Non-Coding RNAs* (eds. Feng, Y. & Zhang, L.) vol. 1402 119–134 (Springer New York, 2016).

260. Pratt, A. J. & MacRae, I. J. The RNA-induced Silencing Complex: A Versatile Gene-silencing Machine. *J. Biol. Chem.* **284**, 17897–17901 (2009).

261. Wilson, R. C. & Doudna, J. A. Molecular Mechanisms of RNA Interference. *Annu. Rev. Biophys.* **42**, 217–239 (2013).

262. Miao, H. *et al.* A long noncoding RNA distributed in both nucleus and cytoplasm operates in the PYCARD-regulated apoptosis by coordinating the epigenetic and translational regulation. *PLOS Genet.* **15**, e1008144 (2019).

263. Gudenas, B. L. & Wang, L. Prediction of LncRNA Subcellular Localization with Deep Learning from Sequence Features. *Sci. Rep.* **8**, 16385 (2018).

264. Palazzo, A. F. & Lee, E. S. Sequence Determinants for Nuclear Retention and Cytoplasmic Export of mRNAs and lncRNAs. *Front. Genet.* **9**, 440 (2018).

265. Zerbino, D. R. *et al.* Ensembl 2018. *Nucleic Acids Res.* **46**, D754–D761 (2018).

266. Hon, C.-C. *et al.* An atlas of human long non-coding RNAs with accurate 5′ ends. *Nature* **543**, 199–204 (2017).

267. Kanamori-Katayama, M. *et al.* Unamplified cap analysis of gene expression on a single-molecule sequencer. *Genome Res.* **21**, 1150–1159 (2011).

268. Noguchi, S. *et al.* FANTOM5 CAGE profiles of human and mouse samples. *Sci. Data* **4**, 170112 (2017).

269. Itoh, M. *et al.* Automated Workflow for Preparation of cDNA for Cap Analysis of Gene Expression on a Single Molecule Sequencer. *PLoS ONE* **7**, e30809 (2012).

270. Hubé, F., Velasco, G., Rollin, J., Furling, D. & Francastel, C. Steroid receptor RNA activator protein binds to and counteracts SRA RNA-mediated activation of MyoD and muscle differentiation. *Nucleic Acids Res.* **39**, 513–525 (2011).

271. Gascoigne, D. K. *et al.* Pinstripe: a suite of programs for integrating transcriptomic and proteomic datasets identifies novel proteins and improves differentiation of protein-coding and non-coding genes. *Bioinformatics* **28**, 3042–3050 (2012).

272. Banfai, B. *et al.* Long noncoding RNAs are rarely translated in two human cell lines. *Genome Res.* **22**, 1646–1657 (2012).

273. Wang, L. *et al.* CPAT: Coding-Potential Assessment Tool using an alignment-free logistic regression model. *Nucleic Acids Res.* **41**, e74–e74 (2013).

274. Sun, K. *et al.* iSeeRNA: identification of long intergenic non-coding RNA transcripts from transcriptome sequencing data. *BMC Genomics* **14 Suppl 2**, S7 (2013).

275. Han, S., Liang, Y., Li, Y. & Du, W. Lncident: A Tool for Rapid Identification of Long Noncoding RNAs Utilizing Sequence Intrinsic Composition and Open Reading Frame Information. *Int. J. Genomics* **2016**, 9185496 (2016).

276. Kang, Y.-J. *et al.* CPC2: a fast and accurate coding potential calculator based on sequence intrinsic features. *Nucleic Acids Res.* **45**, W12–W16 (2017).

277. Choi, M. & Lee, C. Immortalization of Primary Keratinocytes and Its Application to Skin Research. *Biomol. Ther.* **23**, 391–399 (2015).

278. Stöppler, H., Hartmann, D.-P., Sherman, L. & Schlegel, R. The Human Papillomavirus Type 16 E6 and E7 Oncoproteins Dissociate Cellular Telomerase Activity from the Maintenance of Telomere Length. *J. Biol. Chem.* **272**, 13332–13337 (1997).

279. Dickson, M. A. *et al.* Human Keratinocytes That Express hTERT and Also Bypass a p16INK4a-Enforced Mechanism That Limits Life Span Become Immortal yet Retain Normal Growth and Differentiation Characteristics. *Mol. Cell. Biol.* **20**, 1436–1447 (2000).

280. Smits, J. P. H. *et al.* Immortalized N/TERT keratinocytes as an alternative cell source in 3D human epidermal models. *Sci. Rep.* **7**, 11838 (2017).

281. Boukamp, P. *et al.* Normal keratinization in a spontaneously immortalized aneuploid human keratinocyte cell line. *J. Cell Biol.* **106**, 761–771 (1988).

282. Cong, L. *et al.* Multiplex genome engineering using CRISPR/Cas systems. *Science* **339**, 819–823 (2013).

283. Ran, F. A. *et al.* Genome engineering using the CRISPR-Cas9 system. *Nat. Protoc.* **8**, 2281–2308 (2013).

284. Eckert, R. L. *et al.* Keratinocyte Survival, Differentiation, and Death: Many Roads Lead to Mitogen-Activated Protein Kinase. *J. Investig. Dermatol. Symp. Proc.* **7**, 36–40 (2002).

285. Lee, M.-H., Padmashali, R. & Andreadis, S. T. JNK1 Is Required for Lentivirus Entry and Gene Transfer. *J. Virol.* **85**, 2657–2665 (2011).

286. Simon, M. D. *et al.* High-resolution Xist binding maps reveal two-step spreading during X-chromosome inactivation. *Nature* **504**, 465–469 (2013).

287. Nicholson, D. W. & Thornberry, N. A. Caspases: killer proteases. *Trends Biochem. Sci.* **22**, 299–306 (1997).

288. Weil, M., Raff, M. C. & Braga, V. M. M. Caspase activation in the terminal differentiation of human epidermal keratinocytes. *Curr. Biol.* **9**, 361–365 (1999).

289. Rendl, M. *et al.* Caspase-14 Expression by Epidermal Keratinocytes is Regulated by Retinoids in a Differentiation-associated Manner. *J. Invest. Dermatol.* **119**, 1150–1155 (2002).

290. Lachner, J., Mlitz, V., Tschachler, E. & Eckhart, L. Epidermal cornification is preceded by the expression of a keratinocyte-specific set of pyroptosis-related genes. *Sci. Rep.* **7**, 17446 (2017).

291. Denecker, G. *et al.* Caspase-14 protects against epidermal UVB photodamage and water loss. *Nat. Cell Biol.* **9**, 666–674 (2007).

292. Denslow, S. A. & Wade, P. A. The human Mi-2/NuRD complex and gene regulation. *Oncogene* **26**, 5433–5438 (2007).

293. Bowen, N. J., Fujita, N., Kajita, M. & Wade, P. A. Mi-2/NuRD: multiple complexes for many purposes. *Biochim. Biophys. Acta BBA - Gene Struct. Expr.* **1677**, 52–57 (2004).

294. Zhang, Y. *et al.* Analysis of the NuRD subunits reveals a histone deacetylase core complex and a connection with DNA methylation. *Genes Dev.* **13**, 1924–1935 (1999).

295. Torchy, M. P., Hamiche, A. & Klaholz, B. P. Structure and function insights into the NuRD chromatin remodeling complex. *Cell. Mol. Life Sci.* **72**, 2491–2507 (2015).

296. McDonel, P., Costello, I. & Hendrich, B. Keeping things quiet: Roles of NuRD and Sin3 co-repressor complexes during mammalian development. *Int. J. Biochem. Cell Biol.* **41**, 108–116 (2009).

297. Toh, Y. & Nicolson, G. L. The role of the MTA family and their encoded proteins in human cancers: molecular functions and clinical implications. *Clin. Exp. Metastasis* **26**, 215–227 (2009).

298. Kashiwagi, M., Morgan, B. A. & Georgopoulos, K. The chromatin remodeler Mi-2 is required for establishment of the basal epidermis and normal differentiation of its progeny. *Development* **134**, 1571–1582 (2007).

299. Lu, X. *et al.* Inactivation of NuRD Component Mta2 Causes Abnormal T Cell Activation and Lupus-like Autoimmune Disease in Mice. *J. Biol. Chem.* **283**, 13825–13833 (2008).

300. Chu, C., Qu, K., Zhong, F. L., Artandi, S. E. & Chang, H. Y. Genomic Maps of Long Noncoding RNA Occupancy Reveal Principles of RNA-Chromatin Interactions. *Mol. Cell* **44**, 667–678 (2011).

301. Zhang, Y. *et al.* Model-based analysis of ChIP-Seq (MACS). *Genome Biol.* **9**, R137 (2008).

302. Kong, L.-J., Chang, J. T., Bild, A. H. & Nevins, J. R. Compensation and specificity of function within the E2F family. *Oncogene* **26**, 321–327 (2007).

303. Dimova, D. K. & Dyson, N. J. The E2F transcriptional network: old acquaintances with new faces. *Oncogene* **24**, 2810–2826 (2005).

304. DeGregori, J. & Johnson, D. Distinct and Overlapping Roles for E2F Family Members in Transcription, Proliferation and Apoptosis. *Curr. Mol. Med.* **6**, 739–748 (2006).

305. Xu, X. *et al.* A comprehensive ChIP chip analysis of E2F1, E2F4, and E2F6 in normal and tumor cells reveals interchangeable roles of E2F family members. *Genome Res.* **17**, 1550–1561 (2007).

306. Wu, C. L., Zukerberg, L. R., Ngwu, C., Harlow, E. & Lees, J. A. In vivo association of E2F and DP family proteins. *Mol. Cell. Biol.* **15**, 2536–2546 (1995).

307. Justus, C. R., Leffler, N., Ruiz-Echevarria, M. & Yang, L. V. In vitro Cell Migration and Invasion Assays. *J. Vis. Exp. JoVE* (2014) doi:10.3791/51046.

308. Peter, C. *et al.* Migration to Apoptotic "Find-me" Signals Is Mediated via the Phagocyte Receptor G2A. *J. Biol. Chem.* **283**, 5296–5305 (2008).

309. Junger, W. G. Purinergic regulation of neutrophil chemotaxis. *Cell. Mol. Life Sci.* **65**, 2528–2540 (2008).

310. Lazennec, G. & Richmond, A. Chemokines and chemokine receptors: new insights into cancer-related inflammation. *Trends Mol. Med.* **16**, 133–144 (2010).

311. Stamm, A. *et al.* In vitro wound healing assays – state of the art. *BioNanoMaterials* **17**, (2016).

312. Liang, C.-C., Park, A. Y. & Guan, J.-L. In vitro scratch assay: a convenient and inexpensive method for analysis of cell migration in vitro. *Nat. Protoc.* **2**, 329–333 (2007).

313. Ziegler, C. & Kretz, M. The More the Merrier—Complexity in Long Non-Coding RNA Loci. *Front. Endocrinol.* **8**, (2017).

314. Derrien, T. *et al.* The GENCODE v7 catalog of human long noncoding RNAs: analysis of their gene structure, evolution, and expression. *Genome Res.* **22**, 1775–1789 (2012).

315. Iyer, M. K. *et al.* The landscape of long noncoding RNAs in the human transcriptome. *Nat. Genet.* **47**, 199–208 (2015).

316. Hon, C.-C. *et al.* An atlas of human long non-coding RNAs with accurate 5′ ends. *Nature* **543**, 199–204 (2017).

317. Oh, I. Y. *et al.* Regulation of the Dynamic Chromatin Architecture of the Epidermal Differentiation Complex Is Mediated by a c-Jun/AP-1-Modulated Enhancer. *J. Invest. Dermatol.* **134**, 2371–2380 (2014).

318. Ziegler, C. *et al.* The long non-coding RNA LINC00941 and SPRR5 are novel regulators of human epidermal homeostasis. *EMBO Rep.* **20**, (2019).

319. Chu, C., Qu, K., Zhong, F. L., Artandi, S. E. & Chang, H. Y. Genomic Maps of Long Noncoding RNA Occupancy Reveal Principles of RNA-Chromatin Interactions. *Mol. Cell* **44**, 667–678 (2011).

320. Feng, S., Jacobsen, S. E. & Reik, W. Epigenetic Reprogramming in Plant and Animal Development. *Science* **330**, 622–627 (2010).

321. Clapier, C. R. & Cairns, B. R. The Biology of Chromatin Remodeling Complexes. *Annu. Rev. Biochem.* **78**, 273–304 (2009).

322. Campos, E. I. & Reinberg, D. Histones: Annotating Chromatin. *Annu. Rev. Genet.* **43**, 559–599 (2009).

323. Eskiw, C. H. *et al.* Transcription Factories and Nuclear Organization of the Genome. *Cold Spring Harb. Symp. Quant. Biol.* **75**, 501–506 (2010).

324. Shi, D. *et al.* LncRNA AFAP1-AS1 promotes tumorigenesis and epithelial-mesenchymal transition of osteosarcoma through RhoC/ROCK1/p38MAPK/Twist1 signaling pathway. *J. Exp. Clin. Cancer Res.* **38**, 375 (2019).

325. Wu, W. *et al.* Hypomethylation of Noncoding DNA Regions and Overexpression of the Long Noncoding RNA, AFAP1-AS1, in Barrett's Esophagus and Esophageal Adenocarcinoma. *Gastroenterology* **144**, 956-966.e4 (2013).

326. El-Guendy, N., Zhao, Y., Gurumurthy, S., Burikhanov, R. & Rangnekar, V. M. Identification of a Unique Core Domain of Par-4 Sufficient for Selective Apoptosis Induction in Cancer Cells. *Mol. Cell. Biol.* **23**, 5516–5525 (2003).

327. Zhao, H., Zhang, X., Frazão, J. B., Condino-Neto, A. & Newburger, P. E. HOX antisense lincRNA HOXA-AS2 is an apoptosis repressor in all *Trans* retinoic acid treated NB4 promyelocytic leukemia cells: lincRNA HOXA-AS2 suppresses apoptosis in NB4 cells. *J. Cell. Biochem.* **114**, 2375–2383 (2013).

328. Luo, J., Su, F., Chen, D., Shiloh, A. & Gu, W. Deacetylation of p53 modulates its effect on cell growth and apoptosis. *Nature* **408**, 377–381 (2000).

329. Feng, Q. & Zhang, Y. The NuRD Complex: Linking Histone Modification to Nucleosome Remodeling. in *Protein Complexes that Modify Chromatin* (ed. Workman, J. L.) vol. 274 269–290 (Springer Berlin Heidelberg, 2003).

330. Torchy, M. P., Hamiche, A. & Klaholz, B. P. Structure and function insights into the NuRD chromatin remodeling complex. *Cell. Mol. Life Sci.* **72**, 2491–2507 (2015).

331. Basta, J. & Rauchman, M. The nucleosome remodeling and deacetylase complex in development and disease. *Transl. Res.* **165**, 36–47 (2015).

332. Dege, C. & Hagman, J. Mi-2/NuRD chromatin remodeling complexes regulate B and T-lymphocyte development and function. *Immunol. Rev.* **261**, 126–140 (2014).

333. Zhao, Z., Sentürk, N., Song, C. & Grummt, I. lncRNA PAPAS tethered to the rDNA enhancer recruits hypophosphorylated CHD4/NuRD to repress rRNA synthesis at elevated temperatures. *Genes Dev.* **32**, 836–848 (2018).

334. Buenrostro, J. D., Giresi, P. G., Zaba, L. C., Chang, H. Y. & Greenleaf, W. J. Transposition of native chromatin for fast and sensitive epigenomic profiling of open chromatin, DNA-binding proteins and nucleosome position. *Nat. Methods* **10**, 1213–1218 (2013).

335. Orlando, V. & Paro, R. Mapping polycomb-repressed domains in the bithorax complex using in vivo formaldehyde cross-linked chromatin. *Cell* **75**, 1187–1198 (1993).

336. Naumova, N. & Dekker, J. Integrating one-dimensional and three-dimensional maps of genomes. *J. Cell Sci.* **123**, 1979–1988 (2010).

337. Sen, G. L., Reuter, J. A., Webster, D. E., Zhu, L. & Khavari, P. A. DNMT1 maintains progenitor function in self-renewing somatic tissue. *Nature* **463**, 563–567 (2010).

338. Sardet, C. *et al.* E2F-4 and E2F-5, two members of the E2F family, are expressed in the early phases of the cell cycle. *Proc. Natl. Acad. Sci. U. S. A.* **92**, 2403–2407 (1995).

339. Ginsberg, D. *et al.* E2F-4, a new member of the E2F transcription factor family, interacts with p107. *Genes Dev.* **8**, 2665–2679 (1994).

340. Zhang, Y., Venkatraj, V. S., Fischer, S. G., Warburton, D. & Chellappan, S. P. Genomic cloning and chromosomal assignment of the E2F dimerization partner TFDP gene family. *Genomics* **39**, 95–98 (1997).

341. Trimarchi, J. M. *et al.* E2F-6, a member of the E2F family that can behave as a transcriptional repressor. *Proc. Natl. Acad. Sci. U. S. A.* **95**, 2850–2855 (1998).

342. Oberley, M. J., Inman, D. R. & Farnham, P. J. E2F6 negatively regulates BRCA1 in human cancer cells without methylation of histone H3 on lysine 9. *J. Biol. Chem.* **278**, 42466–42476 (2003).

343. Lee, E. Y. *et al.* E2F4 loss suppresses tumorigenesis in Rb mutant mice. *Cancer Cell* **2**, 463–472 (2002).

344. Xu, N. *et al.* MicroRNA-125b Down-regulates Matrix Metallopeptidase 13 and Inhibits Cutaneous Squamous Cell Carcinoma Cell Proliferation, Migration, and Invasion. *J. Biol. Chem.* **287**, 29899–29908 (2012).

345. Ridky, T. W., Chow, J. M., Wong, D. J. & Khavari, P. A. Invasive three-dimensional organotypic neoplasia from multiple normal human epithelia. *Nat. Med.* **16**, 1450–1455 (2010).

346. Lazarov, M. *et al.* CDK4 coexpression with Ras generates malignant human epidermal tumorigenesis. *Nat. Med.* **8**, 1105–1114 (2002).

347. Bolger, A. M., Lohse, M. & Usadel, B. Trimmomatic: a flexible trimmer for Illumina sequence data. *Bioinformatics* **30**, 2114–2120 (2014).

348. External RNA Controls Consortium. Proposed methods for testing and selecting the ERCC external RNA controls. *BMC Genomics* **6**, 150 (2005).

349. Dobin, A. *et al.* STAR: ultrafast universal RNA-seq aligner. *Bioinformatics* **29**, 15–21 (2013).

350. Kolde, R. Pheatmap: pretty heatmaps. *R Package Version* **61**, (2012).

351. Hartley, S. W. & Mullikin, J. C. QoRTs: a comprehensive toolset for quality control and data processing of RNA-Seq experiments. *BMC Bioinformatics* **16**, 224 (2015).

352. Kent, W. J. *et al.* The Human Genome Browser at UCSC. *Genome Res.* **12**, 996–1006 (2002).

353. Thorvaldsdóttir, H., Robinson, J. T. & Mesirov, J. P. Integrative Genomics Viewer (IGV): high-performance genomics data visualization and exploration. *Brief. Bioinform.* **14**, 178–192 (2013).

354. Robinson, J. T. *et al.* Integrative genomics viewer. *Nat. Biotechnol.* **29**, 24–26 (2011).

355. Love, M. I., Huber, W. & Anders, S. Moderated estimation of fold change and dispersion for RNA-seq data with DESeq2. *Genome Biol.* **15**, (2014).

356. Benjamini, Y. & Hochberg, Y. Controlling the False Discovery Rate: A Practical and Powerful Approach to Multiple Testing. *J. R. Stat. Soc. Ser. B Methodol.* **57**, 289–300 (1995).

357. Huang, D. W., Sherman, B. T. & Lempicki, R. A. Systematic and integrative analysis of large gene lists using DAVID bioinformatics resources. *Nat. Protoc.* **4**, 44–57 (2009).

358. Huang, D. W., Sherman, B. T. & Lempicki, R. A. Bioinformatics enrichment tools: paths toward the comprehensive functional analysis of large gene lists. *Nucleic Acids Res.* **37**, 1–13 (2009).

359. Chen, E. Y. *et al.* Enrichr: interactive and collaborative HTML5 gene list enrichment analysis tool. *BMC Bioinformatics* **14**, 128 (2013).

360. Kuleshov, M. V. *et al.* Enrichr: a comprehensive gene set enrichment analysis web server 2016 update. *Nucleic Acids Res.* **44**, W90–W97 (2016).

361. R Core Team. *R: A Language and Environment for Statistical Computing*. (R Foundation for Statistical Computing, YEAR).

362. Lin, M. F., Jungreis, I. & Kellis, M. PhyloCSF: a comparative genomics method to distinguish protein coding and non-coding regions. *Bioinformatics* **27**, i275–i282 (2011).

363. Raney, B. J. *et al.* Track data hubs enable visualization of user-defined genome-wide annotations on the UCSC Genome Browser. *Bioinformatics* **30**, 1003–1005 (2014).

364. Sun, K. *et al.* iSeeRNA: identification of long intergenic non-coding RNA transcripts from transcriptome sequencing data. *BMC Genomics* **14**, S7 (2013).

365. Kong, L. *et al.* CPC: assess the protein-coding potential of transcripts using sequence features and support vector machine. *Nucleic Acids Res.* **35**, W345-349 (2007).

366. Afgan, E. *et al.* The Galaxy platform for accessible, reproducible and collaborative biomedical analyses: 2018 update. *Nucleic Acids Res.* **46**, W537–W544 (2018).

367. Zhang, Y. *et al.* Model-based Analysis of ChIP-Seq (MACS). *Genome Biol.* **9**, R137 (2008).

368. Feng, J., Liu, T., Qin, B., Zhang, Y. & Liu, X. S. Identifying ChIP-seq enrichment using MACS. *Nat. Protoc.* **7**, 1728–1740 (2012).

369. Heinz, S. *et al.* Simple combinations of lineage-determining transcription factors prime cis-regulatory elements required for macrophage and B cell identities. *Mol. Cell* **38**, 576–589 (2010).

370. Barrett, T. *et al.* NCBI GEO: archive for functional genomics data sets—update. *Nucleic Acids Res.* **41**, D991–D995 (2013).

371. Edgar, R., Domrachev, M. & Lash, A. E. Gene Expression Omnibus: NCBI gene expression and hybridization array data repository. *Nucleic Acids Res.* **30**, 207–210 (2002).

372. Langmead, B. & Salzberg, S. L. Fast gapped-read alignment with Bowtie 2. *Nat. Methods* **9**, 357–359 (2012).

373. Mayer, A. *et al.* Native Elongating Transcript Sequencing Reveals Human Transcriptional Activity at Nucleotide Resolution. *Cell* **161**, 541–554 (2015).

374. Chu, C., Qu, K., Zhong, F. L., Artandi, S. E. & Chang, H. Y. Genomic Maps of Long Noncoding RNA Occupancy Reveal Principles of RNA-Chromatin Interactions. *Mol. Cell* **44**, 667–678 (2011).

375. Streit, S., Michalski, C. W., Erkan, M., Kleeff, J. & Friess, H. Northern blot analysis for detection and quantification of RNA in pancreatic cancer cells and tissues. *Nat. Protoc.* **4**, 37–43 (2009).

376. Livak, K. J. & Schmittgen, T. D. Analysis of Relative Gene Expression Data Using Real-Time Quantitative PCR and the 2−ΔΔCT Method. *Methods* **25**, 402–408 (2001).

11 Acknowledgements

This thesis could not have been completed without the help and support of many people.

First of all, I really feel to say many thanks to my supervisor PD Dr. Markus Kretz for the opportunity to start my PhD project in his laboratory. I am more than grateful for the great opportunity to conduct my doctoral research in his group. I want to thank him for his constant support, his enthusiasm, his positive attitude, many inspiring discussions, and for enabling experimental freedom.

I want to thank Prof. Dr. Gunter Meister and Prof. Dr. Melina Musri for being my PhD thesis mentors and giving me helpful suggestion for this project.

Many thanks to all members of my thesis comitee.

Thanks to all members of the AG Kretz (present and alumni). The unconditional support of Bianca, her always positive attitude and always open ear during countless discussions made every challenge feasible. Additionally, I want to thank Daniela for assisting in every situation and her ability to always create a cheerful atmosphere in the lab. Also, many thanks to Sonja for scientific productive discussions and inspirations. Moreover, my PhD colleagues Chris and Fabi for discussions and support along the way.

Many thanks to the whole AG Meister and AG Medenbach, especially Gerhard and Norbert for their endless help and support for all bioinformatic obstacles. Furthermore, I want to thank the 11 o´ clock lunch group for many hours of relaxing and cheerful breaks. I had so much fun all the time. I want to thank Kevin, Franzi and Fabi for reading and giving input for this manuscript.

Furthermore, I want to thank Kevin who made lab-life and many evenings more enjoyable on numerous occasions.

Last but most important to my family for their unconditional support throughout this long and sometimes challenging journey. Thank you for always being there as a fixed point and for giving new impulses when they are needed. That was without a doubt crucial for this work. I am very grateful to have so many people at my side, who always supported me.